Subduction and continental collision in the Lufilian Arc-Zambesi Belt orogen: A petrological, geochemical, and geochronological study of eclogites and whiteschists (Zambia)

Dissertation
zur Erlangung des Doktorgrades
der Mathematisch-Naturwissenschaftlichen Fakultät
der Christian-Albrechts-Universität
zu Kiel

vorgelegt von
Timm John

Kiel
2001

Vorwort

Diese Arbeit besteht aus drei Kapiteln, denen eine allgemeine Einführung und Zusammenfassung vorangestellt ist. Die Kapitel sind so konzipiert, daß sie zwar getrennt voneinander als Artikel publiziert werden können, aber auch eine zusammenhängende Monographie darstellen.

Die Arbeit entstand im Rahmen eines von der Deutschen Forschungsgemeinschaft geförderten und von Volker Schenk initiierten Forschungsprojekts (Sche 265/10-1 und Sche 265/10-2). Volker Schenk möchte ich an dieser Stelle in besonderem Maße danken: für die Gelegenheit an diesem Projekt mitzuarbeiten und die Möglichkeit zu promovieren. Auch seinem großen Engagement, dem intensiven Einsatz und der fördernden Betreuung während des Geländeaufenthaltes in Zambia und der Bearbeitung der Proben hier in Kiel gilt mein herzlicher Dank. Von seiner Leidenschaft für die Petrologie habe ich mich gern anstecken lassen.

Klaus Mezger hat mich während meines Gastaufenthaltes am Zentrallaboratorium für Geochronologie der Universität Münster hervorragend betreut und stets nach “Niederlagen” im Labor wieder aufgebaut. Vielen Dank für die kompetente Einführung in die Geochronologie, unzählige Denkanstöße, viele Lacher und nicht zuletzt die Gewährung von Unterschlupf.

Für die gute Zusammenarbeit in der Arbeitsgruppe in Kiel bedanke ich mich bei Petra Herms, Peter Raase und Peter Appel, die mir stets hilfreich zur Seite standen. Besonders die Ratschläge zu Fragen der Dünnschliffmikroskopie haben mir immer wieder geholfen. Karsten Haase hat mir in vielen langen Diskussionen die Geochemie näher gebracht, unter anderem danke ich ihm dafür. Dieter Garbe-Schönberg danke ich herzlichst für die Durchführung der Messungen von Spurenelementen an der ICP-MS. Bei der Probenaufbereitung wurde ich hervorragend von Stefan Bredemeyer und Frau Astrid Weinkauf unterstützt. Andreas Fehler danke ich für die Herstellung vieler Gesteins-Dünnschliffe. Herr Dr. Dietrich Ackermand, Frau Barbara Mader und Peter Appel halfen mir tatkräftig bei der Durchführung der Mikrosondenanalysen.

Der Münster-Crew sei erst einmal im Gesamten gedankt. Ihr wißt schon wofür. Bei Bart Willigers, Erik Scherer, Kilian Pollok und Thorsten Kleine möchte ich mich vor allem für die anregenden Diskussionen bedanken. Erik, danke für much more than the big Lu’s and Hf‘s. Ohne die vielen Hilfestellungen von Heidi Baier im Labor und an den Massenspektrometern wäre wohl kein Isotop von mir gemessen worden.

Ein Dank geht auch an Andreas Kronz vom Institut für Geochemie der Universität Göttingen, der mir bei Messungen an der dortigen Mikrosonde geholfen hat.

I greatfully acknowledge the support of the Geology Department of the University of Zambia and the Zambian Geological Survey. I am especially thankful for the strong support I had from Francis Tembo during the whole study. Pete and Spana Mosley and Bill Barclay, I thank you for the support and the nice time in Lusaka. Last but not least, thanks to Ben Mapani.

Andrea, Klaus, Evi, Geli, Alex, Dirk, Imke, Lutz, Martin und Uwe – danke. Außerdem danke ich allen, die mir über die Jahre geholfen, mich zum Lachen gebracht oder einfach in Ruhe gelassen haben.

Introduction and Summary

The study is focused on eclogites and other potentially subduction related rocks from the late Proterozoic orogenic belts in south central Africa in order to get new insights into subduction zone processes at Precambrian times and, moreover, to clarify their geodynamic relation to the Pan-African orogenic cycle.

Eclogites are formed from rocks of basaltic bulk-composition due to crustal thickening or subduction zone processes. Rocks transform to eclogites at great depth under low geothermal gradients, and thus, the occurrence of eclogites indicates specific plate-tectonic processes. If eclogites are formed from oceanic crust, their outcrops may mark a suture zone, which is the region where two blocks of lithosphere are welded together (e.g., Condie, 1989). Other potentially subduction related rocks besides eclogites are whiteschists (talc-kyanite schists) (Schreyer, 1973). Whiteschists typically are found in Alpine-type orogens, e.g., Western Alps, Trans-Himalaya (Sar e Sang - Afghanistan), and are usually interpreted as being of metasomatic origin (e.g., Schreyer & Abraham, 1976). The stability field of the talc-kyanite assemblage is restricted to temperatures between c. 600 and 800 °C, and pressures from c. 6 kbar up to conditions of ultra-high-pressure metamorphism (Chopin, 1984; Schreyer, 1988; Massonne, 1989). Whiteschists of all known occurrences are formed during crustal thickening under low geothermal gradients.

Ocean basins form by seafloor spreading processes following the rifting of continental lithosphere. In some cases, the closure of an ocean basin occurred repeatedly between the same parts of continental lithosphere which formed one continuous block prior to rifting. This process of ocean basin formation and closure, resulting in a continent-continent collision, is called a Wilson cycle. During the closure of an ocean basin, oceanic crust consumption occurs at convergent plate boundaries (subduction zones) where oceanic lithosphere descends beneath less dense continental lithosphere, or older (denser) beneath younger (lighter) oceanic lithosphere. Orogens usually form by the closure of an ocean basin (e.g., Alps), or subduction of oceanic beneath continental lithosphere (e.g., Andes). In rare cases, orogens may form by compression of sedimentary basins in continental rifts. Thus, ophiolites and eclogites representing relics of oceanic basins can provide key information to distinguish between different former large-scale geodynamic processes. They provide geochemical information about the geotectonic setting in which they were generated, the time of their formation, and can preserve a record of the pressure-temperature conditions within the subduction zone in which they were metamorphosed. In addition, whiteschists usually contain monazite which is suitable for high-precision U-Pb geochronology due to the incorporation of uranium into the structure. Since whiteschists and monazites are formed by metamorphic processes, they provide, similar to eclogites, information about the conditions and the time of their formation.

The Proterozoic mobile belts of central southern Africa (e.g., Irumide Belt and Lufilian Arc-Zambesi Belt) formed between the Congo and Kalahari cratons during the evolution of the supercontinents Rodinia and Gondwana (e.g., Unrug, 1996; Weil et al., 1998). Two contrasting models exist to explain the origin of these mobile belts: one suggesting an intracratonic formation (Daly, 1986; Hanson et al., 1994), and the other involves the formation of an ocean basin (Coward & Daly, 1984, Porada & Berhorst, 2000). Central Zambia exhibits the largest occurrence of Precambrian eclogites in southern Africa (Vrana et al.,

1975). Only two other eclogite localities exist in this region, one in northern Zambia (Cosi et al., 1992) and the other in northern Zimbabwe (Dirks and Sithole, 1999). Both could be related to the main central Zambian occurrence, because they are situated within the same Pan-African belt. However, different times for eclogite formation have been proposed. Vrana et al. (1975) relate the eclogites of central Zambia to the evolution of the Pan-African Zambesi Belt, and thus to the Gondwana formation (720 to 520 Ma). In contrast, based on a study of the eclogites from northern Zimbabwe, Dirks & Sithole (1999) suggest that the eclogites formed during the assembly of Rodinia (1300 to 1000 Ma). Neither the geochemical nature of the protoliths nor the age or the pressure-temperature conditions of formation of the Zambian eclogites is known. This resulted in contrasting models of eclogite formation in central Zambia and hence in the contrasting geodynamic models for the related mobile belts. Consequently, several objectives are addressed in this thesis: one is to verify whether the eclogites were formed from oceanic crust, and another is to characterize the pressure-temperature evolution of these rocks. Therefore Zambian eclogites and basic magmatic rocks have been analysed for their major- and trace-element as well as Nd-isotopic compositions, and geothermobarometric methods have been applied. Another goal of this study is to identify the orogenic cycle during which the eclogite facies metamorphism took place by applying Sm-Nd garnet geochronology. Moreover, the occurrence of co-genetic eclogitic and gabbroic rocks along a 200-km long and up to 40-km wide area in central Zambia provides a unique possibility to investigate the behaviour of gabbroic rocks during subduction zone metamorphism. On the basis of a detailed petrographic and mineral chemical study it is aimed to characterize the main metamorphic processes that control the gabbro-to-eclogite transformation. Furthermore, Zambia hosts one of the largest occurrences of whiteschists in the world with several exposures along a c. 700 km northwest-southeast striking zone. Mineral-chemical and textural investigations in combination with quantitative geothermobarometry were applied to reconstruct the metamorphic evolution of the whiteschists, in order to clarify their relationship to the Zambian eclogites. In addition, peak metamorphic conditions have been dated with U-Pb monazite geochronology to compare the time of whiteschist formation with that of the eclogites.

The thesis is subdivided into three chapters, each written as a manuscript for publication in a scientific journal. The **first chapter** addresses implications of the Zambian eclogites to the regional geology and the assembly of Gondwana. P-T estimates of Ky-bearing eclogites from the entire zone of central Zambia give temperatures between 590 and 750 °C at minimum pressures of about 20 kbar. Phengite-bearing eclogites equilibrated at 720–755 °C and 26–28 kbar, and show evidence for a clockwise P-T path. These P-T conditions imply a low geothermal gradient of c. 8 °C/km and a subduction depth of c. 90 km. The eclogites, metagabbros and gabbros show incompatible element depletion similar to magmatic rocks formed at a recent oceanic spreading centre. Consequently, the investigated basic rocks from Zambia are interpreted to represent part of former oceanic crust. The low geothermal gradient and the great subduction depth suggest the subduction of cold oceanic lithosphere and, accordingly, the former existence of a relatively large oceanic basin. A Sm-Nd garnet-whole rock isochron defines an age of about 595 ±10 Ma for the eclogite facies metamorphism. This

implies that a Neoproterozoic suture zone is located in south central Africa between the Congo and Kalahari cratons. This suture zone was formed during the assembly of Gondwana.

The **second chapter** focuses on the metamorphic processes during the formation of eclogites, i.e., the gabbro-to-eclogite transformation. Gradual stages of prograde transformation from gabbro to eclogite are preserved by incomplete reactions and disequilibrium textures. Undeformed eclogites typically preserved features of the former gabbroic texture, reflected by replacements of plagioclase and pyroxene through eclogite facies minerals. Textures of deformed eclogites range from sheared porphyroclastic to porphyroblastic. Relics of magmatic pyroxene are common and complete eclogitisation occurred only in mm- to cm-scale domains in most of the deformed and undeformed rocks. No evidence for prograde blueschist or amphibolite facies mineral assemblages was found in eclogites. In contrast, the fine grained intergrowth of omphacite, garnet, kyanite and quartz replacing former plagioclase or forming in the pressure shadow of magmatic pyroxene relics indicates that eclogitisation may have affected the gabbroic protoliths directly without any significant intervening metamorphic reactions. Eclogitisation took place at P-T conditions of 605-665 °C and 26-28 kbar and was accompanied by a channelised fluid flow resulting in veins with large, subhedral grains of omphacite, kyanite and garnet. The eclogitisation process was limited by reaction kinetics and dissolution-precipitation rates rather than by the metamorphic P-T conditions. Even though deformation occurred and mineral reaction boundaries were overstepped, the infiltration of fluids was necessary for triggering the gabbro-to-eclogite transformation.

The **third chapter** deals with several whiteschist occurrences in Zambia and their metamorphic evolution and age relation to the Lufilian Arc and Zambesi Belt development. Whiteschists and associated rocks from four localities, three in the Lufilian Arc (NW) and one in the Zambesi Belt (SE) were chosen for this study. In the Lufilian Arc petrological investigations of whiteschists and associated garnet-amphibolites and biotite-kyanite-garnet gneisses record peak-metamorphic conditions of about 750 ±25 °C at 13 ±1 kbar. Using whiteschists, associated gedrite-cordierite-kyanite gneisses and garnet-staurolite-kyanite schists from the Zambesi Belt, estimated peak metamorphic conditions indicate about 700 ±25 °C at 10 ±1 kbar. Mineral reaction textures imply a metamorphic evolution along clockwise P-T paths with peak metamorphism culminating at high-pressure amphibolite facies conditions, which are interpreted as the result of significant crustal thickening. On the basis of the P-T paths and a concordant monazite age of 529 ±2 Ma (biotite-kyanite-garnet gneiss) combined with $^{207}Pb/^{235}U$ ages of 531-532 ±2 Ma from monazites extracted from whiteschists, it is concluded that the crustal thickening event affected the entire Lufilian Arc-Zambesi Belt orogen almost simultaneously. Thus, the whiteschist formation is related to the final continental collision between the Congo and the Kalahari cratons at c. 530 Ma during the assembly of Gondwana, subsequent to the ocean basin subduction and eclogite metamorphism at c. 600 Ma.

CHAPTER ONE

Evidence for a Neoproterozoic ocean in south central Africa from MORB-type geochemical signatures and P-T estimates of Zambian eclogites

1.1 Abstract

Precambrian eclogites, metagabbros, and gabbros occur in a 200 km long and up to 40 km wide zone in central Zambia. Pressure-temperature (P-T) estimates of kyanite-bearing eclogites throughout the entire zone give temperatures of 590-750 °C at minimum pressures of 20 kbar. Phengite-bearing eclogites equilibrated at 720–755 °C and 26–28 kbar and show evidence for a clockwise P-T path. These P-T conditions imply a low geothermal gradient of ca. 8 °C/km and a subduction depth of ca. 90 km. The eclogites, metagabbros, and gabbros show incompatible element depletion similar to that of recent mid-ocean ridge basalts (MORB). These basic rocks are therefore interpreted to represent former oceanic crust. The low geothermal gradient and great subduction depth indicate that the subducted oceanic lithosphere was cold, suggesting the existence of a relatively large ocean basin. A Sm-Nd isochron defines an age of 595 ±10 Ma for the eclogite facies metamorphism. These results imply that a Neoproterozoic suture zone exists between the Congo and Kalahari cratons in south central Africa. This suture zone belongs to the same orogenic cycle that formed the Zambesi Belt and is related to the assembly of Gondwana.

1.2 Introduction

A complete Wilson cycle in the plate tectonic model consists of the opening and closure of an ocean basin and ends with an orogeny. In rare cases however, orogens may form by compression of sedimentary basins in continental rifts (e.g., Condie, 1989). Suture zones in orogenic belts are former plate margins and are often marked by relics of ocean basins in the form of ophiolites and eclogites. These rocks provide geochemical information about the tectonic setting in which they were generated and can preserve a record of the pressure-temperature conditions within the subduction zone in which they were metamorphosed. The Proterozoic mobile belts of central southern Africa formed between the Congo and Kalahari cratons during the development of the supercontinents Rodinia and Gondwana (e.g., Unrug, 1996; Weil et al., 1998). Two contrasting models exist for the origin of these mobile belts: one suggesting formation in an intracratonic setting (Daly, 1986; Hanson et al., 1994) and the other in an oceanic setting (Coward & Daly, 1984, Porada & Berhorst, 2000). The only Precambrian eclogites in this part of Africa are exposed in the central Zambesi Belt and Lufilian Arc (Vrana et al., 1975; Dirks & Sithole, 1999). Here we use new petrologic, geochemical, and age data from these eclogites and associated gabbros to reconstruct the tectonic environment of their formation, which occurred during the dispersal of Rodinia and the assembly of Gondwana.

1.3 Geological overview

The Precambrian orogenic systems of Zambia consist of two major mobile belts: (1) the Mesoproterozoic NE–SW striking Irumide Belt and Choma-Kalomo Block, and (2) the Neoproterozoic to Cambrian Lufilian Arc and Zambesi Belt, which are elongated in E-W direction (Fig. 1.1). The Irumide Belt was formed during the assembly of Rodinia in the large time interval between 1.0 and 1.4 Ga (e.g., Cahen et al., 1984; Hanson et al., 1988; Schenk & Appel, 2001). Importantly, neither evidence for high-pressure / low-temperature metamorphism nor for pressures above ~7 kbar has been found in the Irumide Belt. The Zambesi Belt and the Lufilian Arc are part of a Pan-African orogenic system that crosscuts southern Africa, separating the Congo and Kalahari Cratons. The evolution of the Zambesi Belt is related to the formation of the Gondwana supercontinent, and its peak metamorphism, which occurred between 550-525 Ma (e.g., Goscombe et al., 1998; Vinyu et al., 1999), is attributed to the final collision. The Neoproterozoic Zambesi Belt divides the Mesoproterozoic units of Zambia into the Irumide Belt and the Choma-Kalomo Block (Fig. 1.1). The junction of the Neoproterozoic and Mesoproterozoic belts is marked by a 200 km long and up to 40 km wide zone containing lenses of eclogites, metagabbros, unmetamorphosed gabbros, and rare ultramafic rocks (Vrana et al., 1975). This eclogite-bearing zone is located in the central part of the Zambesi Belt and is elongated parallel to strike (Fig. 1.1). The eclogites and the associated basic rocks form isolated hills of 10 to 100 meters in diameter. Contacts with the country rocks, which consist mainly of kyanite-bearing metapelites, metapsammites, and marbles, are not exposed. These metasedimentary rocks are interpreted to belong to a passive continental margin sequence (Porada & Berhorst, 2000). Neither the strongly weathered metapelitic rocks nor the less altered marbles contain critical mineral assemblages that might attest to the high-pressure evolution of this area. Two different geodynamic scenarios for the eclogite formation have been proposed. Vrana et al.

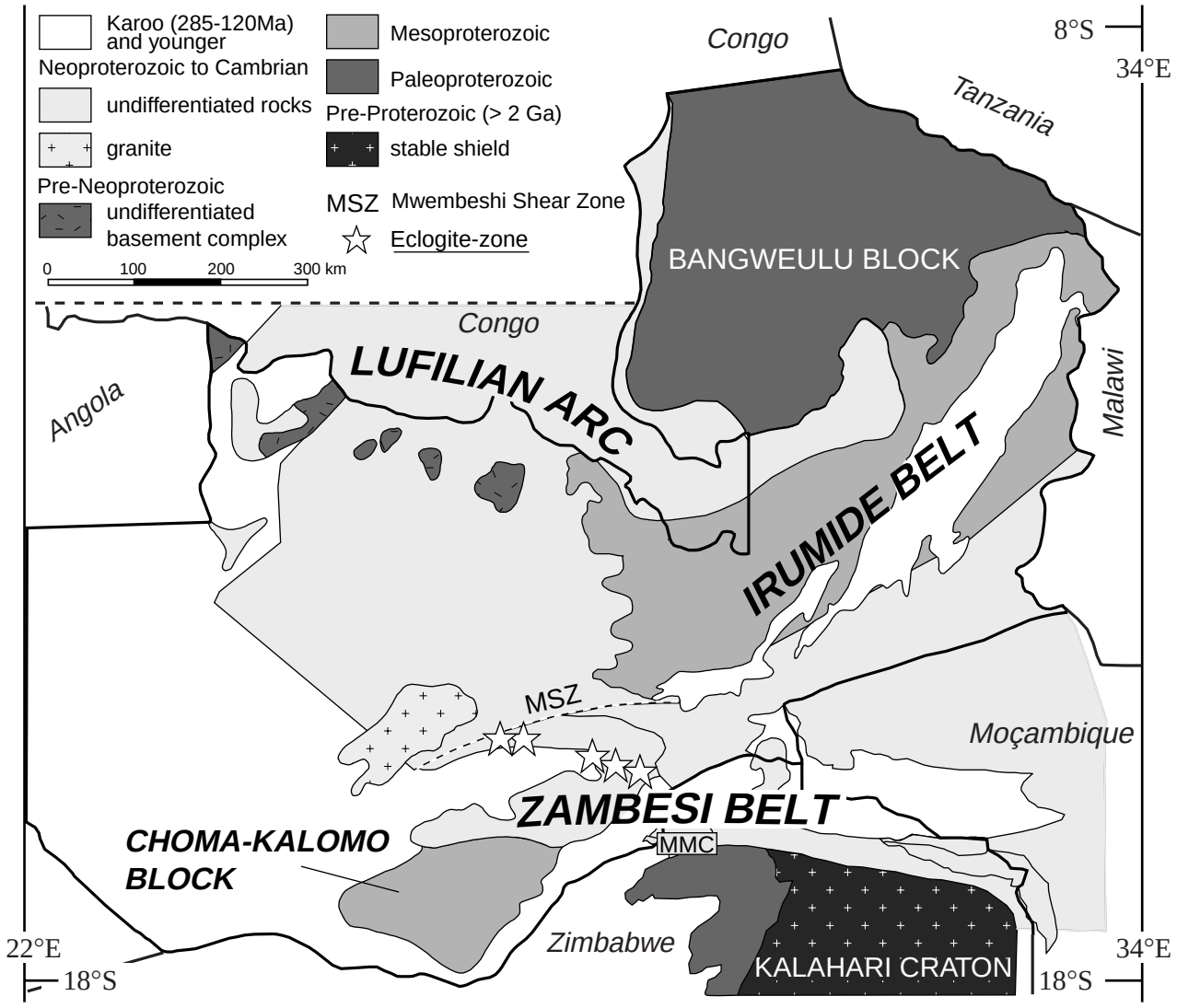

Fig. 1.1 Geological map (after Sikatali et al, 1994; Hanson et al., 1994) showing structural provinces of Zambia and northern Zimbabwe. The northern margin of the Kalahari craton is shown whereas the southern margin of the Congo craton is north of this figure. Stars indicate the eclogite-bearing zone; MMC = Makuti Metamorphic Complex; Thick lines indicate political borders and thin lines geological boundaries.

(1975) related the eclogites to the evolution of the Pan-African Zambesi Belt and thus to the formation of Gondwana (ca. 720 to 520 Ma), because the eclogite occurrences are centrally situated along the belt's strike. In contrast, based on their study of eclogites from the Makuti Metamorphic Complex in northern Zimbabwe (MMC in Fig. 1.1), Dirks & Sithole (1999) suggested that the eclogites formed during the assembly of Rodinia (ca. 1300 to 1000 Ma). They concluded that the eclogite facies metamorphism had to occur before the intrusion of the granitic gneisses (ca. 850 Ma) that enclose the eclogites. However, the tectonic setting of the Mesoproterozoic units of Zambia is regarded as being restricted to intracontinental regimes (e.g., Daly, 1986), whereas for the Pan-African Zambesi Belt the interpretations are more controversial, involving either a complete Wilson cycle with an ocean basin (e.g., Coward & Daly, 1984; Porada & Berhorst, 2000) or a purely ensialic stage of rift evolution (e.g., Hanson et al., 1994).

1.4 Petrography and mineral chemistry

A striking feature of the eclogites and metagabbros in the Zambesi Belt is that they have retained some recognizable ophitic textures of their magmatic protoliths. Ky-bearing eclogites are widespread and typically they have the mineral assemblage garnet + omphacite + rutile ± kyanite. Quartz and phengite are minor phases in some rocks. Retrograde amphibole and plagioclase, commonly replaced by scapolite, are mostly related to late-stage corona textures and symplectites. Garnet (Tab. 1.1) shows preserved growth zoning with core compositions of almandine$_{45-55}$, grossular$_{17-30}$, pyrope$_{10-28}$, and spessartine$_{01-10}$, and rim compositions of almandine$_{38-42}$, grossular$_{15-27}$, pyrope$_{23-40}$, and spessartine$_{00-03}$. X_{Fe}-values [$Fe^{2+}/(Fe^{2+}+Mg)$] of garnet cores vary from sample to sample (0.67 to 0.84), and generally decrease toward the rims (0.49 to 0.78). In some garnets, the grossular-content increases from core to rim. Peak-stage omphacite (Tab. 1.1) contains 40 to 50 mol% jadeite (Jd) and several omphacites show increasing Jd-contents and X_{Fe}–values toward their rims. This zoning of garnet and omphacite suggest that maximum pressure and maximum temperature occurred contemporaneously. During retrograde metamorphism, most omphacites were replaced by symplectites of low-Jd clinopyroxene (Jd_{10-30}) and quartz ± albite ± diopside ± amphibole. Phengite-bearing Ky-eclogites found at one locality contain phengite as either a matrix mineral or as inclusions in garnet. Matrix phengites (Tab. 1.1) have Si-contents ranging from 3.34 to 3.46 per formula unit (pfu), with X_{Fe}-values between 0.12 and 0.19, whereas enclosed phengites have Si-contents and X_{Fe}-values of 3.20 to 3.36 pfu and 0.20 to 0.34, respectively. These phengite inclusions, which occur exclusively in rocks without matrix phengite, probably formed during prograde metamorphism, as suggested by their textural occurrence and low Si-contents. This interpretation is supported by the prograde zoning of the surrounding garnet. In contrast, the high-Si matrix phengite is part of the peak-metamorphic assemblage. Retrograde edenitic amphibole (Tab. 1.1) coexists with garnet + quartz ± plagioclase ± kyanite ± zoisite.

1.5 Thermobarometry and P-T evolution

Temperatures were estimated with the garnet-clinopyroxene (Powell, 1985) and garnet-phengite thermometers (Green & Hellman, 1982). The breakdown of paragonite to kyanite + omphacite(Jd_{50}) + vapor (Holland, 1979) was used to constrain minimum pressures. Peak pressures were estimated with phengite barometry based on the equilibrium assemblage garnet + omphacite + phengite (Waters & Martin, 1993), following the procedure of Carswell et al. (1997). The P-T conditions of a prograde metamorphic stage were deduced from phengite inclusions in garnet. Garnet core, omphacite core and phengite inclusion give 580 ±30 °C at 15.8 ±2.5 kbar (sample Z 101-11a, Fig. 1.2), while peak-metamorphic conditions estimated from garnet and omphacite rims and matrix phengite are 720 ±40 °C at 25.6 ±2.5 kbar (Z 101-5) and 755 ±40 °C at 28.3 ±2.5 kbar (Z 101-7). Applying the internally consistent data set of Berman (1988), we find that these high pressures are supported by the low paragonite content (ca. 3 mol.%) of white mica in equilibrium with omphacite and kyanite (Z 101-7). These results agree with P-T estimates for the phengite-free Ky-eclogites, whose garnet and omphacite rim compositions

Tab. 1.1 Representative major element contents and structural formulae of garnet (Grt), amphibole (Amp), plagioclase (Pl), clinopyroxene (Cpx) and phengite (Phe). Application for thermobarometric calculations is indicated: ga = Grt-Amp thermometry; gc = Grt-Cpx thermometry; ph = phengite barometry.

sample	Z 101-5	Z 101-5	Z 101-5	Z 101-5	Z 101-5	Z 101-7	Z 101-7	Z 101-7	Z 101-7	Z 101-7	Z 101-11	Z 101-11	Z 101-11	Z 101-11	Z 101-11
mineral	Amp	Cpx	Grt	Grt	Phe	Amp	Cpx	Grt	Grt	Phe	Amp	Grt	Grt	Cpx	Phe
analysis	amp1p2	cpx2p5	grt1p7	grt2p78	ph1p17	am4p1	cpxx1p2	grt1ap1	grx1p24	phx1p2	am7p1	grx1p24	grt6p3	cpxx1p3	phx1p3
used for	ga	gc;ph	ga	gc;gp;ph	gp;ph	ga	gc;ph	ga	gc;gp;ph	gp;ph	ga	gc;gp;ph	ga	gc;ph	gp;ph
SiO_2	49.77	55.46	39.95	39.71	51.31	47.36	55.78	40.09	39.63	51.00	49.01	37.87	40.22	55.43	47.93
TiO_2	0.19	0.06	0.04	0.04	0.32	0.32	0.06	0.03	0.09	0.30	0.27	0.10	0.00	0.08	0.54
Al_2O_3	9.40	10.30	22.67	22.42	25.80	13.27	10.34	22.26	22.31	26.08	12.34	21.63	22.01	10.15	29.06
Cr_2O_3	0.02	0.03	0.01	0.02	0.06	n.d.	0.01	0.00	0.10	0.07	n.d.	0.01	0.00	0.14	0.02
FeO	7.37	2.47	18.37	20.90	1.54	7.74	2.52	19.78	18.36	1.24	6.99	25.33	18.38	4.48	1.87
Fe_2O_3	—	2.40	—	0.08	—	—	1.66	0.00	0.24	—	—	—	—	—	—
MgO	16.48	8.51	12.56	9.06	4.28	14.92	9.04	10.22	9.11	4.19	15.08	3.42	12.77	8.78	3.19
MnO	0.03	0.00	0.46	0.41	0.01	0.00	0.02	0.42	0.40	0.00	0.06	2.61	0.52	0.02	0.01
CaO	9.91	12.84	5.70	7.81	0.00	10.64	13.51	8.01	9.73	0.04	8.20	8.90	4.83	12.68	0.01
Na_2O	2.63	6.96	0.00	0.00	0.21	2.94	6.64	0.00	0.00	0.19	4.23	0.00	0.00	7.05	0.70
K_2O	0.65	0.00	0.00	0.00	11.04	1.08	0.00	0.00	0.00	11.14	0.61	0.00	0.00	0.00	10.37
Total	96.44	99.02	99.76	100.45	94.56	98.27	99.58	100.81	99.96	94.25	96.79	99.87	98.73	98.81	93.71
Si	7.119	1.990	5.969	5.996	3.448	6.711	1.988	6.002	5.985	3.436	6.963	5.972	6.057	1.999	3.260
Al^{IV}	0.000	0.010	0.000	0.000	0.552	1.289	0.012	0.000	0.000	0.564	1.037	0.000	0.000	0.001	0.740
Al	1.585	0.426	3.992	3.990	1.491	0.927	0.423	3.928	3.971	1.507	1.029	4.020	3.906	0.431	1.590
Ti	0.021	0.001	0.005	0.005	0.016	0.034	0.002	0.003	0.010	0.015	0.029	0.012	0.000	0.002	0.028
Cr	0.002	0.001	0.001	0.002	0.003	0.000	0.000	0.000	0.011	0.004	0.000	0.001	0.000	0.004	0.001
Fe^{2+}	0.882	0.074	2.295	2.639	0.087	0.917	0.075	2.477	2.318	0.070	0.830	3.341	2.315	0.135	0.106
Fe^{3+}	0.000	0.065	0.000	0.009	0.000	0.000	0.045	0.000	0.027	0.000	0.000	0.000	0.000	0.000	0.000
Mg	3.514	0.455	2.797	2.040	0.429	3.152	0.480	2.281	2.051	0.421	3.194	0.804	2.867	0.472	0.323
Mn	0.004	0.000	0.058	0.052	0.000	0.000	0.001	0.053	0.052	0.000	0.007	0.349	0.066	0.001	0.001
Ca	1.519	0.494	0.912	1.264	0.000	1.615	0.516	1.285	1.574	0.003	1.248	1.504	0.779	0.490	0.001
Na	0.729	0.484	0.000	0.000	0.027	0.808	0.459	0.000	0.000	0.025	1.165	0.000	0.000	0.493	0.092
K	0.118	0.000	0.000	0.000	0.946	0.195	0.000	0.000	0.000	0.958	0.111	0.000	0.000	0.000	0.900
total	15.491	4.000	16.030	15.997	7.000	15.648	4.000	16.030	16.000	7.002	15.613	16.003	15.990	4.027	7.042
XFe	0.20	0.14	0.45	0.56	0.17	0.23	0.14	0.52	0.53	0.14	0.21	0.81	0.45	0.22	0.25
Alm			37.9	44.0				40.6	38.7			55.7	38.4		
Andr			0.0	0.2				0.0	0.7			0.0	0.0		
Grs			15.0	20.8				21.1	25.3			25.0	12.9		
Prp			46.1	34.0				37.4	34.2			13.4	47.6		
Sps			1.0	0.9				0.9	0.9			5.8	1.1		
Uv			0.0	0.0				0.0	0.3			0.0	0.0		

Structural formulae on the basis of: Amp = 23 oxygens; Cpx = 6 oxygens; Grt = 24 oxygens; Phe = 11 oxygens.Fe^{3+} calculated by stoichiometric charge balance.

Tab. 1.1 continued.

sample	Z 139-7	Z 139-7	Z 143-8	Z 143-8	Z 249-6	Z 249-6
mineral	Cpx	Grt	Cpx	Grt	Cpx	Grt
analysis	pyx1p4	grt1p5b	omp2.6	grt1.2	pyx7p1	grx1.94
used for	gc	gc	gc	gc	gc	gc
SiO_2	56.52	38.47	56.30	39.53	56.47	39.01
TiO_2	0.03	0.00	0.05	0.00	0.12	0.00
Al_2O_3	10.18	21.26	11.03	22.24	9.69	22.14
Cr_2O_3	0.00	0.00	0.00	0.00	0.01	0.00
FeO	4.50	25.85	2.01	21.84	5.14	23.90
Fe_2O_3	1.86	0.79	1.39	0.57	—	0.61
MgO	7.86	3.98	8.96	8.99	8.84	6.73
MnO	0.01	0.57	0.04	0.26	0.03	0.23
CaO	12.37	9.74	13.43	7.14	14.22	8.21
Na_2O	7.17	0.00	6.93	0.00	6.53	0.00
K_2O	0.00	0.00	0.00	0.00	0.01	0.00
Total	100.50	100.66	100.14	100.56	101.06	100.83
Si	2.008	6.000	1.988	5.984	1.992	5.969
Al^{IV}	0.000	0.000	0.012	0.000	0.008	0.000
Al	0.426	3.908	0.447	3.968	0.395	3.993
Ti	0.001	0.000	0.001	0.000	0.003	0.000
Cr	0.000	0.000	0.000	0.000	0.000	0.000
Fe^{2+}	0.134	3.372	0.059	2.764	0.099	3.059
Fe^{3+}	0.050	0.093	0.037	0.065	0.053	0.070
Mg	0.416	0.925	0.472	2.029	0.465	1.535
Mn	0.000	0.075	0.001	0.033	0.001	0.029
Ca	0.471	1.628	0.508	1.158	0.537	1.346
Na	0.494	0.000	0.474	0.000	0.447	0.000
K	0.000	0.000	0.000	0.000	0.000	0.000
total	4.000	16.000	4.000	16.000	4.000	16.000
XFe	0.24	0.78	0.11	0.58	0.18	0.67
Alm		56.2		46.2		51.2
Andr		2.3		1.6		1.8
Grs		24.8		17.7		20.8
Prp		15.4		33.9		25.7
Sps		1.3		0.5		0.5
Uv		0.0		0.0		0.0

give peak metamorphic temperatures of 590–750 °C at minimum pressures of 20 kbar (Tab. 1.2).

All of the high-pressure rocks show evidence for a retrograde overprint at P-T conditions transitional between eclogite and amphibolite facies, resulting in a Grt + Ky + Amp + Qtz ± Pl retrograde mineral assemblage. Retrograde temperatures estimated using the garnet-amphibole thermometer of Graham & Powell (1984) give 670 ±60 °C. Some of the kyanites are rimmed by albitic plagioclase, indicating a pressure drop into the albite stability field. Pressures estimated from the breakdown of peak stage omphacite (Jd_{45-50}) into a symplectite of low-Na omphacite (Jd_{30}) and albite in equilibrium with quartz are ca. 12 kbar (Fig. 1.2). The combination of mineral zoning, textural features, and P-T estimates allows the reconstruction of a clockwise P-T path, which shows that these medium-temperature eclogites were subducted to great depth at a low geothermal gradient of ca. 8 °C/km (Fig. 1.2).

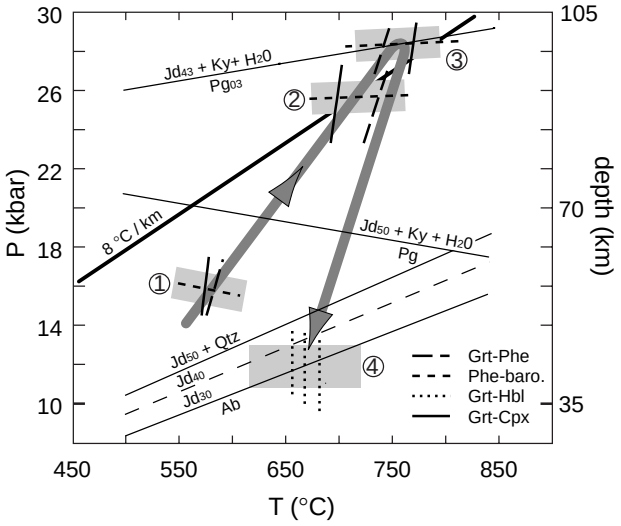

Fig. 1.2 P-T diagram with reaction curves limiting peak-metamorphic conditions and P-T path derived from petrographic observations and thermobarometric results. Shaded boxes indicate pressure and temperature uncertainties for prograde, peak, and retrograde metamorphic stages. (1) Z 101-11a: Grt_{core}-Omp_{core}-Phe_{incl}; (2) Z 101-5: Grt_{rim}-Omp_{rim}-Phe_{matrix}; (3) Z 101-7: Grt_{rim}-Omp_{rim}-Phe_{matrix}; (4) Z 101-5,7,11a: Grt-Amp.

Tab. 1.2 Results of thermobarometric calculations. The applied thermometers and barometers are quoted in the text.

	thermometry [°C]			barometry [kbar]		
sample	Grt - Hbl ± 50	Grt - Cpx ± 25	Grt - Phe ± 25	Phe ± 2.5	Pg#	Remarks
Z 101-5	670	700	735	25.6	—	*; Grt-Hbl only $Fe^{2+} = Fe^{tot}$
Z 101-7	680	770	740	28.3	—	*; Grt-Hbl only $Fe^{2+} = Fe^{tot}$
Z 101-11	655	575	580	15.8	—	all calculations with $Fe^{2+} = Fe^{tot}$
Z 139-7	—	630	—	—	c. 19.7	min T, min P
Z 143-8	—	585	—	—	c. 19.4	min T, min P
Z 249-6	—	640	—	—	c. 20	min T, min P

Paragonite breakdown to Jd_{50} + Ky + H_2O

* Peak-pressures are 1.5 kbar (Z 101-5) and 0.5 kbar (Z 101-7) lower applying the barometer version 1996. (unpubl.- www.earth.ox.ac.uk/~davewa/research/ecbarcal.html)

1.6 Geochemistry

Representative samples were selected for geochemical analysis (Tabs. 1.3, 1.4) to determine the tectonic setting in which the basic rocks were generated (Fig. 1.1). Variations in MgO versus FeO^T (FeO as Fe-total) and TiO_2 reveal typical tholeiitic differentiation trends with Fe- and Ti-enrichment in the early stages of fractionation. Tholeiitic basalts are generated in the upper mantle at different settings, including oceanic spreading axes and island arcs, as well as mantle plumes, which lead to intraplate basalts and continental flood basalts. The metamorphic evolution of the eclogites and the alteration of the unmetamorphosed gabbros suggest interaction with fluids. Thus, only fluid-immobile trace elements can be used for the identification of the tectonic setting (e.g., rare-earth elements, Nb, Zr). The chondrite-normalized rare-earth element (REE) patterns of the samples display MORB-like depletions of the light REE, with heavy REE concentrations that vary from 7 to 20 times chondrite (Fig. 1.3a). The eclogites, gabbros, and metagabbros do not show the strong Nb depletion relative to La that is typical of subduction-related magmas and the bulk continental crust (Figs. 1.3b, 1.4). Island arc basalts (occurring in oceanic and continental arc settings) can be highly depleted in incompatible elements, but have low Nb/La at relatively high $(La/Sm)_N$ ratios due to a subducted slab component (e.g., Hawkesworth

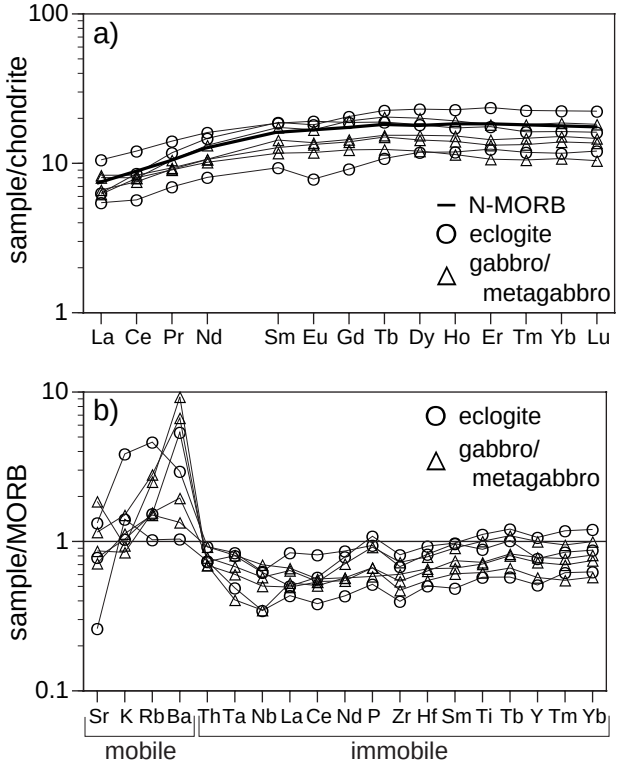

Fig. 1.3 a) REE variation plot, normalized to chondrite (Boynton, 1984) for eclogites, gabbros and, metagabbros, showing their relationship to average mid-ocean ridge basalt (N-MORB). b) Trace element variation plot, normalized to MORB (Hofmann, 1988). Mobility of the trace elements in a fluid phase is indicated.

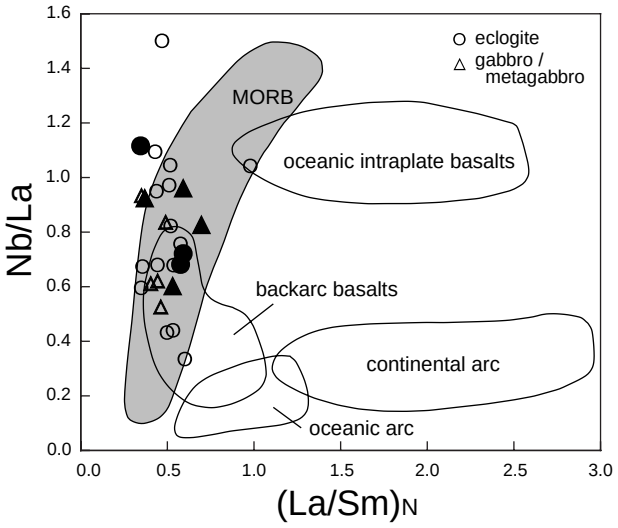

Fig. 1.4 Plot of $(La/Sm)_N$ vs. Nb/La, showing that the origin of the basic rocks of central Zambia is related to a mid-ocean ridge environment. Samples from Fig. 1.3 are indicated by filled symbols. The data used are OIB: Mauna Kea (Frey et al., 1991), continental arc: Andes (Hickey et al., 1986), oceanic arc: Tonga-Kermadec (Turner et al., 1997) back-arc basalts: Lau Basin (Pearce et al., 1995), MORB: Pacific and North Atlantic MORB (Wendt et al., 1999; Hanan et al., 2000).

Tab. 1.3 Complete geochemical data of eclogites (e) and gabbros/metagabbros (g). Ox: wt.%.; trace elements: ppm

sample	Z 142-2	Z 144-2	Z 146-6	Z 201-1	Z 203-9	Z 205-1	Z 249-12
rock-type	e	e	e	g	g	g	g
SiO_2	48.25	48.09	49.81	48.00	47.51	48.71	49.40
Al_2O_3	13.17	14.10	15.22	15.12	13.67	14.16	13.11
TiO_2	1.80	1.43	0.93	1.14	1.62	1.00	1.17
Fe_2O_3	15.32	13.61	10.28	11.91	13.56	10.91	13.87
MnO	0.40	0.28	0.11	0.28	0.25	0.16	0.21
MgO	6.87	7.42	8.81	7.53	7.20	8.61	7.11
CaO	11.35	11.88	12.78	11.85	11.57	12.55	11.02
Na_2O	2.40	2.76	3.05	2.75	3.29	2.31	2.64
K_2O	0.11	0.41	0.15	0.10	0.16	0.09	0.12
P_2O_5	0.13	0.11	0.06	0.07	0.11	0.08	0.08
LOI	0.74	0.57	0.53	N.D.	N.D.	N.D.	N.D.
total	100.54	100.66	101.73	98.75	98.94	98.58	98.73
Mg#	0.34	0.39	0.50	0.42	0.38	0.48	0.37
K	913	3404	1245	830	1328	747	996
P	732	637	349	394	620	451	451
Ti	10791	8573	5575	6834	9712	5995	7014
Rb	1.93	5.83	1.29	3.16	3.54	1.97	1.90
Sr	88.4	150.5	29.5	209.9	130.6	97.8	80.8
Y	38.1	27.5	18.3	26.0	35.8	20.5	28.0
Zr	84.9	70.7	41.4	62.8	75.7	49.2	56.4
Nb	2.17	2.21	1.21	1.22	1.76	2.02	2.45
Cs	0.05	0.31	0.07	0.08	0.04	0.10	0.01
Ba	74.5	40.8	14.4	128.8	93.0	27.1	18.6
La	1.96	3.27	1.69	2.06	1.93	2.49	2.58
Ce	6.90	9.76	4.60	6.08	6.42	6.47	6.73
Pr	1.44	1.72	0.85	1.11	1.28	1.10	1.14
Nd	8.81	9.64	4.83	6.37	7.92	6.10	6.39
Sm	3.66	3.63	1.82	2.49	3.39	2.28	2.79
Eu	1.33	1.41	0.58	0.98	1.23	0.87	1.01
Gd	5.32	4.86	2.37	3.60	4.97	3.19	3.74
Tb	1.07	0.90	0.51	0.71	0.97	0.59	0.73
Dy	7.42	5.84	3.81	4.62	6.46	3.89	4.96
Ho	1.64	1.24	0.85	1.01	1.38	0.82	1.10
Er	4.96	3.70	2.61	2.78	3.81	2.24	3.02
Tm	0.73	0.53	0.38	0.43	0.59	0.34	0.48
Yb	4.69	3.41	2.44	2.91	3.89	2.25	3.16
Lu	0.72	0.52	0.39	0.44	0.59	0.34	0.47
Hf	2.77	2.44	1.50	1.95	2.35	1.63	1.89
Ta	0.15	0.16	0.09	0.08	0.12	0.13	0.16
Pb	1.06	2.34	0.74	3.05	0.89	1.18	0.76
Th	0.14	0.17	0.14	0.13	0.13	0.15	0.17
U	0.06	0.42	0.05	0.03	0.04	0.04	0.05

N.D. = not determined

Tab. 1.4 $(La/Sm)_N$ and Nb/La ratios of the Zambesi Belt samples; e=eclogite; g=gabbro/metagabbros.

sample		$(La/Sm)_N$	Nb/La
Z 101-7	e	0.498	0.429
Z 138-1	e	0.345	0.671
Z 138-3	e	0.430	0.947
Z 138-5	e	0.352	0.594
Z 138-10	g	0.417	0.611
Z 139-7	e	0.460	1.497
Z 140-1	g	0.391	0.600
Z 140-5	e	0.592	0.331
Z 142-1	e	0.527	0.675
Z 142-2	e	0.337	1.110
Z 143-8	e	0.508	1.041
Z 144-1	e	0.510	0.819
Z 144-2	e	0.567	0.675
Z 146-1	e	0.502	0.968
Z 146-6	e	0.583	0.715
Z 147-3	e	0.567	0.754
Z 200-2	g	0.480	0.831
Z 201-1	g	0.521	0.591
Z 203-1	g	0.334	0.926
Z 203-9	g	0.358	0.914
Z 205-1	g	0.686	0.812
Z 206-9	e	0.970	1.039
Z 210-1	g	0.453	0.517
Z 216-1	e	0.507	0.436
Z 216-9	e	0.434	0.676
Z 249-1	e	0.422	1.041
Z 249-12	g	0.581	0.949

et al., 1993). In contrast, continental flood basalts are generally enriched in light REE, a feature that is attributed to enriched mantle sources or crustal contamination (e.g., Carlson, 1991) and would plot in the $(La/Sm)_N$ >1 part of figure 1.4. In addition, oceanic intraplate basalts form from enriched mantle plume sources and generally have $(La/Sm)_N$ >1 (Fig. 1.4). The eclogites and gabbros of the Zambesi Belt, however, display a large range of Nb/La but generally have low $(La/Sm)_N$; these characteristics strongly resemble those of average MORB (Figs. 1.3b, 1.4). Furthermore, these rocks show no evidence of contamination by enriched continental crustal material. The variations in incompatible element

Tab. 1.5 Sm-Nd data.

Sample		Sm (ppm)	Nd (ppm)	$^{147}Sm/^{144}Nd$	$^{143}Nd/^{144}Nd$ (now)	εNd (now)	$^{143}Nd/^{144}Nd$ (720 Ma)	εNd (720 Ma)
Gabbros and Metagabbros								
Z 201-1*	wr	2.18	5.74	0.2296	0.513175 (11)	+10.5	0.512091	+7.5
Z 203-9*	wr	3.01	7.16	0.2546	0.513292 (10)	+12.8	0.512090	+7.4
Z 205-1	wr	2.01	5.54	0.2196	0.513150 (8)	+10.0	0.512114	+7.9
Z 249-12†	wr	N.D.§	5.50	N.D.	0.513216 (8)	+11.3	N.D.	N.D.
Ky-bearing Eclogites								
Z 143-8	wr	0.809	2.14	0.2283	0.513076 (8)	+ 8.5	0.511998	+5.6
	grt	0.0128	0.0180	0.4280	0.513911 (75)	+24.8	N.A.#	N.A.
Z 309-5	wr	1.29	3.04	0.2563	0.513305 (5)	+13.0	0.512095	+7.5
	grt**	0.225	0.153	0.8880	0.515766 (19)	+61.0	N.A.	N.A.
Other Eclogites								
Z 142-2	wr	3.36	8.43	0.2407	0.513241 (7)	+11.8	0.512105	+7.7
Z 144-2	wr	3.27	8.88	0.2225	0.513123 (9)	+ 9.5	0.512073	+7.1
Z 146-6	wr	1.61	4.48	0.2165	0.513115 (10)	+ 9.3	0.512093	+7.5

Note: Garnet separates were prepared at Universität Kiel and Universität Münster using a steel jaw crusher, magnetic separator, and hand picking. To remove surface contamination, garnets were washed for 10 minutes in cold 1M HCl, then rinsed with distilled water. All samples were spiked with a mixed ^{149}Sm-^{150}Nd tracer before being digested with HF-HNO_3-$HClO_4$ in bombs at 180°C. Sm and Nd data were measured on a VG Sector 54 TIMS at the Zentrallabor für Geochronologie in Münster. Nd isotope ratios were normalized to $^{146}Nd/^{144}Nd = 0.7219$. The mean $^{143}Nd/^{144}Nd$ of the La-Jolla Nd standard was 0.511858 during this study; no correction for instrumental bias has been applied here. Procedural blanks for Nd and Sm were less than 200 pg and 50 pg, respectively. Chondritic uniform reservoir (CHUR) parameters used for calculating ε_{Nd} values are $^{143}Nd/^{144}Nd = 0.512638$, $^{147}Sm/^{144}Nd = 0.1967$.

*Garnet-bearing gabbros.

†Amphibole-bearing gabbro.

§N.D. = not determined.

#N.A. = not applicable.

**Impure garnet separate.

contents are within the range of basaltic rocks produced by various crystal fractionation processes or different extents of partial melting (Fig. 1.3). The range in present-day Nd isotope compositions (Tab. 1.5) of the eclogites (ε_{Nd} = +8.5 to +13.0, n = 5) overlaps that of the gabbros and metagabbros (ε_{Nd} = +10.0 to +12.8, n = 4). All samples scatter closely around a 720 Ma Sm-Nd reference line (n = 7, Z 143-8 excluded, M.S.W.D = 1.1). At that time, their ε_{Nd} values only ranged from +7.1 to +7.9 (+5.6 for Z 143-8), consistent with their derivation from a relatively homogeneous, long-term depleted mantle source during the Neoproterozoic.

We conclude that the source of the magmas of the Zambesi Belt samples was depleted upper mantle and that no chemical interaction with continental crust occurred. Thus, the eclogites and gabbros preserve typical geochemical signatures of rocks that were formed in a mid-ocean ridge or a back-arc spreading environment.

1.7 Geochronology

To constrain the timing of eclogite facies metamorphism, Sm-Nd data were also acquired for garnets from two of the eclogites (Tab. 1.5). The garnet-whole rock (Grt-wr) isochron for sample Z 309-5 yielded an age of 595 ±10 Ma. Due to the very low REE concentrations in the Z 143-8 garnet, the measured Grt-wr age for that sample, 638 ±61 Ma, is imprecise. Nevertheless, the two ages agree within error and place the eclogite facies metamorphism in the Pan-African orogenic cycle and thus with

the Zambesi Belt orogen (Fig. 1.5). Neither petrologic nor isotopic indications for an older, Mesoproterozoic metamorphism were found. Instead, these ages support the earlier suggestions of Vrana et al. (1975) that the eclogites have a Pan-African origin.

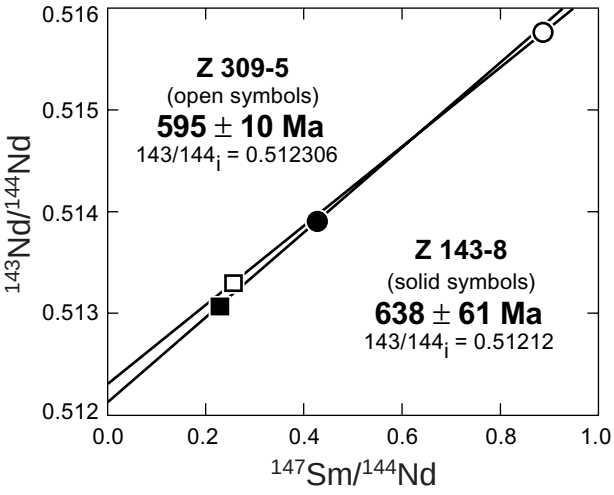

Fig. 1.5 Sm-Nd isochrons for Zambian eclogites. Symbols: solid = Z 143-8, open = Z 309-5, squares = whole rocks, circles = garnets. Errors in $^{147}Sm/^{144}Nd$ and $^{143}Nd/^{144}Nd$ used in the regressions are the larger of external reproducibility (i.e., 0.5%, and 0.5 ε-units, respectively) or 2 s.e. in-run statistics. Age errors are reported at the 2 s.d. level.

1.8 Conclusions

The medium-temperature eclogites studied here represent parts of Neoproterozoic oceanic crust that were subducted to a depth of ca. 90 km. The gabbros and metagabbros have geochemical features that are similar to those of the eclogites, indicating that they also formed in an oceanic setting. However, they were either not subducted to great depth, or they survived subduction within an undeformed, anhydrous environment (e.g., Hacker, 1996). The 90 km subduction depth, as well as the low geothermal gradient of ca. 8 °C/km implied by the eclogite facies conditions, suggest a tectonothermal evolution similar to those of cold Phanerozoic subduction zones. Assuming a fast convergence rate, the thermal evidence in turn requires subduction of oceanic crust that was at least 30 Myr old (Cloos, 1993), implying the existence of a relatively large ocean basin between the Kalahari and the Congo cratons. The age of the eclogite facies metamorphism, and therefore the timing of subduction, is constrained by Grt-wr Sm-Nd ages of 595 ±10 Ma and 638 ±61 Ma.

Taken together, these results have major consequences for the reconstruction of Gondwana and support the interpretations of Meert et al. (1995) and Porada & Berhorst (2000). On the basis of paleomagnetic studies, Meert et al. (1995) suggested that the Damara-Zambesi Belt may represent a closed ocean basin. Porada & Berhorst (2000) concluded that a passive continental margin at the northern boundary of the Lufilian-Zambesi basin was formed during rifting which began at ca. 880 Ma during Rodinia dispersal. Other possible remnants of oceanic crust between the Congo and the Kalahari cratons are located in Namibia (Barnes & Sawyer, 1980) and Zimbabwe (Oliver et al. 1998; Johnson & Oliver, 2000), and these are assumed to be of Neoproterozoic and Mesoproterozoic age. Since these rocks were not formed during the same orogenic cycle, the possibility arises that ocean basins may have existed at different times in south central Africa. However, we conclude that the suture zone in the Zambesi Belt represents the site of a subducted Neoproterozoic ocean that may have connected the Moçambique Ocean in the north with the Adamastor Ocean in the south (e.g., Coward & Daly, 1984). Furthermore, considering the timing of initial rifting, this ocean might have been formed during the dispersal of Rodinia and closed during the assembly of Gondwana. The evolution of the Zambesi Belt could thus represent a complete Wilson cycle.

CHAPTER TWO

Partial eclogitisation of gabbroic rocks in a late Precambrian subduction zone (Zambia): prograde metamorphism triggered by fluid infiltration

2.1 Abstract

Gabbros and eclogites occur closely associated in a 200-km long and up to 40-km wide area of the Zambesi Belt in central Zambia. This area is interpreted to represent part of a late Precambrian suture zone, with the mafic rocks being relics of the subducted crust. Gradual stages of prograde transformation from gabbro to eclogite are preserved by incomplete reactions and disequilibrium textures. Undeformed eclogites typically preserved features of the former gabbroic texture, reflected by replacements of plagioclase and pyroxene through eclogite facies minerals. Textures of deformed eclogites range from sheared porphyroclastic to porphyroblastic. Relics of magmatic pyroxene are common and complete eclogitisation occurred only in mm- to cm-scale domains in most of the deformed and undeformed rocks. No evidence for prograde blueschist or amphibolite facies mineral assemblages was found in eclogites. In contrast, the fine grained intergrowth of omphacite, garnet, kyanite and quartz which replace former plagioclase or was formed in the pressure shadow of magmatic pyroxene relics, indicates that eclogitisation might have affected the gabbroic protoliths directly without any significant intervening metamorphic reactions. Eclogitisation took place at P-T conditions of 605-665 °C and 26-28 kbar and was accompanied by a channelised fluid flow resulting in veins with large, subhedral grains of omphacite, kyanite and garnet. Growth zonings of the vein-omphacites and coexisting garnets, indicate a simultaneous increase in pressure and temperature during vein formation. The gabbro-to-eclogite transformation was enhanced by a fluid allowing the nessacary material transport for the dissolution-precipitation mechanism that characterizes the mineral replacements during metamorphism. The eclogitisation process was limited by reaction kinetics and dissolution-precipitation rates rather than by the metamorphic P-T conditions. Even though deformation occurred and mineral reaction boundaries were overstepped, the infiltration of fluids was necessary for triggering the gabbro-to-eclogite transformation.

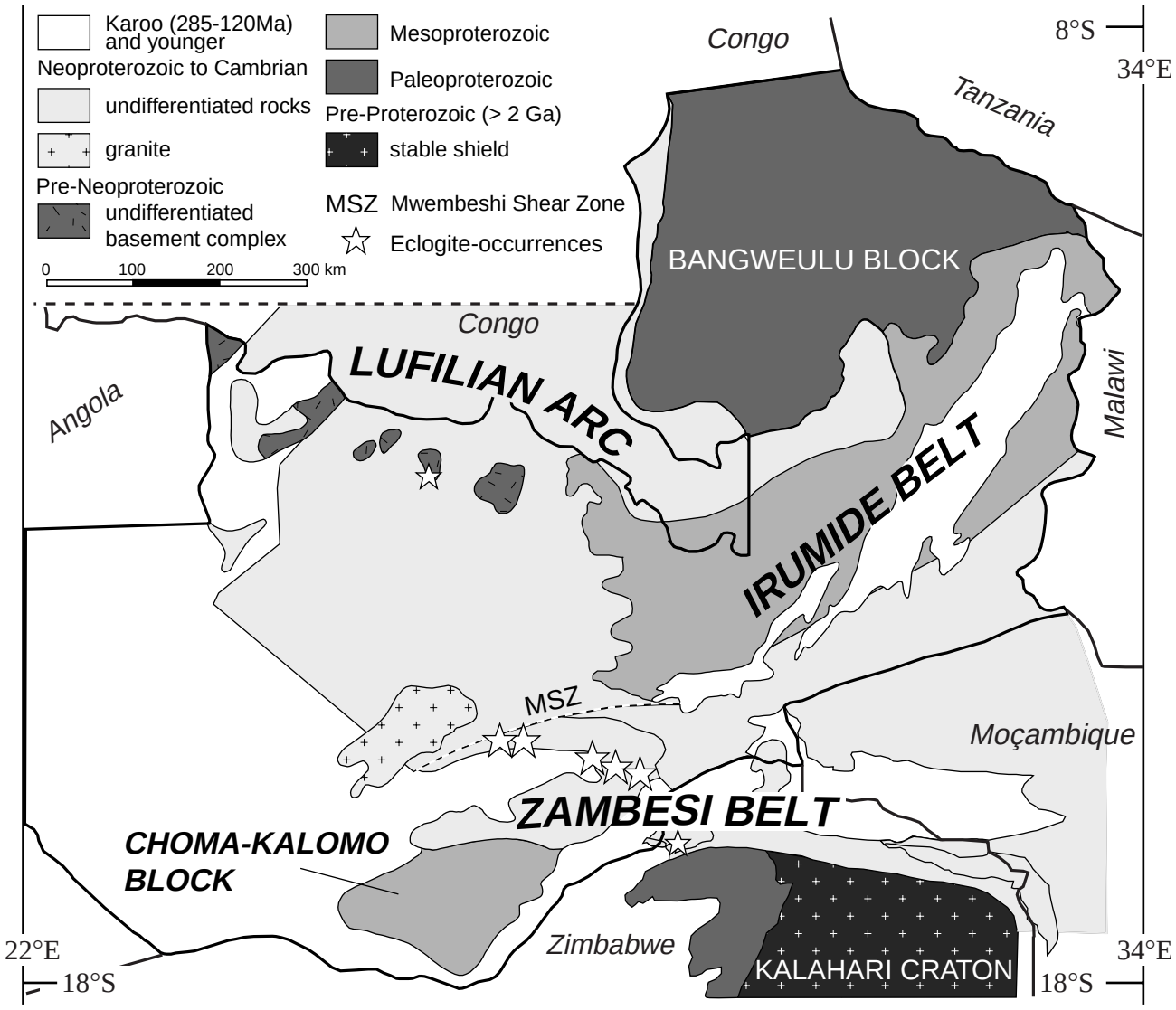

Fig. 2.1 Geological map (after Sikatali et al, 1994; Hanson et al., 1994) showing structural provinces of Zambia and northern Zimbabwe. The northern margin of the Kalahari craton is shown while the southern margin of the Congo craton is north of this figure. Political borders have thick lines, while geological boundaries have thin lines. The eclogite-bearing zone is indicated by the white stars, two other eclogite occurrences (single outcrops) are indicated by the small stars (see text).

2.2 Introduction

Precambrian eclogites are rare rocks (e.g., Sanders et al., 1984; Möller et al., 1995; Jahn, et al., 2001), which results in a poor knowledge of processes in subduction zones for this time interval. However, central Zambia exhibits the largest number of Precambrian eclogite occurrences in Africa (Vrana et al., 1975) and consequently offers a unique opportunity to study Precambrian eclogite metamorphism. In addition to the outcrops studied here, two futher eclogite localities exist in this region, one in northern Zambia (Cosi et al., 1992) and one in northern Zimbabwe (Dirks and Sithole, 1999). Both could be

related to the main central Zambian occurrence, because they are situated within the same Pan-African orogenic belt. The central Zambian eclogites and the associated gabbros (Fig. 2.1) are interpreted as relics of a fossil subducted slab, marking the suture zone between the Congo craton to the north and the Kalahari craton to the south (chapter one). Disequilibrium textures, incomplete reactions, and metastabilities due to sluggish nucleation and/or low diffusion and reaction kinetic rates are commonly observed in low-T / high-P environments (Mørk, 1985 a, b; Koons et al., 1987; Wayte et al., 1989; Rubie, 1998). Within dry, coarse-grained rocks, high-pressure mineral assemblages are sometimes formed only within fluid veins or in deformed domains. In such rocks, low-pressure minerals can persist metastably at conditions well above their equilibrium boundaries if no catalyst triggers metamorphic reactions (e.g., Åustrheim, 1986/87; Hacker, 1996; Rubie, 1998). With respect to the Zambian eclogites, Vrana et al. (1975) already suggested that in addition to the P-T conditions, the fluid pressure and fluid composition, as well as the permeability of the rocks, were all crucial factors that controlled the transformation of gabbroic protoliths into the eclogites. Assuming that the Zambian eclogites and gabbros are co-genetic and both belonged to the same subducted oceanic lithosphere (chapter one), these rocks provide an exceptional opportunity to study the fate of subducting gabbroic rocks. This paper describes the Precambrian eclogites and gabbros of central Zambia and the transformation processes by which the gabbroic protoliths were eclogitised. These processes are predominantly fluid controlled dissolution, transport and precipitation. Using textural and mineral chemical data, we document the importance of a fluid phase as a catalyst for eclogitisation even in rocks which were deformed during metamorphism.

2.3 Geological setting

The Precambrian orogenic systems of Zambia consist of two major mobile belts (Fig. 2.1): (1) the Mesoproterozoic NE–SW striking Irumide Belt and Choma-Kalomo Block and (2) the Neoproterozoic to Cambrian Lufilian Arc and Zambesi Belt which are elongated in E-W direction. The Irumide Belt formed during the assembly of Rodinia in the large time-interval between 1.0–1.4 Ga (e.g., Cahen et al., 1984; Hanson et al., 1988, Porada & Berhorst, 2000), with the peak of ultra-high temperature metamorphism occurring at ca. 1.05 Ga (Schenk & Appel, 2001). Neither evidence for high-pressure / low-temperature metamorphism nor for metamorphic conditions above ~7 kbar has been found in the Irumide Belt.
The Zambesi Belt and the Lufilian Arc are part of a Pan-African orogenic system that crosscuts southern Africa, separating the Congo and Kalahari Cratons and their respective Paleo- and Mesoproterozoic units. The evolution of these Pan-African belts is related to the assembly of the Gondwana supercontinent. Eclogite facies metamorphism occurred at ca. 600 Ma (chapter one), whereas peak metamorphism during the subsequent continental collision occurred between 550-525 Ma, with metamorphic P-T conditions reaching the high-pressure amphibolite facies (Goscombe et al., 1998; 2000; Vinyu et al., 1999; Johnson & Oliver, 2001; chapter three). The Zambesi Belt divides the Mesoproterozoic units of Zambia into the Irumide Belt and the Choma-Kalomo Block (Fig. 2.1). The junction of the Neoproterozoic belts and the Mesoproterozoic units is marked by a 200-km long and up to 40-km wide zone containing lenses of Ky-eclogites, metagabbros, gabbros, and rare ultramafic rocks (Fig. 2.2). This eclogite-bearing zone is located in the central part of the Zambesi Belt and is oriented parallel to its strike. The eclogites and associated basic rocks form isolated hills of ten to a hundred

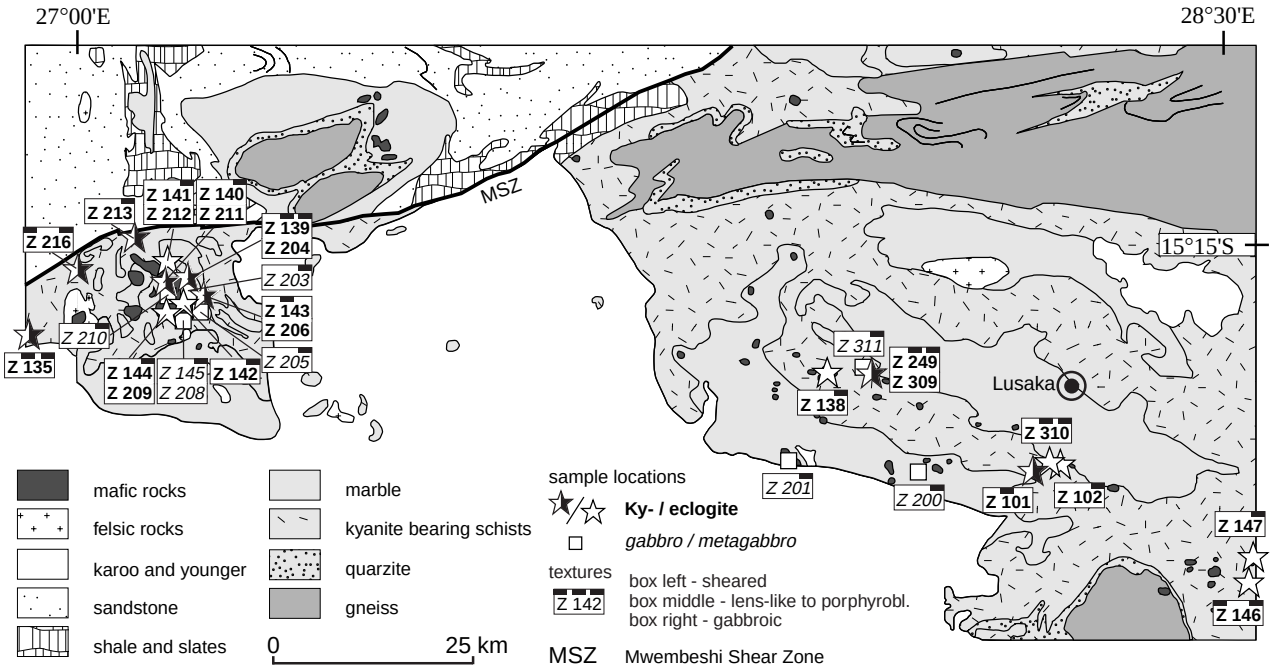

Fig. 2.2 Enlarged and simplified geological map of central Zambia after Thieme (1984) showing the sample locations. Eclogite occurrences are indicated by stars (half black stars = Ky-bearing) and bold sample numbers; gabbro occurrences are indicated by squares and italic sample numbers. The black boxes at the top of the sample-labels indicate the observed textures in samples from this locality (see legend).

metres in diameter. Neither contacts with the country rocks nor between the eclogites and the other basic rocks are exposed. The country rocks consist mainly of kyanite-bearing metapelites, metapsammites, and marbles (Fig. 2.2). Due to the strong weathering of metapelitic outcrops, useful petrological information about their metamorphic evolution is not preserved. The less altered marbles contain rare calcsilicate bands which lack critical mineral assemblages that could be used to determine the metamorphic evolution of this area. According to the tectonic model of Porada & Berhorst (2000), the basic rocks of the Lufilian Arc-Zambesi Belt were incorporated into the platform and shelf sediments of the northern, i.e., the lower plate during collisional overthrusting and backthrusting. This might explain the occurrence of isolated basic blocks within the sedimentary country rocks. Porada & Berhorst (2000) proposed that during rifting, which is assumed to have started ca. 880 Ma ago, a passive continental margin was formed at the southern edge of the Congo craton. The authors pointed out, that their depositional and tectonic model for the Lufilian Arc and northern Zambesi Belt requires the opening and closure of a major ocean. However, a geochemical study of gabbros and metagabbros from the Lufilian Arc suggested that the rifting probably did not significantly overstep an intracontinental stage (Tembo et al., 1999). In contrast, geochemical and P-T data of gabbros and eclogites from central Zambia which are considered here, imply that the parental magmas of these rocks were formed at an oceanic spreading centre, and consequently it is argued that these rocks are relics of a subducted oceanic crust (chapter one).

2.4 Petrology

Eclogites were found at 16 of 23 investigated outcrops of basic rocks, nine of which include Ky-bearing eclogites (Fig. 2.2). At 12 of the 23 localities amphibolites, Grt-amphibolites and gabbros occur (Tab. 2.1). Even when eclogites and gabbros occur together in a single outcrop, contacts between them were not found. A typical feature of most of the Zambian eclogites is that they usually contain only small domains in which the complete transformation to eclogite occurred. Partially eclogitised rocks with disequilibrium textures are more common.

Tab. 2.1 Textures and rock types of investigated basic rocks. Localities are shown in Fig. 2.2.

textures of eclogites			non-eclogites
ophitic (Group 1)	porph.-banded (Group 2)	mylonitic (Group 3)	gabbro metagabbro
Z 102	**Z 101**	Z 146*	Z 145/208
Z 135*	**Z 135***	**Z 216***	Z 200
Z 138 §	**Z 139/204**		Z 201
Z 139/204	**Z 143/206§**		Z 203
Z 140/211	**Z 249§**		Z 205
Z 141/212	**Z 310*§**		Z 311
Z 142 §			
Z 144/209			
Z 146*			
Z 147 §			
Z 213			
Z 216*			
Z 310*§			

bold = Ky-bearing rocks; * = magmatic relics; § = with gabbro/metagabbro

To simplify the description of the studied rocks, all samples that contain an eclogite facies mineral assemblage (i.e., omphacite and garnet), at least in subdomains, are named eclogites in this paper. Retrograde overprinting affected eclogite facies assemblages to varying, but mostly minor degrees; pervasive amphibolitisation is rare but a late stage scapolitisation is found in many outcrops. The Zambian eclogites can be subdivided into three groups based on their dominant textures: The first group has preserved gabbroic (i.e., igneous) textures, the second group has lens-like to porphyroblastic textures, and the third group has sheared porphyroclastic textures. The textures of the eclogites are highly variable, even at the thin section scale, with many outcrops displaying two of the textural types. The eclogitisation was accompanied by channelised fluid infiltration, which is visible in form of veins with large omphacite, garnet, kyanite and rare epidote crystals. Mineral relics of the magmatic protoliths are restricted to clinopyroxene, plagioclase is not preserved.

2.4.1 Petrography

Group 1: eclogites with gabbroic textures

Eclogites that contain relics of a medium grained gabbroic texture are common, occurring at 13 of the 16 eclogite localities (Fig. 2.2; Tab. 2.1). The former gabbroic texture is reflected by the shape of garnet which replaces plagioclase laths, and omphacite which replaces the magmatic, interstitial clinopyroxene (Fig. 2.3a). Magmatic clinopyroxene relics are common, and in most cases, complete eclogitisation occurred only in mm-scale domains. In some samples a complete eclogitisation occurred only along vein-like fluid paths (Fig. 2.3b). These eclogites contain epidote group minerals, occurring mainly in the matrix, and as rare inclusions in garnet. In this case, the epidote-group minerals, instead of garnet, replace the plagioclase laths, and garnet is only a minor phase. Very fine-grained quartz and kyanite typically occur within the matrix and as inclusions in garnet of the less eclogitised rocks. This kyanite is anhedral or forms tiny needles. The rims of the magmatic clinopyroxene relics are usually strongly affected by omphacite formation, whereas the cores of the grains have almost perfectly preserved magmatic compositions. Former plagioclase laths located close to clinopyroxene relics are pseudomorphically replaced by a fine grained intergrowth of anhedral garnet, omphacite, kyanite, and quartz (Fig. 2.3c).

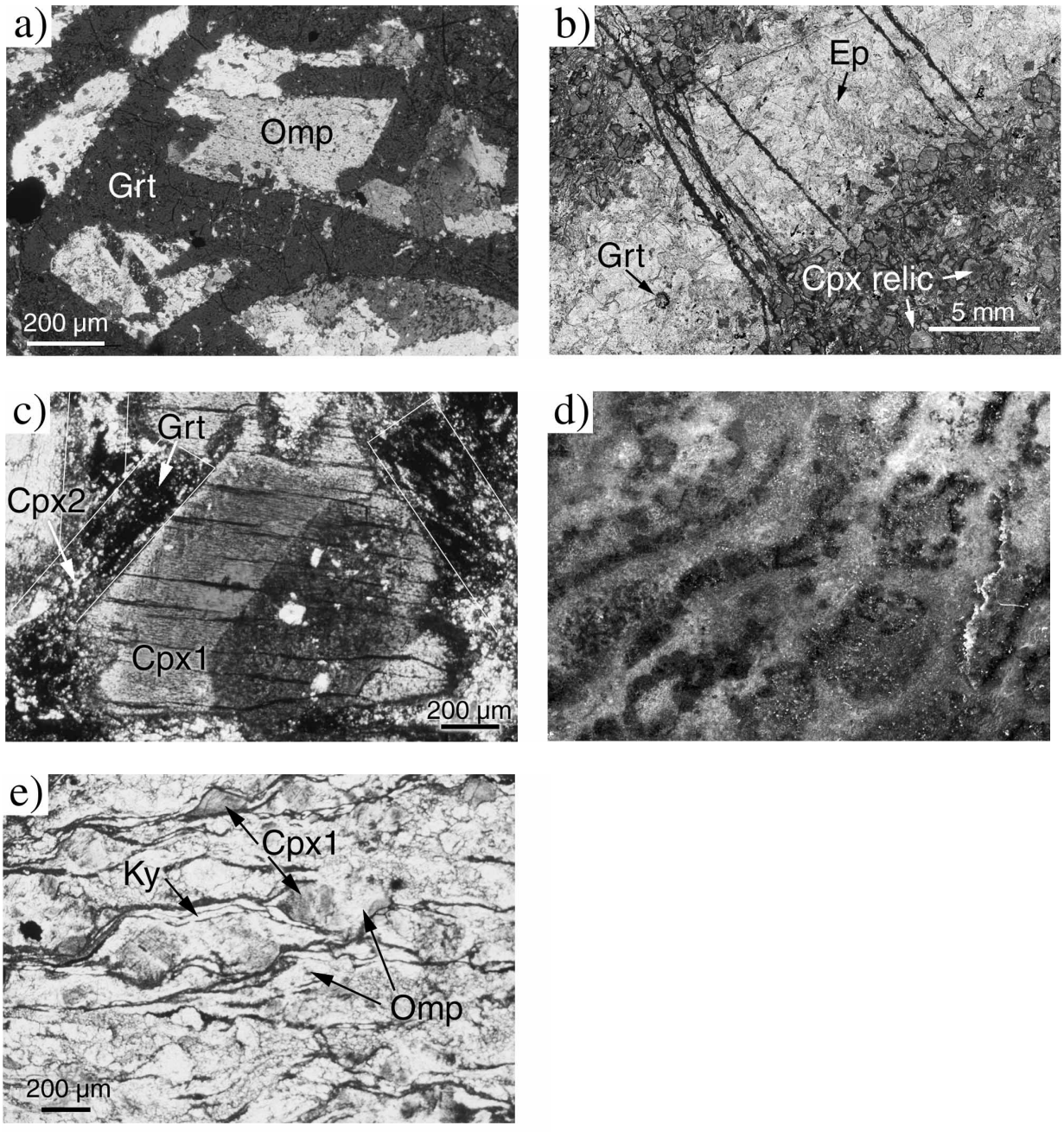

Fig. 2.3 a) Preserved gabbroic texture in an eclogite. Garnet forms pseudomorphs after plagioclase (dark) and omphacite after magmatic pyroxenes (bright). Note lack of strain fabric in the replacement assemblage (Z146-1);
b) A major fluid infiltration vein (bright) in a partially eclogitised rock (Z310-4). The darker region consists of omphacite-garnet-kyanite-quartz symplectites between magmatic clinopyroxene relics. The vein consists of epidote-group minerals (darker grey), omphacite (brighter grey) composed of ca. 10µm subgrains, and rare garnet. Late stage thin vein (dark) of greenschist facies assemblages are cutting the eclogite facies vein;
c) Relic of a magmatic pyroxene (Cpx1) showing preserved magmatic twinning (enlarged from Fig. 2.3b). The bright patches within the crystal is late-stage hornblende. The dark (Grt) and bright (Cpx2) intergrowth that surrounds the magmatic relic is the replacement product of former plagioclases (indicated by white outlines), consisting of fine-grained garnet, omphacite (Cpx2), quartz and kyanite;
d) Lens-like eclogite (Z143-8). Garnet (black) forms lenses within a omphacitic matrix (bright). Field of view ca. 4cm;
e) Sheared porphyroclastic eclogite (Z 216-7). Most omphacite (white) has grown in the pressure shadow of magmatic clinopyroxene relics (Cpx1; dark). Thin bands of kyanite surround these clinopyroxenes porphyroclast.

Group 2: eclogites with lens-like to porphyroblastic textures

Eclogites with lens-like and/or porphyroblastic textures were found at six localities (Fig. 2.2; Tab. 2.1). The textures are combined to one group since a gradual transition between the textures exists. The more segregated parts contain garnet-rich and omphacite-rich domains that sometimes stretch into parallel lenses up to a few cm in length (Fig. 2.3d). Some of the omphacites display an orientation parallel to the lenses. The more porphyroblastic parts are characterised by large (up to 1 cm) garnet porphyroblasts in an omphacite matrix. These garnets are mostly ellipsoidal, and their rims are typically clouded with minute omphacite inclusions. Some garnets form large anhedral porphyroblasts containing several garnet cores. The garnets are in a fine-grained omphacitic matrix with mostly amoeboid grain boundaries. In some domains the omphacite crystals are coarser-grained due to recrystallisation and display equilibrium grain boundaries. Relics of magmatic textures or minerals are not preserved in these group 2 eclogites.

Group 3: sheared porphyroclastic eclogites

Sheared eclogites were found at only two localities (Fig 2.2; Tab. 2.1). Most of these rocks are partially sheared to varying extents, but a strong, pervasive deformation is rare. The eclogites contain porphyroclastic relics of magmatic clinopyroxene (Fig. 2.3e) and as for the eclogites of the group 1, complete eclogitisation occurred only within mm-scale domains. The relics of magmatic clinopyroxenes and the garnets are forming orientated and elongated porphyroclasts in a matrix of very fine grained (ca. 10 µm) omphacite, quartz, and kyanite. The magmatic pyroxene relics have small omphacitic rims which increase in thickness towards the sides where pressure solution occurred. However, the largest amount of omphacite grew within the pressure shadows and the fine grained matrix. Thin, mm-long bands of kyanite follow the foliation and wrap around the clinopyroxene relics (Fig. 2.3e). Garnet typically occurs in these assemblages as subparallel oriented laths and, within the strongly sheared parts, as deformed porphyroclasts.

Eclogitic veins

Eclogitic veins occur in almost all investigated eclogites. They are composed of large (mm-scale) omphacite grains, which are sometimes associated with kyanite, garnet, or apatite (Figs. 2.4a, b). However, some veins consist mostly of garnet, with omphacite only occurring in the centres of these veins (Fig. 2.4c). Other veins contain garnet, omphacite, amphibole, and kyanite. In these veins omphacite and garnet are usually cut and healed several times during multiple opening of the vein (Fig. 2.4d). The veins have randomly distributed orientations (Fig. 2.4e), and in most cases, they crosscut the main fabric. They range in width from less than 1 mm up to more than 1 cm. In rare cases, veins contain epidote group minerals instead of garnet (Fig. 2.3b), associated with very fine grained (ca. 10 µm) omphacite.

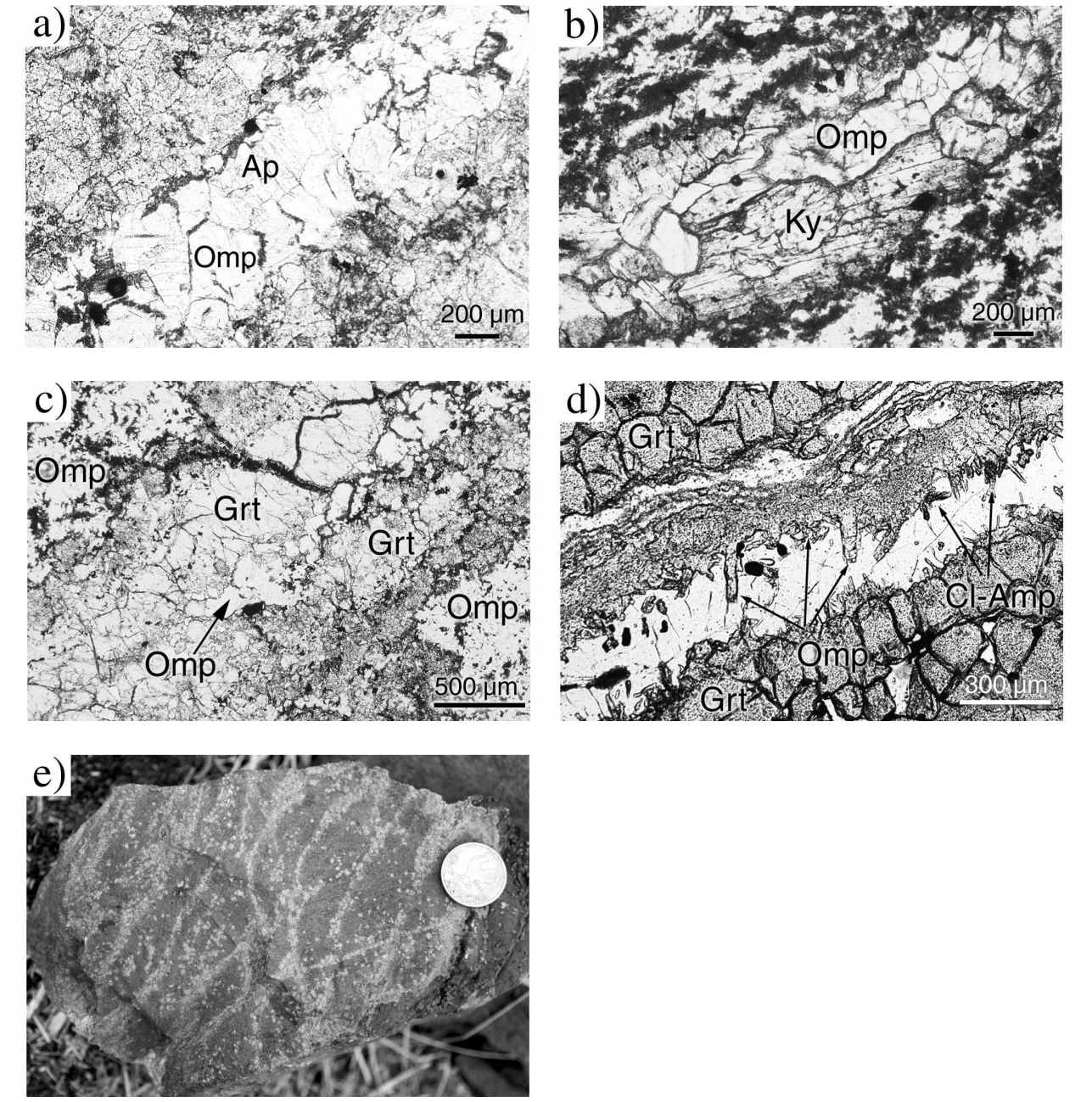

Fig. 2.4 a) Vein in eclogite consisting of large, subhedral omphacite and apatite crystals. The surrounding matrix consists of fine-grained garnet and omphacite replacing the former magmatic texture (Z 146-2);
b) Vein consisting of kyanite and omphacite with preserved growth zoning. The vein follows the fabric of the host eclogite (Z 143-8);
c) Garnet-omphacite vein in a porphyroblastic eclogite (Z 139-3). The vein consists of large omphacites in the centre surrounded by garnet. At the rim of vein, the garnet is clouded with omphacite inclusions (darker grey). The rock matrix consists of omphacite;
d) Vein in a porphyroblastic eclogite (Z 249-6). The vein consists of euhedral omphacites (grey) with preserved growth zoning, potassium-rich Cl-amphiboles (dark), garnet (at the rim), quartz (white), and apatite (not shown);
e) Eclogite crosscut by randomly orientated veins (locality Z 249).

2.4.2 Mineral chemistry and growth history

Elemental analyses of minerals (Tabs. 2.2-2.4) were performed on JEOL 8900 electron microprobes in Kiel and Göttingen, both equipped with five wavelength-dispersive spectrometers (WDS). For mineral analyses, these instruments were typically operated with a 15 kV acceleration voltage and a focussed, 15 nA beam. Sample spot sizes were ca. 1 µm in diameter. Citzaf was used for the matrix correction of the raw counts. Natural mineral and synthetic standards were used for analyses.

To illuminate the formation history of the eclogite facies assemblages, the relevant mineral reactions will be introduced here. Only generalised, non-stoichiometric reactions are given (mineral abbreviations after Kretz, 1983). The plagioclase components convert to eclogite facies phases through reactions of the kind

(1) An ⇒ Grs + Ky + Qtz

(2) An + H_2O ⇒ Czo/Zo + Ky

(3) Ab ⇒ Jd + Qtz.

These result for a near isochemical plagioclase breakdown in (Wayte et al., 1989)

(4) Pl ⇒ Grs + Jd + Ky + Qtz

in a dry system, or

(5) Pl + H_2O ⇒ Czo/Zo + Jd + Ky +Qtz

if H_2O is available.

The augitic clinopyroxene (Cpx1) convert to omphacite through

(6) Aug + Jd ⇒ Omp + $(Ca, Fe, Mg)_2Si_2O_6$

while the excess Ca, Mg, and Fe of the augite were incorporated in garnet and epidote

(7) $(Ca, Mg, Fe^{2+})_2Si_2O_6$ + Ky ⇒ Grs + Pyr + Alm

(8) Ca, Fe^{3+} + Ky + H_2O ⇒ Ep.

During retrograde metamorphism, the eclogites were partially transformed to amphibolite according to a reaction of the type

(9) Omp + Grt + H_2O ⇒ Prg + Pl + Qtz ± Czo/Ep,

while the plagioclase is usually replaced by scapolite.

Garnet

Garnet occurs as ellipsoidal porphyroblasts as well as pseudomorphic laths after plagioclase. Growth zoning, characterized by pyrope-enriched rims with almandine- and sometimes spessartine-rich cores, is preserved

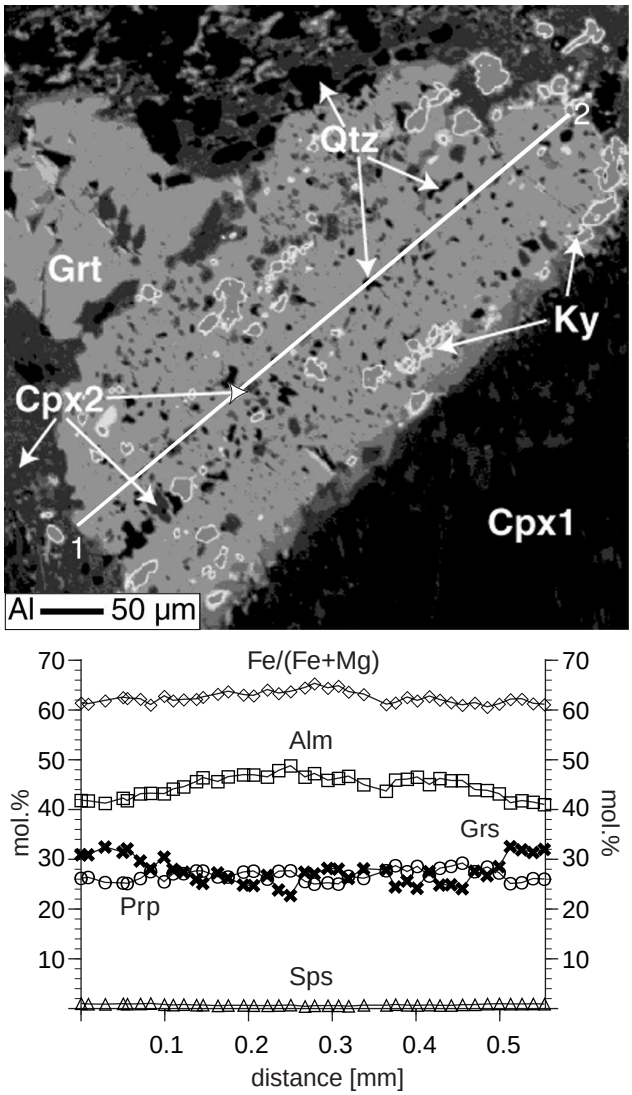

Fig. 2.5 Aluminium element mapping and chemical profile of a garnet which is part of the plagioclase replacement assemblage (see text). The garnet grew next to a magmatic pyroxene relic (Cpx1) and shows a preserved growth zoning (X_{Fe} decreases and Grs-content increases towards the rim). The garnet (light grey) is lath-shaped and is intergrown with quartz (black), omphacite (Cpx2, dark grey) and kyanite (grey with white rim). The intergrowth indicates that the garnet grew under eclogite facies conditions. The magmatic relic (Cpx1) is also shown in Fig. 2.3b.

Tab. 2.2 Representative garnet analyses and structural formulae.

sample	Z 101-5	Z 101-7	Z 135-6	Z 139-3	Z 139-7	Z 143-8	Z 146-1	Z216-5	Z 249-6	Z310-4a
Analyses	grt2.78	grx1.24	grt1-1.5	Grt2.3	grt1.5b	grt1.2	grt2.14	ogo1g.21	grx1.94	grt6.4
Location	rim	rim	rim	rim	rim	rim	rim	rim	rim	rim
SiO_2	39.71	39.63	39.44	38.97	38.47	39.53	38.87	39.17	39.01	39.19
Al_2O_3	22.42	22.31	22.54	22.05	21.26	22.24	21.98	22.00	22.14	22.46
FeO	20.97	18.57	20.28	25.24	26.56	22.35	21.23	21.48	24.45	20.01
MgO	9.06	9.11	9.29	7.58	3.98	8.99	7.41	6.66	6.73	6.70
MnO	0.41	0.40	0.33	0.36	0.57	0.26	0.45	0.42	0.23	0.46
CaO	7.81	9.73	8.62	5.88	9.74	7.14	9.65	10.49	8.21	11.61
Total	100.38	99.75	100.50	100.08	100.58	100.51	99.59	100.22	100.77	100.43
Si	3.000	2.997	2.967	2.999	3.000	2.992	2.982	2.996	2.984	2.980
Al	1.996	1.988	1.999	2.000	1.954	1.984	1.987	1.983	1.996	2.013
Fe^{2+}	1.321	1.156	1.210	1.621	1.686	1.382	1.312	1.350	1.529	1.245
Fe^{3+}	0.004	0.019	0.066	0.003	0.046	0.032	0.050	0.024	0.035	0.028
Mg	1.020	1.027	1.042	0.870	0.463	1.014	0.847	0.759	0.768	0.759
Mn	0.026	0.026	0.021	0.023	0.038	0.016	0.029	0.027	0.015	0.030
Ca	0.632	0.788	0.695	0.485	0.814	0.579	0.793	0.860	0.673	0.946
Total	8.000	8.000	8.000	8.000	8.000	8.000	8.000	8.000	8.000	8.000
Alm*	44	39	42	54	57	47	45	45	52	42
Grs*	21	26	23	16	27	19	26	28	22	31
Prp*	34	34	34	29	15	34	28	25	25	25
Sps	1	1	1	1	1	1	1	1	0	1
Fe^{3+}/Fe^{ToT}	0.003	0.016	0.052	0.002	0.027	0.023	0.037	0.018	0.022	0.022
XFe*	0.56	0.53	0.55	0.65	0.79	0.58	0.62	0.64	0.67	0.63

Structural formulae on a basis of 12 oxygens. Fe^{3+} calculated by stoichiometric charge balance. * Fe^{2+} as Fe^{ToT}.

in almost all samples (Tab. 2.2; Fig. 2.5). The X_{Fe}-value varies from sample to sample (X_{Fe} = 53-78), and generally decreases towards the rims. If garnet is zoned in grossular content, it increases rimwards. The zoning pattern indicates that garnet grew during increasing temperatures and, in cases of a rimward grossular increase, during a simultaneously increase in pressure. Some garnets have numerous inclusions of quartz, kyanite and omphacite. In some cases, garnet is intergrown with omphacite, kyanite, and quartz, replacing former plagioclase laths. This intergrowth (related to reactions (4), (6), and (7)), together with the prograde growth zoning of the garnet indicates that for these rocks, the metamorphic reactions started under eclogite facies conditions (Fig. 2.5). Usually, quartz inclusions are randomly distributed, whereas most kyanite and omphacite inclusions occur in the outer parts of the pseudomorphic garnet-laths. This inclusion pattern points to garnet growth, or at least to continued growth under eclogite facies conditions. Other inclusions are rutile and, rarely, epidote group minerals and phengite. At locality Z 101, a second generation of garnet grew at lower pressure and temperature conditions. This garnet (Grt2) is only slightly zoned with a retrograde zoning at the rim. Grt2 has lower almandine$_{(38-40)}$ and grossular$_{(12-21)}$ and higher pyrope$_{(37-48)}$ components as compared to the rim compositions of prograde garnet (Grt1 = almandine$_{(38-45)}$, grossular$_{(21-35)}$, pyrope$_{(32-34)}$).

Clinopyroxene

Omphacite is usually anhedral, with subhedral grains occurring only rarely in veins and the eclogites of group 2. Different stages of the transformation from magmatic pyroxene to omphacite are preserved (Fig. 2.6; Tab. 2.3).

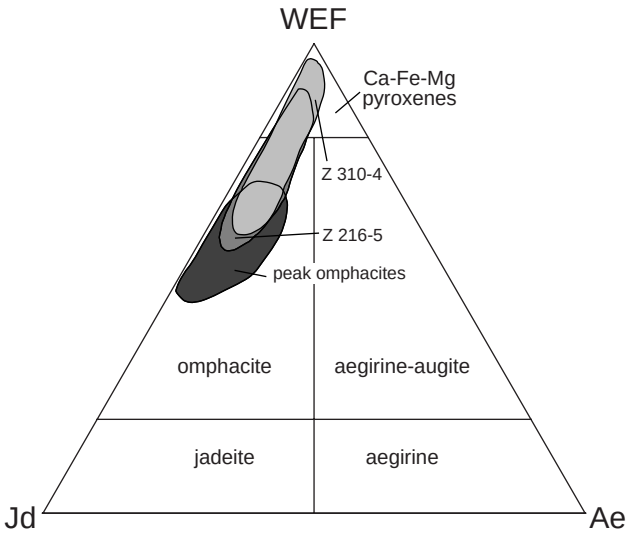

Fig. 2.6 Compositional ranges of pyroxenes (after Morimoto, 1988) from eclogites, including the compositions of magmatic relics from sheared eclogites (Z216-5) and eclogites with relic gabbroic textures (Z 310-4). Peak omphacite compositions several samples are also shown (Tab. 2.3).

The sheared porphyroclastic eclogites (group 3) contain magmatic pyroxene relics of diopsidic composition ($Wo_{49}Cfs_{43}Cen_{8}$–Jd_{10}; Tab. 2.3). The Jd-content of these pyroxenes increases considerably towards the rims (Jd_{10} to Jd_{35}). The compositional gradient is less pronounced on the side of a grain that underwent pressure solution, whereas towards the pressure shadow, the transition from diopsidic to omphacitic composition is sharp (Fig. 2.7a). Since these pressure shadows contain only eclogite facies minerals formed through reactions (4), (6), and (7), it may indicate that deformation, as well as the metamorphic reactions, started under eclogite facies conditions. The magmatic pyroxene relics of the group 1 rocks (relic gabbroic texture) are seldom completely converted to omphacite. Their compositions normally range between Jd_{10} and Jd_{25}, and some grains contain unaffected domains with compositions of ca. $Wo_{43}Cfs_{49}Cen_{8}$–Jd_{2} (Figs. 2.3c, 2.7b). In most samples, at least a thin rim of the magmatic pyroxenes is strongly affected by metamorphic reactions indicated by the corroded grain boundaries and the sudden increase of the Jd-content (Fig. 2.7b). Omphacite that is part of the plagioclase-replacing assemblage (Figs. 2.5, 2.7b) was formed mainly by reactions (4) and (6). Within these small-scale subsystems, omphacite has Jd-contents of 35-45 mol.% (e.g., Cpx2 in Fig. 2.7b). Omphacite that formed along grain boundaries and cracks also contain 35-45 mol.% jadeite. Peak-stage omphacite in the matrix of well-equilibrated eclogites (usually from group 2), as well as vein omphacites have 40-50 mol.% jadeite (Fig. 2.6). Although they cannot be distinguished chemically from matrix omphacites in terms of Jd-content, vein omphacites typically show growth zoning with increasing Jd-contents and X_{Fe}-values towards their rims. This is interpreted to reflect growth under increasing pressure and temperature conditions. The Jd-content of the magmatic relics (Figs. 2.7a, b) is not well understood. One possible interpretation is that the Jd-content resulted from retrograde processes. The replacement may have taken place in pyroxenes that were entered by a fluid along cleavage planes and which dissolved parts of the host crystal during prograde metamorphism. During retrogression, amphiboles grew within the widened cleavage planes and equilibrated with low-jadeite pyroxenes at lower P-T conditions (Figs. 2.7a, b). A more common feature of the retrogression is the replacement of omphacites with high jadeite contents by symplectites of clinopyroxenes with lower, varying jadeite contents (10-30 mol.%) and by quartz±albite±diopside±amphibole.

Tab. 2.3 Representative pyroxene analyses and structural formulae.

Sample	Z101-5	Z101-7	Z 135-6	Z 139-3	Z139-7	Z 143-8	Z 146-1	Z216-5	Z 216-5	Z249-6	Z 310-4	Z 310-4a
Analysis	cpx2.5	cpxx1.2	grt1omp1.1	omp4.2	pyx1.4	omp2.6	omp4.5	ogo1.1	cpx5L.53	pyx7.11	cpx1.4	cpx1L.64
Location	rim	rim	rim	rim	rim	rim	rim	rim	core of relic	rim	rim	core of relic
SiO_2	55.46	55.78	55.35	56.19	56.52	56.30	54.58	56.29	52.86	56.47	55.59	54.16
TiO_2	0.06	0.06	0.00	0.04	0.03	0.05	0.09	0.02	0.66	0.12	0.05	0.19
Al_2O_3	10.30	10.34	8.48	10.99	10.18	11.03	7.98	10.14	2.87	9.69	9.01	2.33
FeO	4.63	4.01	3.12	5.14	6.17	3.26	4.12	3.25	4.50	5.14	3.85	4.75
MgO	8.51	9.04	10.71	7.81	7.86	8.96	11.00	9.20	14.03	8.84	10.14	17.16
MnO	0.00	0.02	0.07	0.03	0.01	0.04	0.00	0.00	0.12	0.03	0.01	0.17
CaO	12.84	13.51	16.28	12.40	12.37	13.43	17.07	14.44	22.63	14.22	16.82	20.81
Na_2O	6.96	6.64	5.10	7.55	7.17	6.93	4.44	6.61	1.41	6.53	5.18	0.29
K_2O	0.00	0.00	0.00	0.00	0.00	0.00	0.00	0.00	0.00	0.01	0.00	0.00
Total	98.75	99.40	99.11	100.14	100.31	100.00	99.28	99.95	99.08	101.05	100.64	99.86
T_Si	1.991	1.989	1.989	1.988	2.008	1.988	1.971	1.993	1.947	1.992	1.974	1.974
T_Al	0.009	0.011	0.011	0.012	0.000	0.012	0.029	0.007	0.053	0.008	0.026	0.026
M1_Al	0.426	0.423	0.348	0.446	0.426	0.447	0.310	0.416	0.071	0.395	0.351	0.074
M1_Ti	0.001	0.002	0.000	0.001	0.001	0.001	0.002	0.001	0.018	0.003	0.001	0.005
M1_Fe^{3+}	0.063	0.043	0.017	0.080	0.049	0.036	0.024	0.042	0.000	0.053	0.028	0.000
M1_Fe^{2+}	0.054	0.052	0.061	0.061	0.108	0.045	0.071	0.054	0.136	0.085	0.083	0.000
M1_Mg	0.455	0.480	0.574	0.412	0.416	0.472	0.592	0.486	0.770	0.465	0.537	0.915
M2_Mg	0.000	0.000	0.000	0.000	0.000	0.000	0.000	0.000	0.000	0.000	0.000	0.017
M2_Fe^{2+}	0.022	0.024	0.016	0.011	0.026	0.016	0.029	0.000	0.003	0.014	0.003	0.145
M2_Mn	0.000	0.001	0.002	0.001	0.000	0.001	0.000	0.000	0.004	0.001	0.000	0.005
M2_Ca	0.494	0.516	0.627	0.470	0.471	0.508	0.660	0.548	0.893	0.537	0.640	0.813
M2_Na	0.484	0.459	0.355	0.518	0.494	0.475	0.311	0.454	0.101	0.447	0.357	0.021
M2_K	0.000	0.000	0.000	0.000	0.000	0.000	0.000	0.000	0.000	0.000	0.000	0.000
Total	4.000	4.000	4.000	4.000	4.000	4.000	4.000	4.000	3.996	4.000	4.000	3.995
Wo	45	46	48	45	44	47	48	48	49	47	50	43
Clino-En	42	43	44	40	39	44	43	43	43	40	42	49
Clino-Fs	13	11	7	15	17	9	9	9	8	13	9	8
WEF	51	54	64	48	51	52	69	55	90	55	64	98
Jd	42	42	34	44	44	44	29	41	10	39	33	2
Ae	6	4	2	8	5	4	2	4	0	5	3	0
XFe *	0.14	0.14	0.12	0.15	0.24	0.11	0.14	0.10	n.d	0.18	0.14	n.d
XFe **	0.23	0.20	0.14	0.27	0.31	0.17	0.17	0.17	0.15	0.25	0.17	0.13
Fe^{3+}/Fe^{total}	0.45	0.36	0.18	0.53	0.27	0.37	0.19	0.44	n.d	0.35	0.25	n.d

Structural formulae on a basis of 6 oxygens; * included Fe^{3+} calculation (stoichiometric charge balance); ** Fe^{2+} as Fe^{total}; n.d. not determined.

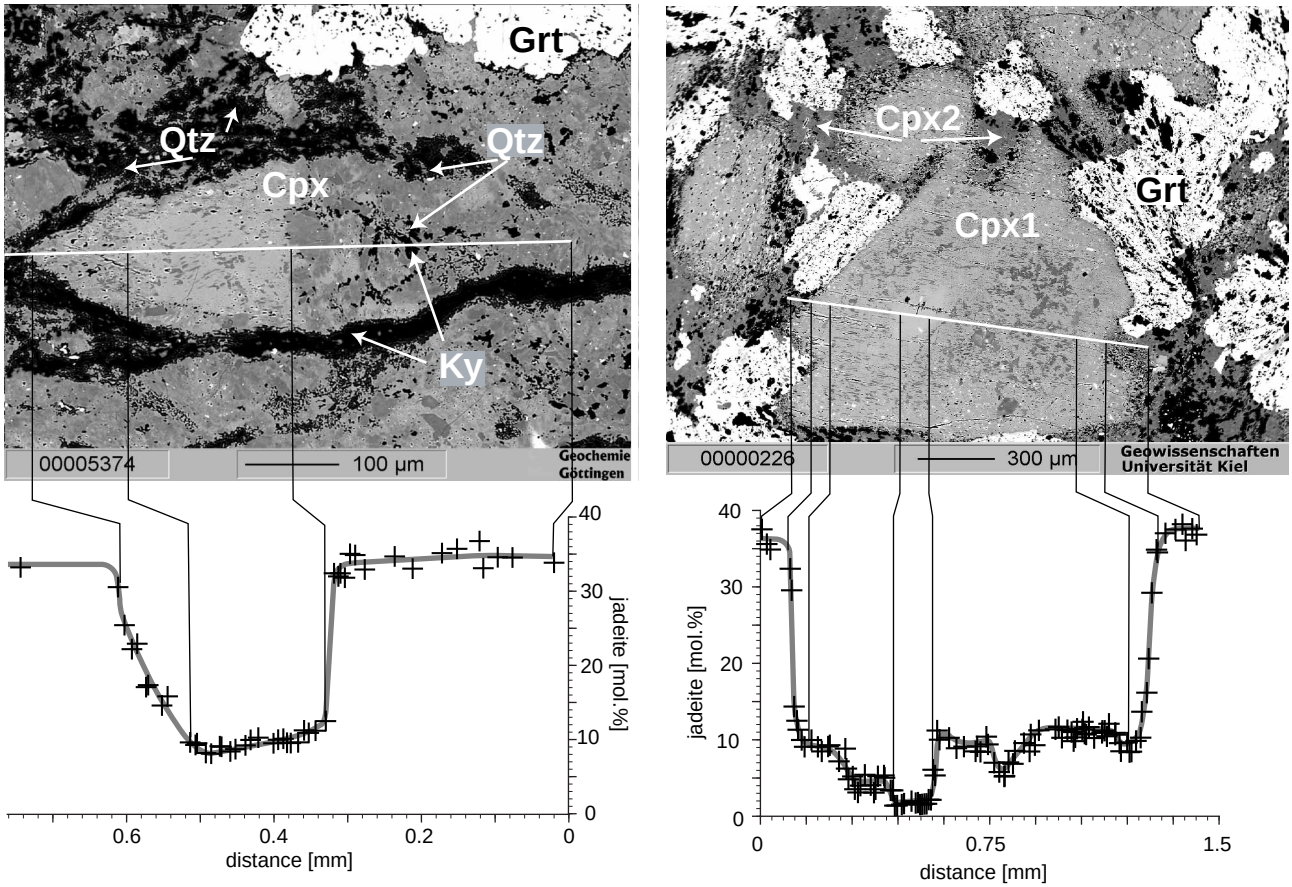

Fig. 2.7 a) Back-scattered electron (BSE) image and chemical profile of clinopyroxenes in a sheared eclogite (Z 216-5) with magmatic relics. Following the profile from left, it starts in the matrix (not shown) with ca. 35 mol.% jadeite, crosses a kyanite band (black), and enters the magmatic relic (Cpx). At this side of the grain, there is smooth transition from Jd_{35} at the rim to Jd_{10} in the core. In contrast, the boundary between the magmatic pyroxene relic and the omphacite (dark grey) occurring in the pressure shadow is marked by a sharp compositional transition. The mineral assemblage in the pressure shadow is omphacite, quartz and kyanite;
b) BSE image and chemical profile of a magmatic pyroxene relic (Cpx1) in an undeformed eclogite (same grain as in Fig. 2.3b; Z 310-4). Garnet (white), kyanite (black), quartz (black), and omphacite (Cpx2, dark grey) with 35-40 mol.% jadeite have replaced plagioclase, while the augite was replaced by low-jadeite omphacite (Cpx1, Jd_{10}, bright grey). Note that only a thin rim of the Cpx1 shows a sharp increase of the jadeite-content towards the matrix (see bright rim in Fig. 2.3b) and one area has an almost unaffected composition. The dark grey patches within Cpx1 are hornblende.

Amphibole

Amphiboles usually grew during the retrograde evolution of the rocks, and are edenitic to pargasitic hornblende in composition. They are found in omphacite replacing symplectites, in coronas surrounding garnet, or as euhedral grains in the matrix. Hornblende in textural equilibrium with prograde omphacite was found at one locality (Z 249) and is thus interpreted as being formed under eclogite facies conditions. All hornblendes usually contain significant amounts of chlorine, ranging from 0.5 up to 5.8 wt.%. These chlorine contents are positively correlated with potassium contents, e.g. a chlorine content of about 5-6 wt.% is associated with a potassium content of up to ~3.3 wt.% (Tab. 2.4). The unusual chlorine-rich amphiboles typically occur as vein-forming minerals (Fig. 2.4d).

Tab. 2.4 Representative analyses of chlorine-rich amphiboles from locality Z 249.

Sample	Z 249-6	Z 249-6
Analysis	amp1.3	amp4.4
Location	core	rim
SiO_2	38.67	38.11
Al_2O_3	14.46	15.45
TiO_2	0.35	0.44
FeO	19.57	19.41
MgO	6.42	6.35
MnO	0.00	0.01
CaO	10.31	10.53
Na_2O	1.83	1.65
K_2O	3.23	3.31
H_2O-	0.41	0.44
F-	n.d.	n.d.
Cl-	5.78	5.71
Total	99.73	100.12
Si	6.166	6.049
Al^{IV}	1.834	1.951
Sum_T	8.000	8.000
Al^{VI}	0.883	0.940
Ti	0.042	0.053
Mg	1.526	1.503
Fe^{2+}	2.549	2.505
Mn	0.000	0.000
Sum_C	5.000	5.000
Fe^{2+}	0.061	0.072
Mn	0.000	0.001
Mg	0.000	0.000
Ca	1.761	1.791
Na	0.178	0.136
Sum_B	2.000	2.000
Ca	0.000	0.000
Na	0.388	0.372
K	0.657	0.670
Sum_A	1.045	1.042
Sum_Tot	16.045	16.042
OH	0.438	0.464
F	0.000	0.000
Cl	1.562	1.536

Structural formulae on a basis of 24 oxygens,
n.d. not detected.

Epidote group minerals

Minerals of the epidote group usually occur as anhedral grains grown at the rim of former plagioclases. In this case, they may have been part of the prograde plagioclase replacement assemblage or they may have replaced garnet. Prograde epidote group minerals also occur in veins as subhedral to anhedral grains consisting sometimes of very fine subgrains (ca .10µm). Pistacite content is not uniform, ranging between 0.3 and 0.6. Chlorine was not detectable within the epidote-group minerals.

Phengite

Phengites were found only in samples of locality Z 101, where they are occur either in the matrix as part of the peak assemblage, or as inclusions in garnet. The phengite inclusions occur exclusively in rocks without matrix phengite. Si-contents of matrix phengite range between 3.34 and 3.46 pfu, with X_{Fe}-values between 0.12 and 0.19, whereas enclosed phengite has lower Si-contents between 3.20 and 3.36 pfu and X_{Fe}-values between 0.20 and 0.34. Their textural occurrence and lower Si-contents indicate that phengite inclusions probably formed during the prograde evolution. These prograde phengite inclusions have somewhat lower chlorine-contents (ca. 0.1 wt.%) than the matrix phengites (> 0.2 wt.%).

2.4.3 P-T conditions and phase relations

Peak metamorphic mineral assemblages are omphacite-garnet-rutile±kyanite with rare quartz in the matrix and as inclusions in garnet. Phengite-bearing eclogites were found at one locality. Temperatures were estimated with the garnet-clinopyroxene thermometer (Powell, 1985), and minimum pressures were constrained by the breakdown of paragonite to kyanite+omphacite(Jd_{50})+vapour (Holland, 1979). Temperature estimates were obtained from eight localities distributed throughout the eclogite zone (Fig. 2.2; Tab. 2.5). Although disequilibrium textures are common features of these eclogites, only eclogites that were well equilibrated or that contain equilibrated subdomains were used for P-T estimates. The attainment of equilibrium during eclogite facies metamorphism within subdomains was

Tab. 2.5 Temperature estimates for eight localities.

temperature estimates (for minimum pressures of 20 kbar)								
location		Z 101 [°C]	Z 135 [°C]	Z 139 [°C]	Z 143 [°C]	Z 146 [°C]	Z 216 [°C]	Z 249 [°C]	Z 310 [°C]
mean Fe^{2+}	*	885	725	755	725	730	715	760	730
error	#	±25	±25	±40	±25	±25	±25	±25	±42
mean Fe^{3+}	§	715	630	605	635	630	625	640	665
error	#	±32	±25	±28	±50	±40	±48	±25	±40

* Fe^{2+} as Fe^{tot}; # minimum error 25 °; § Fe^{3+} calculated by stoichiometric charge balance

tested by comparing P-T results from five to ten mineral pairs. Assuming $Fe^{2+} = Fe^{tot}$, garnet and omphacite rim compositions give peak-metamorphic temperatures between 710 and 760 °C for seven localities, and ca. 885 °C for the eighth locality (Z 101), at minimum pressures of 20 kbar suggested by Jd_{50} in omphacite (Tab. 2.5). The temperatures are ca. 100 °C lower if calculated Fe^{3+}-values of omphacite and garnet are considered, yielding values between 605 and 665 °C, and 715 °C (Z 101). Due to uncertainties in calculating Fe^{3+}-contents from microprobe analyses, the spread of calculated temperatures for each locality are greater than for the ones using Fe^{2+} as Fe^{tot} (Tab. 2.5). Temperature calculations assuming Fe^{2+} as Fe^{tot} give maximum values whereas the temperature calculations considering Fe^{3+}-contents give lower values, since the Fe^{3+}/Fe^{tot} ratios can reach ca. 0.5 in omphacite but only ca. 0.05 in garnet (Tabs. 2.2, 2.3). The calculated Fe^{3+}/Fe^{tot} ratios are in agreement with values obtained at other eclogite occurrences, where omphacite usually has almost ten-times higher Fe^{3+}/Fe^{tot} ratios than coexisting garnet (Carswell et al., 1997; 2000). Thus, the temperatures from the calculations considering Fe^{3+}-contents are interpreted to be more realistic than the ones assuming Fe^{2+} as Fe^{tot}. Excluding the higher temperatures from locality Z 101, all eclogites equilibrated in a small temperature interval of ca. 60 °C which is situated somewhere between 600 and 760 °C. The small temperature range is remarkable, considering the great spatial distribution of the eclogite occurrences regarded here (Fig. 2.2). Pressure estimates for the eclogite occurrences, obtained from phengite-bearing eclogites, are about 26-28 kbar (chapter one). Since evidence for a direct transformation from gabbro to eclogite (Figs. 2.5, 2.7a, b) were found in many samples, we infer that metamorphism and thus eclogitisation took place probably at temperatures between 605 and 665 °C and pressures of about 26-28 kbar. Schmid and Poli (1998) determined the stability field of epidote-eclogite (Grt-Omp-Ep) between ca. 20 and 30 kbar and 660 and 800°C for MORB-like bulk compositions in a water-saturated system. The vein shown in Fig. 2.3b (Z 301-4), containing omphacite, epidote-group minerals, and garnet, is mineralogical similar to the epidote-eclogites of Schmid and Poli (1998) and the P-T estimates obtained for the host rock of this vein is in agreement with the experimental results.

The protoliths of the Zambian eclogites have a MORB-like (mid-ocean ridge basalt) bulk-chemistry (chapter one) and the formation of Ky-bearing eclogites from such protoliths is unusual, since average MOR-basalts are Al-poor rocks and kyanite is not expected to be formed. The changing phase relations during the prograde metamorphic evolution of eclogites will be described, in order to explain the occurrence of kyanite in eclogites with such an Al-poor bulk-chemistry. Assuming

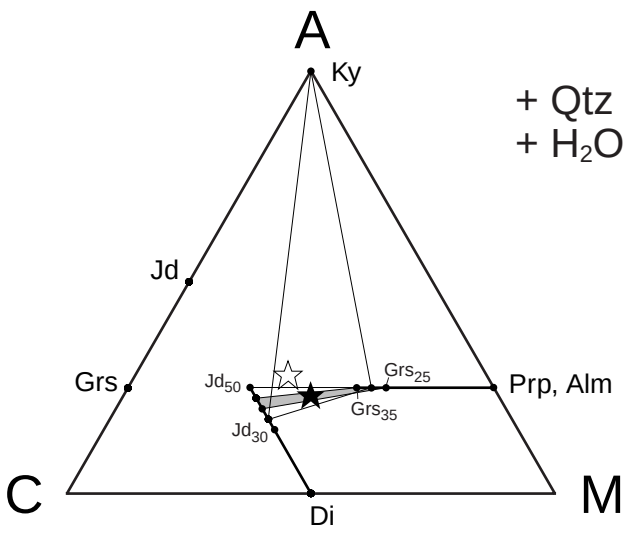

Fig. 2.8 ACM diagram (after Thompson, 1981) illustrating the phase relation of the Zambian basic rocks during their metamorphic evolution. Condensed CMASH composition space, with projection from Qtz and H_2O and condensation along $NaSiCa_{-1}Al_{-1}$ (for more details see Thompson, 1981). The mean composition of the rocks is indicated by the black star; the white star indicates the possible composition of Al-enriched subdomains. The shaded triangle represents the peak metamorphic assemblages of the "completely" equilibrated eclogites, while the three-phase field represents the peak assemblage of eclogites containing relics (i.e., Z 216-5 and Z 310-4).

somewhat lower P-T conditions at the beginning of eclogitisation than during peak metamorphism, plagioclase and diopsidic pyroxene were consumed and low-jadeite omphacite, kyanite, and garnet with moderate grossular contents was formed (Fig. 2.8). After consumption of plagioclase, low-jadeite omphacite and kyanite became the sources of Na and Al to form high-jadeite omphacite at higher P-T conditions. For the given bulk-chemistry (black star in Fig. 2.8), kyanite will become consumed during continuously increasing P-T conditions and more garnet will be produced, since garnet will shift to more grossular-rich compositions whereas the pyroxene will become more jadeitic. As it is evident from figure 2.8, the bulk-chemistry of the Zambian eclogites does not have enough Al to form kyanite beside garnet and omphacite at peak metamorphic conditions, and consequently a more Al-rich composition is required. For certain subdomains within the Ky-bearing eclogites, the necessary shift to Al-rich composition (white star in Fig. 2.8) resulted from the complete breakdown of plagioclase, while relics of the Al-poor magmatic, diopsidic pyroxene remained intact (e.g., Figs. 2.7a, b). Another possible scenario for such a shift is that kyanite precipitated from an Al-supersaturated fluid in a vein (e.g., Fig. 2.4b). Thus, the occurrence of kyanite in eclogite facies rocks with MORB-like compositions is only possible at (1) moderate P-T conditions (lower Jd-content in omphacite and lower Grs-content in garnet), in (2) incompletely equilibrated rocks that contained magmatic pyroxene relics (extraction of Al-poor parts from the bulk-chemical system), or (3) in Al-rich chemical subdomains (e.g., veins or former plagioclase sides - precipitated from supersaturated fluids).

2.5 Processes occurring during eclogitisation

The eclogites of group 2 contain no textural evidence for specific kinematic conditions which may have occurred during the transformation to an eclogite. In contrast, the preserved gabbroic textures in group 1 eclogites clearly indicate that eclogitisation occurred in this case without deformation (Fig. 2.3a) and omphacite inclusions in garnet (Figs. 2.5, 2.7b) are evidence that metamorphism commenced under eclogite facies conditions. In addition, the sheared porphyroclastic textures of group 3 eclogites are the result of deformation. The mineral assemblage formed within pressure shadows (Fig. 2.7a) again indicates that the

transformation took place under eclogite facies conditions. Hence, the different textures of the Zambian eclogites are evidence for different kinematic conditions during the eclogitisation process. However, all reactions in the different types of eclogites, which are related to the gabbro-to-eclogite transformation base on net transfer reactions. There is always more than one reactant necessary to produce the eclogite facies peak assemblages. Therefore, once the transformation had started, material transport was essential for the continued production of eclogite facies assemblages during metamorphism. Some processes of material transport and features of the gabbro-to-eclogite transformation are discussed below.

2.5.1 Dissolution and precipitation mechanism

Element exchange between minerals, resulting from variations in P, T, and X, occurs by diffusion or net transfer reactions. Diffusion in a rock occurs in response to chemical potential gradients and results in element exchange within a mineral or between minerals over grain boundaries and has no effect on the physical characteristics of the related minerals like the structure, size, form, and the modal amount. In contrast, net transfer reactions between minerals are based on dissolution of mineral phases and growth of one or more mineral phases, which might result in changed structures of minerals or even new mineral phases (e.g., Carmichael, 1969; Ridley & Thompson, 1985; Spear, 1993). The preservation of undeformed, gabbroic textures in group 1 eclogites must be the result of pure fluid-rock interaction. Plagioclase breakdown (Pl $\Rightarrow$ Grs + Jd + Ky + Qtz, reaction (4)), the breakdown of augitic pyroxene, and the related growth of omphacite (e.g., $CaMg_{(\text{in augite})} \Leftrightarrow NaAl_{(\text{in fluid})}$) are all based on net transfer reactions. In the first case, the consumption of plagioclase and the production of quartz, jadeite, grossular, and kyanite clearly affect the modal proportions of the involved minerals. During the replacement of magmatic augite by omphacite (Fig. 2.9), grain boundaries move as a consequence of coupled augite consumption and omphacite growth. The importance of the dissolution and precipitation mechanisms for

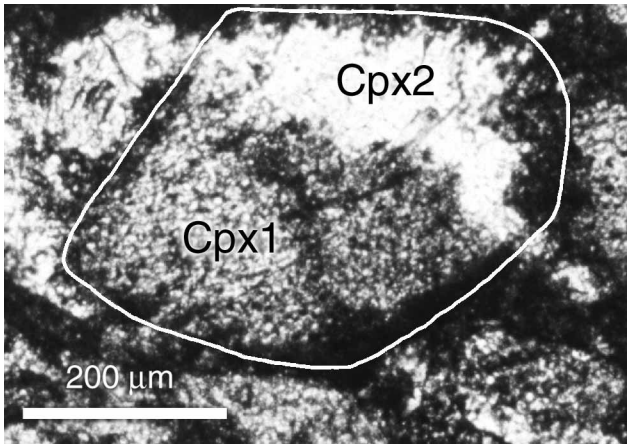

Fig. 2.9 Omphacite (Cpx2) with Jd_{35} replaces former magmatic pyroxene (Cpx1) with Jd_{10} (Z 310-4). Note that the grain boundary between Cpx1 and Cpx2 moved during replacing by consumption and growth.

the gabbro-to-eclogite transformation is also demonstrated by the sheared eclogites (group3). The chemical profile across the pyroxene pophyroclasts (Fig. 2.7a) shows a characteristic asymmetry. A less steep compositional gradient is observed on the side of the grain that underwent pressure-solution. The formation of this less steep gradient at the reaction front is related to a continuous dissolution of the magmatic pyroxene (Cpx1), and a simultaneous precipitation of omphacite (Cpx2) that grew topotactically on Cpx1, direct at the side where dissolution was taking place. This may occur when a fluid, saturated with Al and Na (from dissolved Pl), arrived at a magmatic relic. After dissolving some of the Cpx1, the fluid became supersaturated with respect to Cpx2 components for the P-T conditions of the given subdomain, leading to precipitation of Cpx2 (direct at the solution

front). Continued dissolution of Cpx1 and precipitation of Cpx2 decrease the amount of Al and Na within this particular subdomain, whereas the amounts of Ca, and Mg, and Fe increases in the fluid that continued dissolving Cpx1 and precipitating Cpx2. This resulted in a decrease of the Jd-content towards the core of the magmatic relic and created the smooth transition between the rim and unaffected core in areas undergoing pressure solution. If the whole magmatic relic is considered as a subsystem, omphacite, quartz, and kyanite precipitated from the fluid within the pressure shadow (Fig. 2.7a), because the fluid was supersaturated with respect to theses minerals. The sharp compositional transition between the core of the magmatic relic and the omphacite grown in the pressure shadow indicates that significant diffusion occurred only within the fluid and not over grain boundaries.

As shown above, all mineral reactions that transformed a gabbro into an eclogite operated with dissolution of the reactant(s), material transport and a fast precipitation of the product(s). Significant diffusion occurred only through the fluid resulting in material transport, which is necessary for mineral reactions (Carmichael, 1969; Walther & Wood, 1984). The development of mineral assemblages which at equilibrium is in agreement with the bulk chemistry is interpreted to depend on deformation combined with fluid availability (e.g., Koons et al., 1987). Since magmatic relics are very common in the sheared eclogites of Zambia and only the fluid related processes produced the eclogite facies minerals, the degree of eclogitisation was apparently controlled by the rates of the dissolution-transport-precipitation processes and thus related to the fluid/rock ratio, rather than the degree of deformation.

2.5.2 Formation of pseudomorphs

Three types of pseudomorphic replacements are responsible for the preservation of gabbroic textures within the eclogites. Two of them developed during prograde metamorphism, and the third during retrogression. The first type of replacement is a polymineralic replacement of plagioclase by garnet, omphacite, kyanite, and quartz (Figs. 2.3c, 2.5, 2.7b), and the second type is the monomineralic replacement of augite by omphacite, as well as plagioclase by garnet (Fig. 2.3a). The third type is the retrograde transformation of the magmatic pyroxene relics to low-Jd omphacites and amphiboles (Figs. 2.3c, 2.7b).

Pseudomorphs were created by the dissolution of the reactant accompanied by the simultaneous precipitation of the product phase(s), which inherited the shape of the reactant crystal (Carmichael, 1969; Merino & Dewers, 1998). Pseudomorphs can be formed during the prograde evolution when the molar volumes of the replacement products are lower than the molar volume of the reactant and the force of crystallisation is supporting the mineral growth at the side of dissolution (Ferry, 2000). They can also be formed during the retrograde evolution if the amount of dissolved material of the host is high enough so that the new mineral can grow contemporaneously within the pseudomorph. This may then depend on the molar volumes (Ferry, 2000), or may be independent on the molar volumes but related to the flux of material (e.g., Merino & Dewers, 1998). The pseudomorphic replacement of plagioclase (type one) by a fine grained intergrowth of eclogite facies assemblage (Grt-Omp-Ky-Qtz) requires that plagioclase persisted as a metastable phase well outside of its stability field. The very fine grain size (ca. 10 µm) of the reaction products is consistent with the model in which rapid nucleation of the product phases is triggered by fluid influx in a metastable system (Rubie, 1983, 1998).

Apparently, the mineral reaction needed to be triggered, in this case by a fluid which strongly dissolved the plagioclase and parts of the also metastable augitic pyroxene. The dissolution of the minerals was accompanied by precipitation of the fine grained intergrowth described above. Metastable plagioclase is rare but have been reported from low-T / high-P milieus (e.g., Åustrheim, 1986/87; Wayte et al., 1989). Rubie (1998) described cases in which plagioclase in a dry system was metastable at pressures >7 kbar above the equilibrium boundary (reaction 4), or >12 kbar above the reaction boundary if a fluid was available (reaction 5).

The monomineralic replacements, such as omphacite pseudomorphs after augite and garnet pseudomorphs after plagioclase (type two), run in two steps. The first step is dissolution of the host mineral and simultaneous nucleation of the new mineral direct at the site of dissolution. After this initial process, effective material exchange between the dissolving plagioclase and magmatic pyroxene (Na + Al ⇔ Fe + Mg + Ca) during the growth of omphacite and garnet is necessary to form the inclusion-poor pseudomorphs. Thus, the amount of fluid had to be reasonably high in these domains (e.g., Mørk, 1985 a, b).

The retrograde pseudomorphic replacements (third type) is characterised by the replacement of the magmatic pyroxenes, which survived the peak eclogite facies metamorphism, by low-jadeite omphacites and amphiboles. The omphacite with a lower molar volume replaces the magmatic relic, while the amphibole with a higher molar volume grew within the former cleavage of the magmatic pyroxene. Both are filling together the available space. The omphacitic replacement products often inherited the twinning from the magmatic relics (Fig. 3c). In this case simultaneous, topotactic growth of the secondary mineral at the site of dissolution is required (Turner & Weiss, 1965; Carmichael, 1987), which in turn demands a restricted amount of reacting material per time so that the product can react with the host crystal during the topotactic growth (e.g., Kleber, 1962).

The transport of material and therefore the amount and the mobility of the transport-medium is important in controlling the textures (Carmichael, 1969). A strong supersaturation of the transport medium (fluid) will result in rapid precipitation and short-distance transport of material (Ferry, 2000). If a large amount of fluid is available, material-transport is enhanced. Because of lower concentrations of mineral components within the fluid, fast precipitation is not forced and transport over longer distances is possible (Walther & Wood, 1984). Hence, the occurrence of prograde and retrograde pseudomorphic replacements is mainly controlled by the fluid/rock ratio during the mineral exchange and thus to the material flux within the particular subdomains.

2.5.3 Vein formation

The veins of the eclogites have random orientations (Fig. 2.4e) and mostly crosscut the main fabric of the host rocks. They are interpreted to be part of a late-stage, prograde fluid infiltration, which is indicated by the prograde chemical zoning of the vein minerals. Veins that were formed during prograde metamorphism and at peak eclogite facies conditions are a common feature elsewhere (e.g., Åustrheim 1986/87, 1990; Brunsmann et al., 2000; Gao & Klemd, 2001). The volume reduction of the host rock during prograde metamorphism may have provided the necessary space. Considering that eclogitisation and thus metamorphism occurred at the time of fluid influx in metastable magmatic assemblages, this space forming mechanism seems to be very efficient. Hydrofracturing could increase the available pore volume, which would result in decreased fluid pressure causing the vein minerals to precipitate

(Brunsmann et al., 2000; Gao & Klemd, 2001). Vein-forming due to hydrofracturing is reasonable since some of the host rocks are undeformed (e.g., host of vein from Fig. 2.3c) and most veins crosscut the fabric of the host. Other veins, however, might be related to fluid-channeling due to shearing (Fig. 2.4b). In most cases, the constituent elements of vein-forming minerals were most likely extracted from the immediately surrounding rock, at or near the time of peak-metamorphic temperature and vein opening and the crystallisation of vein minerals are supposed to occur simultaneously (Vidale, 1974; Ferry, 2000). Since kyanite is a common vein-forming mineral (Fig. 2.4b) in the Al-poor Zambian eclogites, a high mobility of alumina in the eclogitic fluid is required.

2.6 Fluid source

Due to the lack of fluid inclusions in the Zambian eclogites, the ability of OH-bearing minerals to incorporate chlorine was used to estimate roughly the fluid composition during the metamorphic evolution. Kullerud (1996) proposed that the Cl-content of amphibole and biotite is principally controlled by the activity ratio a_{Cl}-/a_{OH}- of the equilibrium fluid during mineral growth. Since silicates prefer to incorporate OH over Cl, a high a_{Cl}-/a_{OH}- ratio is required to form Cl-bearing silicates (Kullerud, 1996). A chlorine-rich fluid can be produced by the desiccation mechanism (Markl & Bucher, 1998), according to which a fluid becomes enriched in chlorine due to continuous hydration reactions in a fluid-poor system. However, the Cl-content of amphiboles and phengites of the Zambian eclogites were high throughout the entire metamorphic evolution (e.g., up to 5.8 wt.% for peak amphiboles and 0.2 wt.% for peak phengites). Evidence for prograde metamorphic reactions prior to eclogite facies conditions was not found, instead all eclogites were formed directly from gabbroic protoliths. Fluid influx into the gabbroic protoliths can occur either during subduction from external rock sources (e.g., Wayte et al., 1989) or prior to subduction, during seawater-alteration of the oceanic crust (e.g., Pognante, 1985; Barnicoat & Cartwright, 1997). Since no petrographic evidences for seawater-alteration in unmetamorphosed gabbros as well as relics of prograde blueschists or amphibolite facies minerals were found, the protoliths of the eclogites were probably too dry to become the source of the eclogitic fluid. Hence, significant interaction with early hydrothermal fluids at the mid ocean ridge can most likely be ruled out for the investigated rocks. Considering the relatively deep position of clinopyroxene–feldspar gabbros in a typical oceanic crust, a possible source for the fluid is the serpentinised part of the underlying slab (Scambelluri et al., 1997; Schmid & Poli, 1998). Scambelluri et al. (1997) deduced from fluid inclusions and mineral chemical data that an eclogitic fluid derived from a seawater-altered peridotite and formed syn-eclogitic veins at about 25 kbar and 550-600°C. This fluid was rich in Cl, Na, K, Mg, and Fe. The high chloride-content of the fluid is interpreted as being the result of hydration of mantle mineral relics and the formation of hydrous vein minerals (desiccation) during prograde metamorphism (Scambelluri et al., 1997). Such a fluid can act as catalyst for the metamorphic reactions within the eclogites and may have delivered the material necessary for the formation of the eclogite facies potassium-rich Cl-amphiboles occurring in veins as well as the peak metamorphic Cl-bearing phengites in the Zambian eclogites. The fluid in these rocks may derive from serpentine and chlorite breakdown in seawater-altered mantle below the gabbroic protoliths of the eclogites (Schmid & Poli, 1998).

2.7 Discussion and conclusions

The dissolution and precipitation features in the Precambrian eclogites described in this study imply that a free fluid phase must have been present during the gabbro to eclogite transformation. This conclusion is confirmed by the occurrence of prograde eclogitic veins which also require a free fluid phase. The fluid had a high chlorinity as indicated by Cl-rich amphiboles and phengites formed during different stages of the metamorphic evolution. Omphacites and most of the epidotes in some eclogitic veins (Fig. 2.3b) consist of very fine subgrains and some eclogite facies plagioclase replacements are formed of very fine grained intergrowths (Fig. 2.7b). These small grain sizes are interpreted as the result of very fast nucleation due to fluid influx into a rock with a metastable mineral assemblage. Thus, the gabbro-to-eclogite transformation is controlled by fluid infiltration and by the fluid/rock ratio rather than the crossing of equilibrium phase boundaries. Even when deformation occurred, the fluid/rock ratio limited reaction rates due to supporting material transport and thus triggering the reactions. Fluid availability is thus the key factor for governing the gabbro-to-eclogite transformation. Considering the very heterogeneous spatial distribution of gabbros and eclogites in the Zambesi Belt and assuming that the mantle underlying these rocks was the fluid-source, it seems that only a small amount of fluid were liberated and that it was a channelised fluid flow which infiltrated the gabbroic part of the oceanic crust. Since the former gabbros transformed directly to eclogites and P-T estimates record 605 to 665 °C at pressures of about 26-28 kbar, it is most likely that the dehydration of the underlying slab started only after reaching a critical depth. The preservation of the incomplete reactions indicates that the processes that transformed the gabbros to eclogites affected some of the investigated eclogites for only a limited time. This suggests that either (1) the eclogites did not remain long enough at great depth for reactions to run to completion or (2) the fluids, which acted as engines for the reactions, left the system. Moreover, the preservation of relic magmatic minerals as well as of gabbroic textures, and the evidences for channelised fluid flow causing eclogitisation, make it reasonable that gabbros and eclogites of the investigated zone are co-genetic but experienced different metamorphic transformation histories. The preservation of prograde disequilibrium features makes a polymetamorphic history for the investigated rocks most unlikely.

CHAPTER THREE

Timing and P-T evolution of whiteschist metamorphism in the Lufilian Arc-Zambesi Belt orogen (Zambia): implications to the Gondwana assembly

3.1 Abstract

One of the world largest occurrence of whiteschist (talc-kyanite schist) is located in south central Africa with several exposures along a c. 700 km northwest-southeast striking zone. Whiteschists and associated rocks from four localities, three in the Lufilian Arc (NW) and one in the Zambesi Belt (SE) were chosen to investigate their metamorphic evolution and age relations in order to elucidate the geodynamic relationship of these belts. In the Lufilian Arc petrological investigations of whiteschists and associated garnet-amphibolites and biotite-kyanite-garnet gneisses record peak-metamorphic conditions of about 750 ±25 °C at 13 ±1 kbar. Using mineral assemblages of whiteschists, associated gedrite-cordierite-kyanite gneisses and garnet-staurolite-kyanite schists from the Zambesi Belt, estimated peak metamorphic conditions indicate about 700 ±25 °C at 10 ±1 kbar. Mineral reaction textures point to a metamorphic evolution along clockwise P-T paths which are interpreted as the result of significant crustal thickening. On the basis of these P-T paths and a concordant monazite age of 529 ±2 Ma (biotite-kyanite-garnet gneiss) combined with $^{207}Pb/^{235}U$ ages of 531-532 ±2 Ma from monazites extracted from whiteschists, it is concluded that the crustal thickening event affected the entire Lufilian Arc-Zambesi Belt orogen almost simultaneously. Thus, the whiteschist formation is related to the final continental collision between the Congo and the Kalahari cratons at c. 530 Ma during the assembly of Gondwana.

3.2 Introduction

The positions of the Congo and the Kalahari cratons within the Rodinia supercontinent are unclear or in debate (e.g., Piper, 2000; Dalziel, 1997; Powell et a., 2001). However, the positions of these cratons within Gondwana are well constraint, but the movement of the cratons during the Gondwana-formation are still under discussion (e.g., Porada, 1989). New palaeomagnetic data indicate that the Kalahari craton converged with Laurentia between 1030 and 1000 Ma, with the Namaqua-Natal belt situated at the edge of Kalahari-Laurentia block far away from the Congo craton (Powell et al., 2001). Other studies postulate a similar position but a 180° rotated orientation of the Kalahari craton (Dalziel et al., 2000). Moreover, Porada and Berhorst (2000) proposed that rifting, which started at c. 880 Ma during Rodinia break-up, separated at least parts of the Kalahari and the Congo craton from each other. The time of initial rifting is in accordance with other estimates for the beginning of the Rodinia break-up (e.g., Hoffman, 1991; Vernikovsky & Vernikovskaya, 2001). A comparison of Mesoproterozoic granulite facies metamorphism from the Namaqua belt (aligned on the Kalahari craton) with that from the Irumide belt (aligned along the Congo craton) shows striking similarities in P-T conditions and ages of the peak-metamorphism, supporting the idea of a possible geographical connection during their formation (Schenk & Appel, 2001). If the Congo and Kalahari cratons became connected during Rodinia assembly, it would have major consequences for the possible orientation of the Congo-Kalahari block in relation to Laurentia. However, palaeomagnetic data indicate that there could have been significant relative movements between the cratonic blocks of Africa prior to Gondwana assembly (e.g., Li and Powell, 1993). This is supported by, e.g., subduction of oceanic crust at around 600 Ma at the eastern edge of the West-Africa craton (Caby et al., 1981; Jahn et al., 2001). Nevertheless, there is only a sparse Neoproterozoic database for the Congo and the Kalahari cratons as pointed out by Meert and Powell (2001). A key location for the understanding of the relationship between the Congo and Kalahari cratons during the Proterozoic is the Pan-African transcontinental belt crosscutting southern Africa in east-west direction (Fig. 3.1) and separating the cratons and the aligned Mesoproterozoic belts (e.g., Hanson et al. 1988a; Porada, 1989).

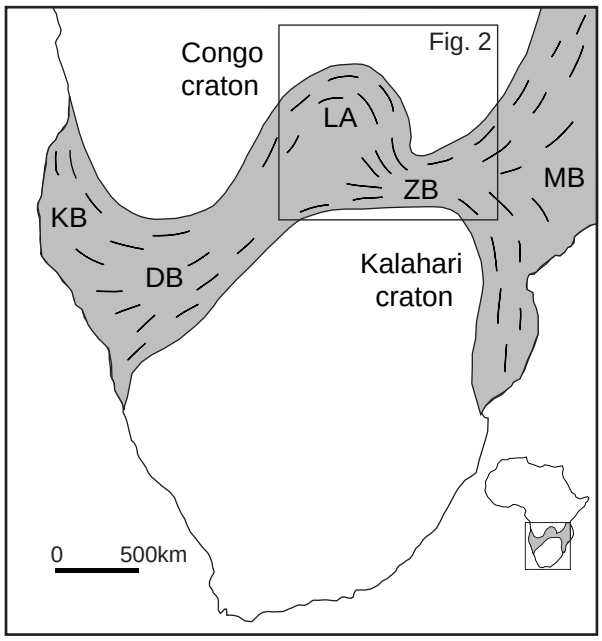

Fig. 3.1 Pan-African Belts in southern Africa. KB = Kaoko Belt; DB = Damara Belt; LA = Lufilian Arc; ZB = Zambesi Belt; MB = Moçambique Belt.

Following Porada and Berhorst (2000), the basin of the Lufilian Arc-northern Zambesi Belt started to develop at c. 880 Ma. Geochemical data and P-T estimates obtained from gabbros and eclogites of the central Zambesi Belt give evidence that Neoproterozoic oceanic crust was formed and subducted in this part of the transcontinental

belt (chapter one). Whiteschists (talc-kyanite schists) as potential subduction related rocks (e.g., Schreyer, 1973) may provide additional information about the Gondwana forming events. Zambia hosts one of the largest occurrences of whiteschists in the world (Vrána & Barr, 1972, Schreyer, 1977). In southern Africa, one additional whiteschist occurrence exists in northern Zimbabwe (Johnson & Oliver, 1998, 2001) within the spatial extension of the Zambian outcrops. Whiteschists typically are found in Alpine-type orogens, e.g., Western Alps, Trans-Himalaya (Sar e Sang - Afghanistan), and Dabie Shan (China) and they are usually interpreted as being of metasomatic origin (Schreyer & Abraham, 1976; Chopin, 1984; Rolfo et al., 2000). The stability field of the talc-kyanite assemblage are restricted to temperatures between c. 600 and 800°C and pressures from c. 6 kbar up to conditions of the ultra-high-pressure metamorphism (Chopin, 1984; Schreyer, 1988; Massonne, 1989) and thus whiteschists are usually formed by crustal thickening under low geothermal gradients. In order to provide more data on the geological evolution of the Lufilian Arc-Zambesi Belt, whiteschists and associated rocks from four whiteschists localities were chosen for petrological and geochronological studies, three within the Lufilian Arc and one within the Zambesi Belt. Mineral-chemical and textural investigations in combination with quantitative geothermobarometry were applied to reconstruct the metamorphic evolution of the investigated rocks. The results are used to identify the geodynamic situation at the time of metamorphism. Peak metamorphism has been dated with monazites, while cooling ages have been obtained with Rb-Sr analyses of micas. In addition, the basement rocks that underlie whiteschists of the Lufilian Arc have been dated with zircons.

3.3 Regional geology

The Precambrian crust of Zambia has been affected by three major orogenic events (Fig. 3.2). Palaeoproterozoic crust occurs in the northeast of Zambia, i.e. in the Bangweulu Block (e.g., Andersen & Unrug, 1984), while the Mesoproterozoic northeast-southwest striking Irumide Belt and Choma-Kalomo Block occur in south and east Zambia (e.g., Ray, 1974; Hanson et al., 1988b). In central Zambia, the Mesoproterozoic units are crosscut by the Neoproterozoic to Cambrian Lufilian Arc and Zambesi Belt, both are part of the transcontinental system (Fig. 3.1) and having a general east-west trend (e.g., Coward & Daly, 1984, Hanson et al. 1988a; Porada, 1989). The two younger orogens are thought to be related to two major supercontinent-forming events, i.e. the Mesoproterozoic Rodinia formation (Hoffman, 1991; Dalziel, 1992) and the late-Proterozoic to Cambrian Gondwana formation (e.g., Porada, 1989, Unrug, 1996).

A continuous transition from the Zambesi Belt into the Moçambique Belt is postulated for the region north-east of the Kalahari craton (Johnson & Vail, 1965; Whittington et al., 1999). The north-western end of the Zambesi Belt is defined by the Mwembeshi Shear Zone (MSZ) separating the Zambesi Belt from the Lufilian Arc (e.g., Porada, 1989) (Fig. 3.2). The importance of this dislocation zone as a dividing line between the Lufilian Arc and the Zambesi Belt is debatable, as shown by Katongo & Tembo (1999), who identified the same lithostratigraphic units in the Neoproterozoic Katangan cover sequence on both sides of the shear zone (detailed discussion in Porada & Berhorst, 2000). Towards the west the Lufilian Arc continues into the Damara Belt (Fig. 3.1). The presence of reworked older basement components is an important feature of the southern Zambesi Belt (Goscombe et al., 1998). In the Lufilian Arc basement rocks are

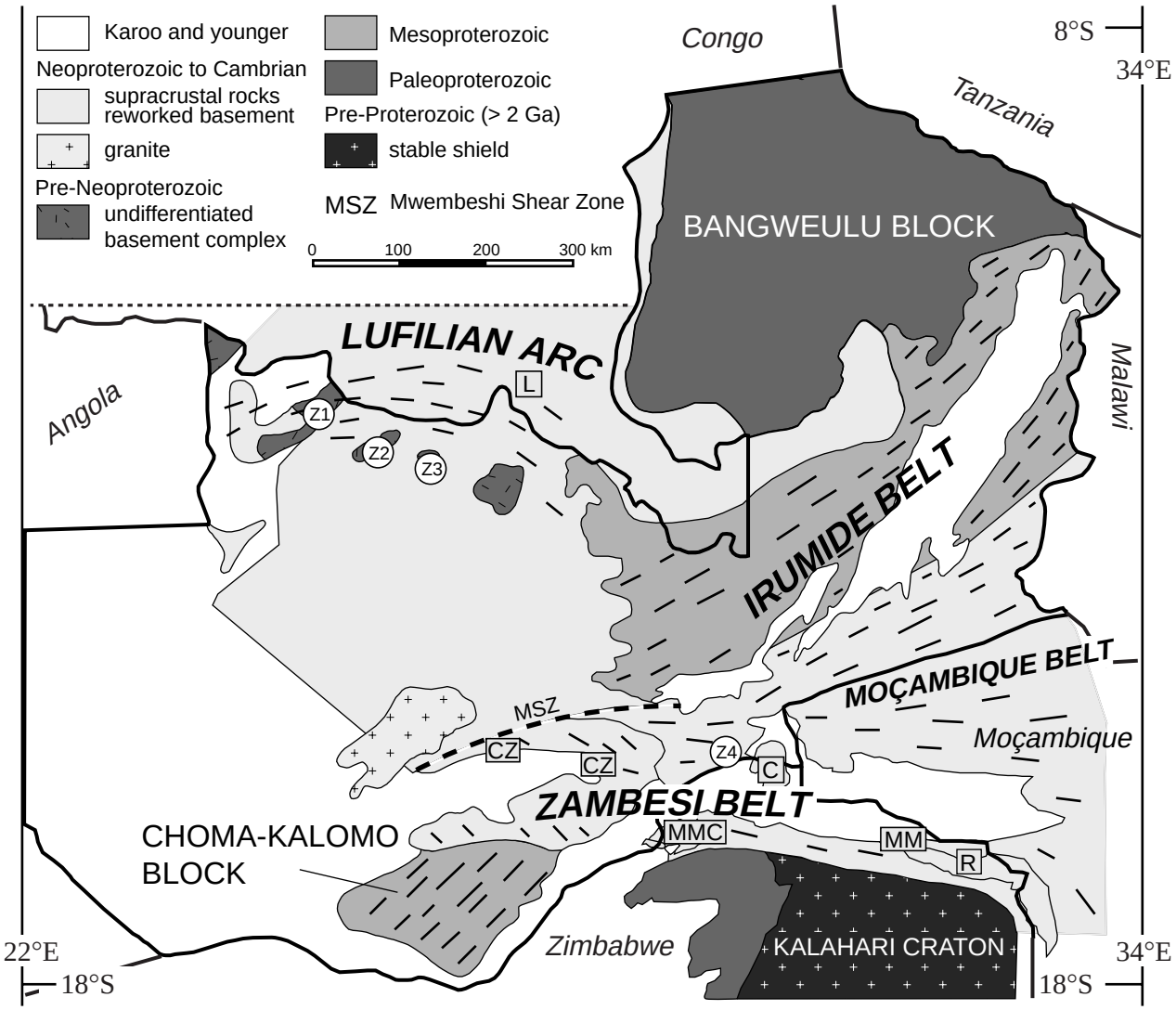

Fig. 3.2 Structural provinces of Zambia, Northern Zimbabwe and Western Moçambique, modified after Sikatali et al. (1994) and Hanson et al. (1994). (Z_{1-4}) investigated areas, 1 = Kabompo Dome, 2 = Mwombezhi Dome, 3 = Solwezi Dome, 4 = Chowe River (Chongwe River Area); (L) Lwiswishi; (CZ) central Zambian eclogites; (MMC) Makuti Metamorphic Complex; (C) Chewore Inliers; (MM) Mavuradonha Mountains; (R) Rushinga Area. Thin lines indicate geological boundaries, while the thick lines indicate political borders.

less reworked and are mainly exposed in the Domes Region, where they are overlain and surrounded by rocks of the Katanga Supergroup (Porada & Berhorst, 2000). Rb-Sr whole-rock and U-Pb zircon SHRIMP analyses (Cahen et al., 1984; Rainaud et al., 1999) yielded Palaeoproterozoic ages between 2.0 and 1.8 Ga for the exposed basement rocks at the eastern margin of the Lufilian Arc. A whole rock Rb-Sr isochron of samples from the basement of the Domes Region defines a Mesoproterozoic age (Cosi et al., 1992). In the central Zambesi Belt, Mesoproterozoic crustal fragments of the Chewore Inliers (Fig. 3.2) gave crystallisation ages of c. 1070 to 1080 Ma. A low-P / high-T metamorphic event was determined at a minimum age of about 945 Ma and a high-P / medium-T metamorphic event was dated at c. 526 Ma, both with the SHRIMP technique on zircon (Goscombe et al, 1998,

2000). In addition, for the Rushinga area in northeast Zimbabwe (Fig. 3.2) two distinguishable metamorphic events are reported. A high-pressure granulite facies migmatisation event between 850-870 Ma and an amphibolite facies event at c. 535 Ma are constrained by zircon and titanite U-Pb ages and Ar-Ar amphibole cooling ages (Vinyu et al. 1997, 1999). On the basis of geochemical and structural studies an extensional regime with intrusions of peralkaline rocks at the time of the high-pressure granulite facies metamorphism has been postulated (Dirks et al., 1998; Vinyu et al., 1999). Furthermore, the widespread granites and volcanic rocks with ages ranging from 840-880 Ma in the Lufilian Arc-Zambesi Belt, are interpreted as indicators of incipient extension (Porada & Berhorst, 2000). According to these authors the Roan basin evolved during rifting and a passive continental margin was formed at the southern edge of the Congo craton. Geochemical investigations of gabbros and metagabbros from the Lufilian Arc suggest that the rifting probably did not significantly overstep a continental stage (Tembo et al., 1999). However, geochemical data and P-T estimates obtained from eclogites and gabbros of central Zambia give evidence that they were formed at an oceanic spreading centre and thus that they are relics of a subducted Neoproterozoic oceanic crust (chapter one). The time of eclogite formation is constrained by Sm-Nd garnet-whole rock ages of c. 600 Ma (chapter one).

3.4 Sample localities

Zambesi Belt – *Chowe River section*

The whiteschist occurrence of the Zambesi Belt belongs to the Chongwe River Area and is located close to the Chowe River (Fig. 3.3 & Z4 in Fig. 3.2). The rock types in this area were first described by Vrana & Barr (1972). Following Barr (mapped in 1970, publ. 1997), the migmatic and leucocratic Chalenga Gneiss, porphyroblastic two-feldspar and muscovite gneisses as well as migmatites form the basement in this area (Fig. 3.3). This basement is locally overlain by the Mesoproterozoic Muva Supergroup which is composed of the Rufunsa Metavolcanic Formation and the Chakwenga River Schist Formation. The Rufunsa Metavolcanic Formation consists of amphibolites and a kyanite-bearing chlorite schist unit to which the investigated metapelites, whiteschists and gedrite-cordierite-kyanite gneisses belong. The Chakwenga River Schist Formation consists of biotite-plagioclase schists, amphibolites and calc-silicate rocks (Fig. 3.3).

Lufilian Arc – *Domes region*

Three localities of whiteschists in the Lufilian Arc were chosen for the investigation. All are situated in the Domes region and each of the localities belongs to a different dome, which are from west to east: the Kabompo Dome, the Mwombezhi Dome and the Solwezi Dome (Fig. 3.4). No significant differences in the lithological composition of the domes have been observed (e.g., Cosi et al., 1992). The contact between rocks of the lower Katanga Supergroup and the basement rocks of the domes are not clearly defined and usually interpreted as sheared. The basement consists of biotite gneisses, schistose gneisses and rare migmatites. The Katanga Supergroup within and around the domes mainly consists of the lower units of the Roan Group, which includes Mg-rich quartzites, quartz-mica schists, metapelites and amphibolites. Whiteschists usually occur close to the contact between the basement and the Roan Group and are interpreted to belong to the lowest part of the cover unit. They are mainly exposed at the rims of the domes, but rare outcrops exists within

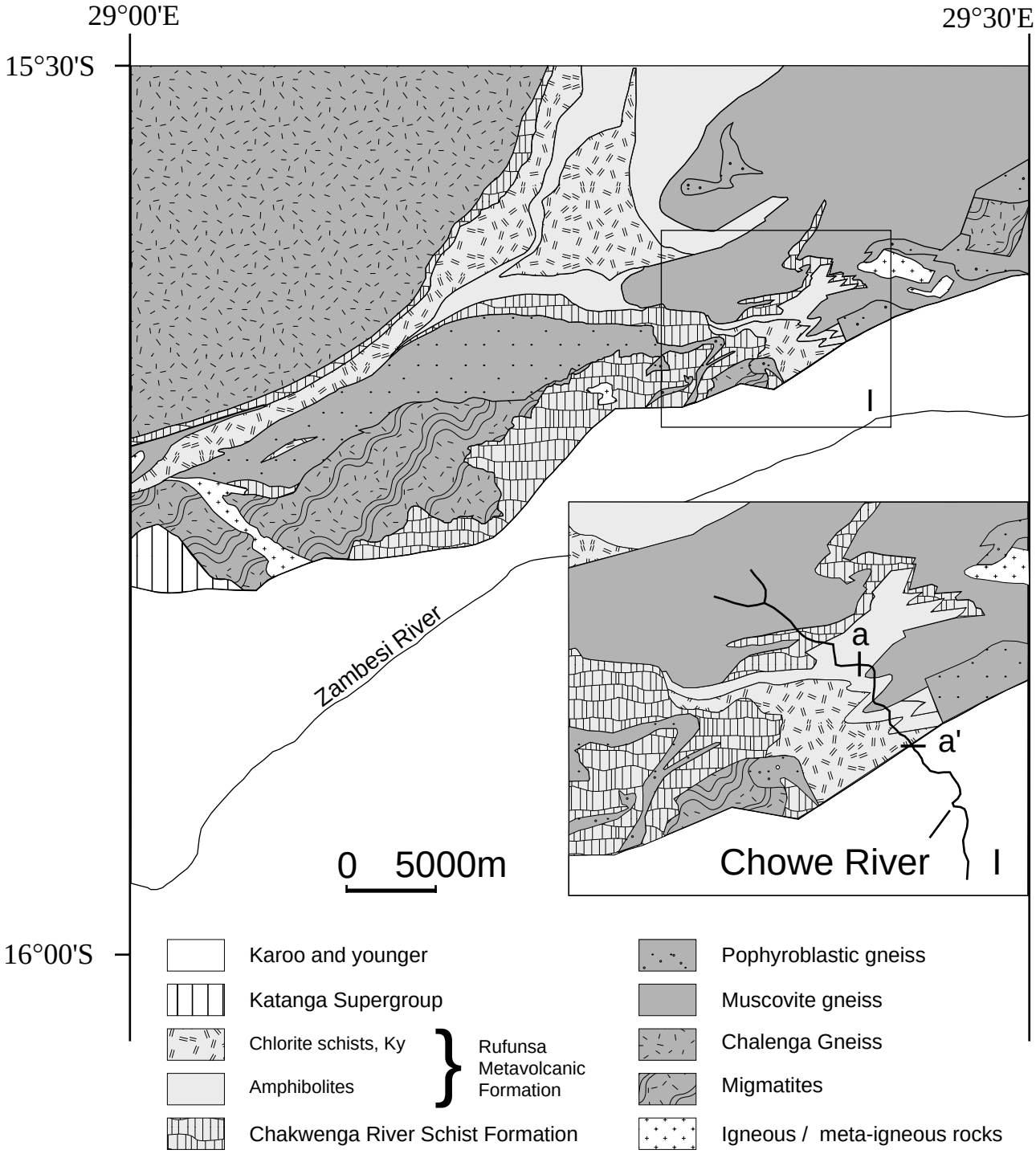

Fig. 3.3 Simplified geological map of the Chongwe River Area after Barr (1997). Inset map shows the sampled river section (a – a').

the domes. In addition, biotite-kyanite-garnet gneisses and garnet-amphibolites were sampled within the Solwezi Dome. The basement rocks came from the Kabompo (tonalitic gneiss) and the Solwezi dome (banded two-mica gneiss) (Fig. 3.4).

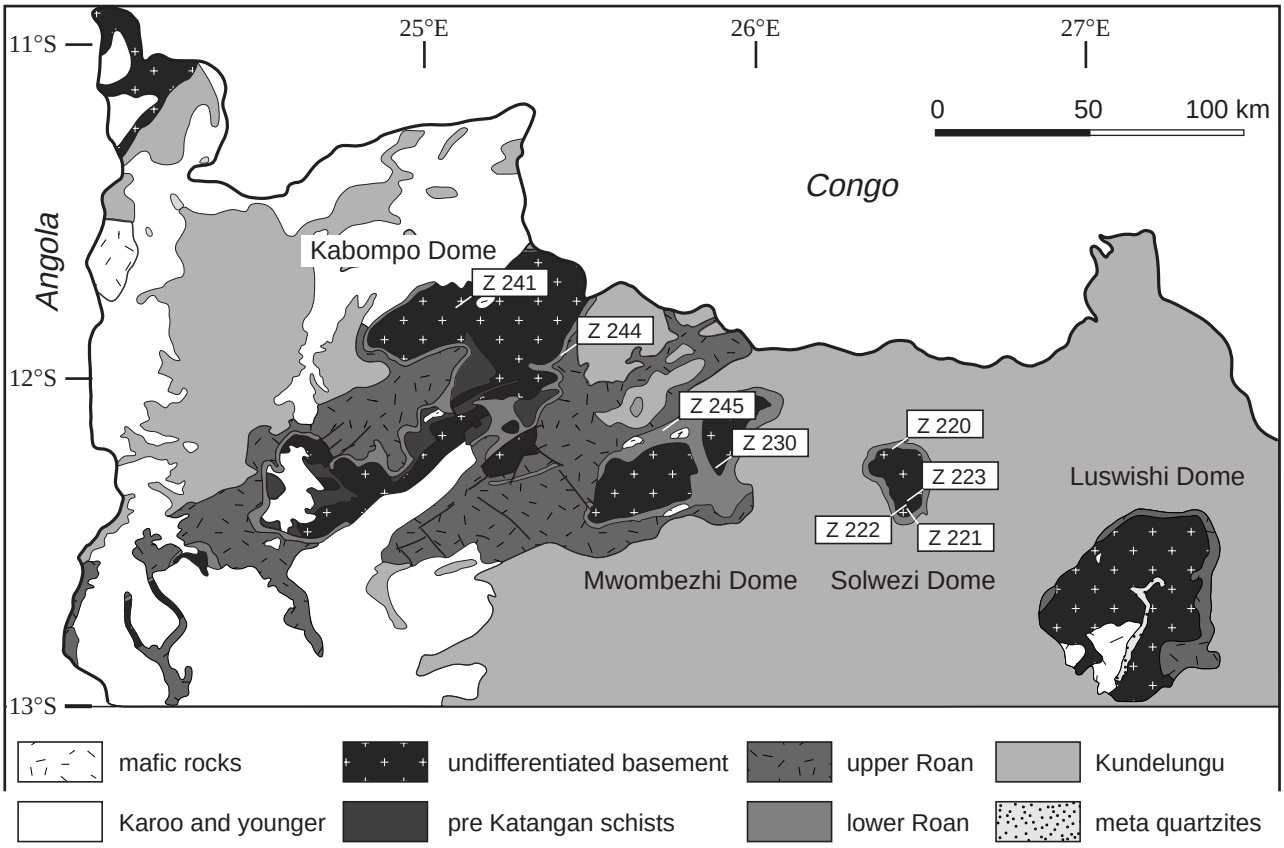

Fig. 3.4 Simplified geological map of the Domes Region with sample localities after Thieme and Johnson (1977). Thin lines indicate geological boundaries, while the thick lines indicate political borders.

3.5 Petrography and mineral chemistry

In order to constrain metamorphic P-T conditions minerals were analysed with the electron microprobe using a CAMECA CAMEBAX and a JEOL 8900 R microprobe at Kiel university. Typical operating conditions were 15 kV acceleration voltage, 15 nA beam current on the Faraday cup and a focussed beam. The matrix correction of the raw counts was made using the PAP- (CAMECA CAMEBAX) and the Citzaf-software (JEOL 8900 R). Mineral assemblages and representative microprobe analyses are given in Tables 3.1 – 3.11. Mineral abbreviations are from Kretz (1983).

3.5.1 Zambesi Belt: Whiteschists and associated rocks

The *whiteschists* of the Chowe river occur as two varieties. The greyish white variety (whiteschist sensu stricto) contains the assemblage talc-kyanite-cordierite-quartz-chlorite-hematite-tourmaline±albite±phlogopite and rutile. Kyanite may be cm-sized, while all other minerals are mainly in the mm-range. The contact between talc and kyanite is characterised by a reaction rim of cordierite (Fig. 3.5a). Cordierite is completely altered to pinite. Poor quality analyses of the pinite suggest low X_{Fe} values of 0.07 to 0.10. Talc has a high alumina content with Al ≈ 0.20-0.40 p.f.u., Cl or F were not detected. The X_{Fe} value is around 0.03. Tourmaline is Fe-rich

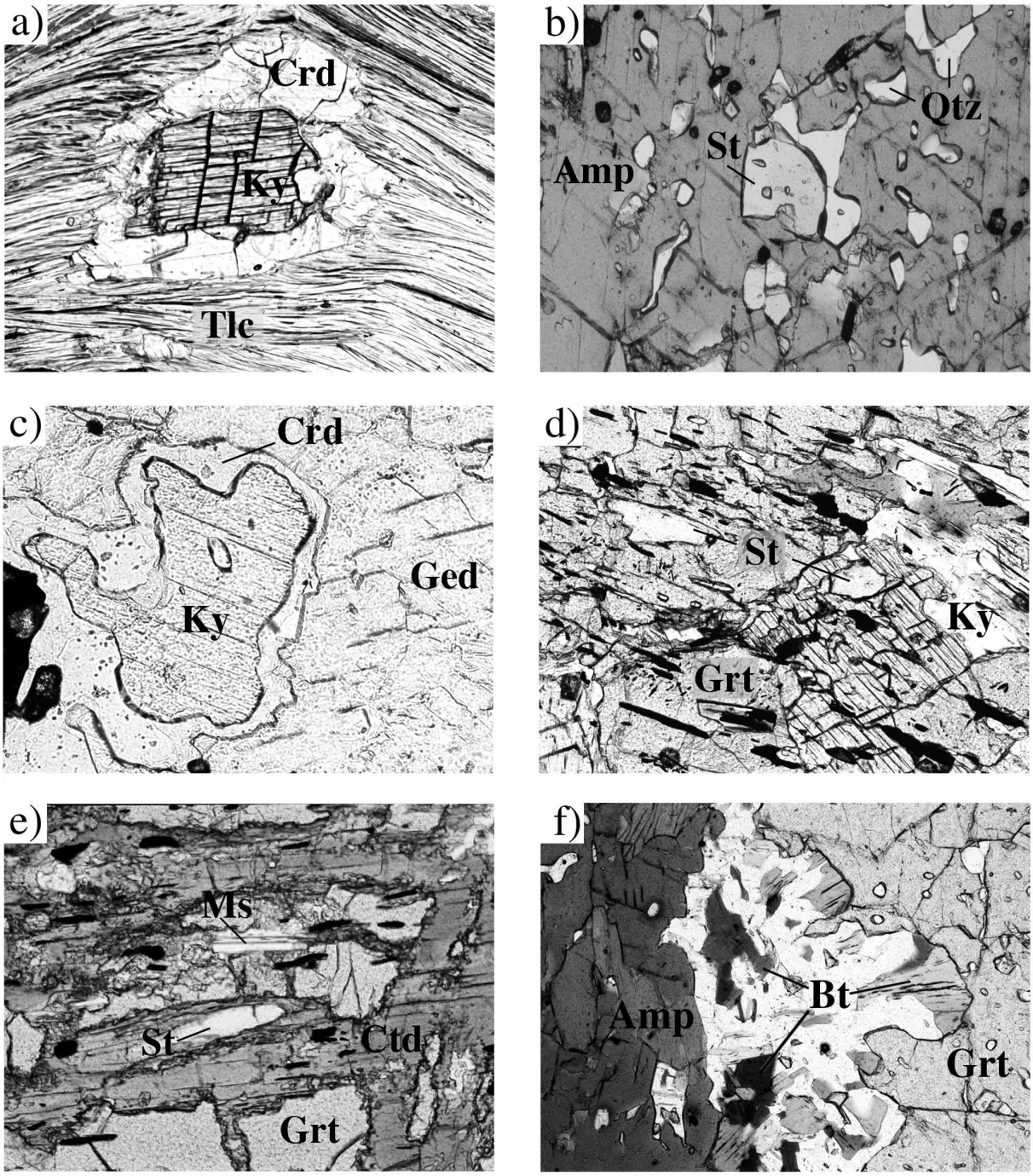

Fig. 3.5 a) Kyanite in a matrix of talc and quartz surrounded by a rim of pinitised cordierite. Quartz is not shown. Chowe River area, whiteschist (Z 103-12). Field of view c. 1 mm;
b) Relic staurolite as inclusion in hornblende. Chowe River area, Ged-Crd-Ky gneiss (Z 103-2). Field of view c. 1mm;
c) Kyanite and gedrite are separated by a cordierite-rim surrounding kyanite, black mineral is ilmenite. Chowe River area, Ged-Crd-Ky gneiss (Z 103-2). Field of view c. 0.75 mm;
d) Staurolite as inclusion in porphyroblastic garnet and kyanite. Black mineral is ilmenite, white lath is muscovite and the dark grey mineral is chlorite. Chowe River area, metapelite (Z 270-5). Field of view c. 1.5 mm;
e) Late stage chloritoide grown along cracks in garnet and surrounding former staurolite inclusions. Chowe River area, metapelite (Z 270-6). Field of view c. 0.75 mm;
f) Garnet resorption and resulting biotite-plagioclase intergrowth. Biotite and plagioclase form rims between garnet and amphibole. Solwezi Dome, Grt-amphibolite (Z 222-1). Field of view c. 10 mm.

Tab. 3.1 Mineral assemblages of analysed samples.

Sample	type	Location	Amp	Bt	Chl	Crd	Ctd	Grt	Ky	Ms	Pl	St	Tlc
8HC 234	+	Z		x	x				x		x		x
Z 103-2	-	Z	x	x	x	x			x			x	x
Z 103-12	+	Z			x	x			x				
Z 270-5	-	Z		x	x			x	x	x	x	x	
Z 270-6	-	Z			x		x	x	x	x	x	x	
Z 272-1b	+	Z			x				x	x	x		x
Z 220-1	-	L	x	x						x	x		
Z 220-7	+	L		x	x				x	x			
Z 221-1	-	L		x				x	x		x		
Z 222-1	-	L	x	x				x			x		
Z 223-1	-	L	x					x			x		
Z 230-1	+	L							x				x
Z 241-1	-	L	x	x							x		
Z 244-1	+	L							x				x
Z 245-1	+	L							x				x

+ indicates whiteschist; - indicates non-whiteschist; Z Zambesi Belt; L Lufilian Arc.

dravite. Sample 8HC 234 (described by Vrana & Barr, 1972) displays an equilibrium mineral assemblage of high-alumina talc-quartz-albite(Ab_{99})-kyanite. This assemblage, which occurs also as inclusions in kyanite, is interpreted to represent the equilibrium assemblage during peak metamorphic conditions. Phlogopite occurs only as matrix mineral and is related to the retrograde evolution of this rock. The more greenish variety of whiteschist, contains less or no talc but more Mg-chlorite (X_{Fe} = 0.03). In some samples kyanite is surrounded by sericite, whereas in other samples kyanite is completely replaced by a fine grained intergrowth of sericite, talc and quartz.

The mineral assemblages of the *gedrite-cordierite-kyanite gneiss* are gedrite-hornblende-quartz-kyanite-cordierite±talc±mg-chlorite ±phlogopite and in some rocks staurolite also occurs as inclusion in both amphiboles and quartz (Fig. 3.5b). The amphiboles are cm-sized nematoblasts, while all other minerals display usually grain sizes in the mm-range. However, cordierite may also form more than 10 cm large crystals segregated along cracks and in veins. Unzoned gedrite (X_{Fe} = 0.17–0.21) and tschermakitic hornblende (X_{Fe} = 0.17–0.20) are intergrown and constitute up to 70 % of the rock. Staurolite inclusions have very low ZnO contents (≤0.1 wt%) and X_{Fe} values are between 0.61 and 0.62. Kyanite is closely associated with orthoamphibole and is always surrounded by a reaction rim of cordierite (X_{Fe} = 0.11–0.12; $Na_2O \leq 0.3$ wt%) (Fig. 3.5c). Cordierite is always formed during the late-stage metamorphic evolution. Quartz is a matrix mineral, but is also common as inclusion in poikiloblastic amphibole and in intergrowths with cordierite. Locally, retrograde talc forms small flakes along rims of gedrite. Fluorine and Cl contents of talc and gedrite are ~0.05 and ~0.01 wt%, respectively. Common accessories are Fe-rich dravite, phlogopite, ilmenite and rutile.

Metapelites are rare in the river section. They have the mineral assemblage garnet-quartz-white mica-plagioclase-kyanite-staurolite-chlorite±biotite±chloritoid. Grain sizes are in the mm-range except for garnet and rare staurolite, which reach cm-size. Garnet shows sigmoidal inclusion trails of kyanite, staurolite and ilmenite, interpreted as indicating synkinematic garnet growth. Garnet is rich in almandine, with Alm_{72-82}, Grs_{06-16}, Prp_{03-13} and Sps_{01-07} (Figs. 3.6a, b). The garnet zonation is interpreted to be of prograde origin with higher X_{Fe} values, spessartine and grossular contents in cores than at rims, while almandine and pyrope contents increase towards the rim. The metapelites display several textural types of muscovite, within and crosscutting the foliation but all have a similar chemical composition. Si-contents cluster around 3.08–3.12 p.f.u. and the X_{Fe} values are around 0.62–0.69. Biotite is only present in some of the studied metapelites and is strongly chloritised in most samples. Biotite grains that are only slightly affected by retrogression show exsolution of ilmenite at the rims and have a low Ti content (0.11–0.12 p.f.u.) and a low X_{Fe} value of around 0.58–0.62. Plagioclase is common as a matrix mineral in almost all samples except in sample Z 270-6, where plagioclase as well as kyanite

Tab. 3.2 Representative amphibole analyses and structural formulae.

Sample	Z 103-2	Z 103-2	Z 103-2	Z 103-2	Z 103-2	Z 103-2	Z 222-1	Z 222-1	Z 223-1	Z 223-1
Analysis	camp1p1	camp1p7	camp1p10	oamp1p1	oamp1p2	oamp2p1	camp1p2	camp1p4	camp5p13	camp2p5
Location	rim-crd	rim-oamp	core	rim-camp	core	rim	rim-grt	core	rim-grt	core
SiO_2	44.97	45.23	44.87	52.82	52.04	50.38	37.83	39.84	38.79	41.42
TiO_2	0.47	0.39	0.37	0.05	0.09	0.15	0.36	0.62	0.49	0.77
Al_2O_3	15.57	14.39	13.55	5.85	6.00	7.79	18.26	16.06	16.90	14.37
FeO	11.07	10.46	10.97	15.39	15.19	16.12	19.23	18.10	19.46	18.34
MgO	14.08	14.67	15.08	23.09	23.18	21.27	6.31	7.54	6.33	8.42
MnO	0.08	0.06	0.01	0.09	0.09	0.09	0.29	0.23	0.27	0.23
CaO	10.55	10.80	10.52	0.49	0.52	0.49	11.49	11.57	11.50	11.70
Na_2O	1.45	1.31	1.22	0.53	0.54	0.65	1.36	1.35	1.49	1.43
K_2O	0.20	0.18	0.19	0.00	0.00	0.01	1.50	1.40	1.09	0.79
Cl	0.04	0.04	0.03	0.01	0.00	0.01	1.17	0.92	0.91	0.59
Total	98.47	97.53	96.79	98.31	97.67	96.97	97.80	97.64	97.22	98.07
Structural formulae on a basis of 23 oxygens										
Si	6.412	6.497	6.512	7.387	7.332	7.188	5.847	6.102	6.004	6.271
Al^{IV}	1.588	1.503	1.488	0.613	0.668	0.812	2.153	1.898	1.996	1.729
Al^{VI}	1.028	0.934	0.830	0.352	0.328	0.499	1.174	1.000	1.088	0.835
Ti	0.050	0.043	0.040	0.006	0.010	0.016	0.042	0.072	0.057	0.088
Fe^{2+}	1.319	1.257	1.331	1.800	1.790	1.924	2.486	2.318	2.519	2.322
Mg	2.992	3.141	3.262	4.814	4.869	4.523	1.454	1.721	1.461	1.900
Mn	0.010	0.007	0.002	0.010	0.010	0.011	0.038	0.030	0.035	0.030
Ca	1.612	1.662	1.635	0.073	0.079	0.076	1.903	1.899	1.907	1.898
Na	0.400	0.366	0.344	0.143	0.148	0.181	0.408	0.401	0.447	0.420
K	0.036	0.032	0.035	0.000	0.000	0.002	0.296	0.274	0.215	0.153
Total	15.447	15.441	15.479	15.197	15.234	15.232	15.799	15.715	15.729	15.646
XFe	0.31	0.29	0.29	0.27	0.27	0.30	0.63	0.57	0.63	0.55

Tab. 3.3 Representative biotite analyses and structural formulae.

Sample	Z 221-1	Z 221-1	Z 222-1	Z 222-1	Z 270-5	Z 270-5
Analysis	bt4p2	bt6p5	bt1p4	bt2p4	bt1p1	bt5p1
Location	near grt	matrix	corona	corona	matrix	matrix
SiO_2	36.56	37.12	36.96	36.47	35.50	35.16
Al_2O_3	18.77	18.33	17.10	16.92	18.48	18.04
TiO_2	0.67	1.25	2.17	2.15	1.97	2.10
Cr_2O_3	0.00	0.05	0.04	0.00	0.01	0.02
FeO	15.39	13.78	17.11	17.73	22.18	23.13
MgO	13.24	14.36	12.21	12.28	8.99	7.86
MnO	0.09	0.03	0.17	0.16	0.06	0.00
CaO	0.00	0.00	0.04	0.03	0.00	0.00
Na_2O	0.30	0.36	0.19	0.18	0.14	0.13
K_2O	8.88	8.61	9.28	9.48	9.74	9.38
Cl	0.34	0.22	0.54	0.51	n.d.	n.d.
Total	94.23	94.10	95.81	95.91	97.07	95.82
Structural formulae on a basis of 11 oxygens						
Si	2.756	2.771	2.780	2.755	2.693	2.713
Al^{IV}	1.245	1.230	1.221	1.245	1.307	1.287
Al^{VI}	0.424	0.383	0.296	0.262	0.346	0.353
Ti	0.038	0.070	0.123	0.122	0.112	0.122
Cr	0.000	0.003	0.002	0.000	0.001	0.001
Fe^{2+}	0.970	0.860	1.076	1.121	1.407	1.493
Mg	1.487	1.598	1.369	1.383	1.017	0.904
Mn	0.006	0.002	0.011	0.010	0.004	0.000
Total	2.924	2.916	2.876	2.897	2.887	2.873
Ca	0.000	0.000	0.003	0.003	0.000	0.000
Na	0.043	0.052	0.028	0.026	0.021	0.019
K	0.854	0.820	0.891	0.914	0.943	0.923
Total	0.897	0.872	0.921	0.942	0.964	0.942
XFe	0.39	0.35	0.44	0.45	0.58	0.62

Tab. 3.4 Representative chlorite analyses and structural formulae.

Sample	Z 270-5	Z 270-5	Z 270-6	Z 270-6	Z 272-1b	Z 272-1b
Analysis	chl4p1	chl5p1	chl1p5	chl2p6	chl1p2	chl2p1
Location	matrix	matrix	matrix	matrix	matrix	matrix
SiO_2	24.50	22.72	22.75	22.49	29.59	30.00
Al_2O_3	22.33	22.41	23.08	22.91	25.44	25.12
TiO_2	0.12	0.06	0.08	0.09	0.07	0.00
Cr_2O_3	0.07	0.03	0.02	0.00	0.00	0.00
FeO	29.06	37.31	35.68	36.68	1.55	1.56
MgO	12.56	6.21	7.47	6.66	31.99	31.74
MnO	0.00	0.03	0.02	0.11	0.10	0.04
CaO	0.00	0.01	0.02	0.00	0.03	0.00
Na_2O	0.00	0.01	0.01	0.03	0.14	0.11
K_2O	0.08	0.01	0.00	0.00	0.28	0.21
Total	88.72	88.8	89.13	88.97	89.18	88.78
Structural formulae on a basis of 28 oxygens						
Si	5.204	5.061	4.997	4.984	5.392	5.479
Al^{IV}	2.796	2.939	3.003	3.016	2.608	2.521
Al^{VI}	2.794	2.945	2.972	2.968	2.855	2.886
Ti	0.019	0.010	0.013	0.015	0.010	0.000
Cr	0.012	0.005	0.003	0.000	0.000	0.000
Fe^{2+}	5.162	6.951	6.554	6.798	0.236	0.238
Mg	3.977	2.062	2.446	2.200	8.689	8.642
Mn	0.000	0.006	0.004	0.021	0.016	0.007
Ca	0.000	0.002	0.005	0.000	0.005	0.000
Na	0.000	0.004	0.004	0.013	0.048	0.040
K	0.022	0.003	0.000	0.000	0.065	0.049
Total	11.987	11.988	12.002	12.015	11.924	11.862
XFe	0.56	0.77	0.73	0.76	0.03	0.03

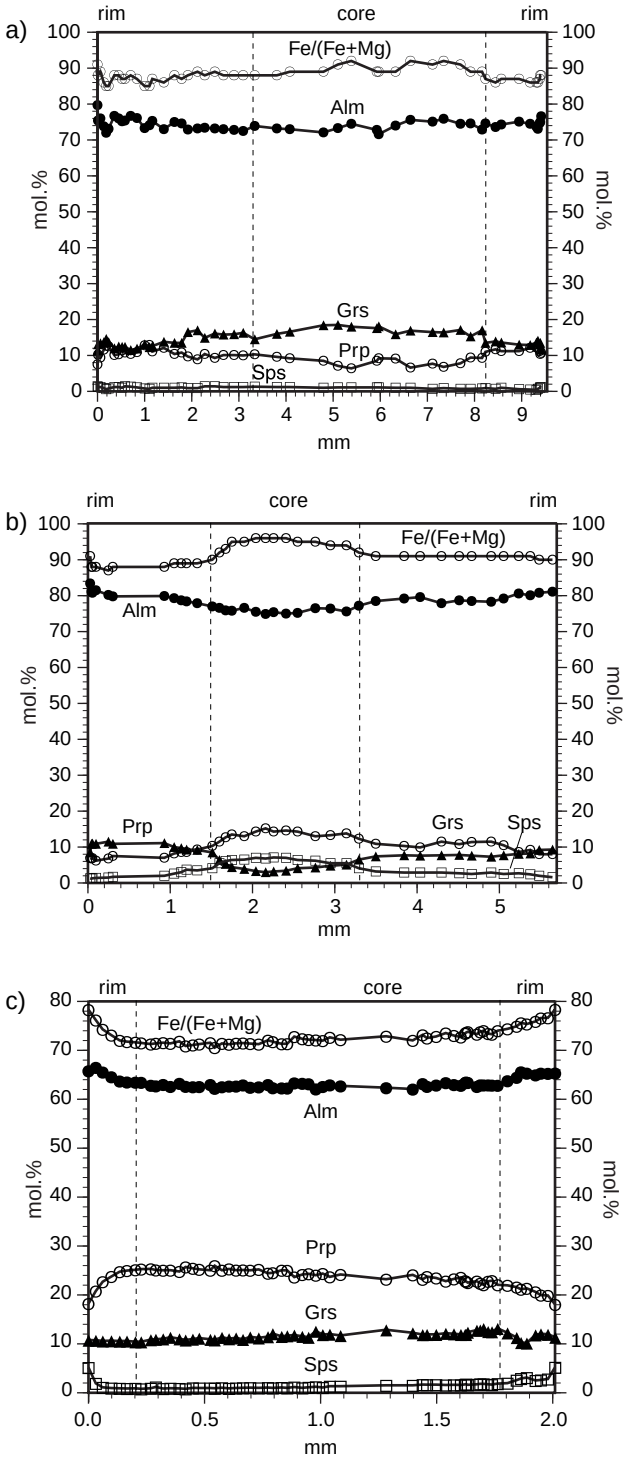

Fig. 3.6 Garnet zoning profiles, a) metapelite with matrix Ky (Z 270-5), b) metapelite with Ky only as inclusion in Grt (Z 270-6) from the Chowe River section and c) Bt-Ky-Grt gneiss from the Solwezi Dome (Z 221-1).

only occurs as tiny inclusions in garnet. The An-content increases slightly from core to rim in the matrix plagioclase (An_{44}-An_{47}) and in plagioclase inclusions in garnet (An_{22}-An_{28}). In some rocks kyanite and garnet contains inclusions of staurolite (X_{Fe} = 0.85–0.93 and ZnO = 1.3–2.4 wt%) (Fig. 5d). Chloritoid (X_{Fe} = 0.91–0.92) formed during retrogression, occurs along cracks in garnet and replaces staurolite inclusions (Fig. 3.5e). Additionally chloritoid surrounds and replaces staurolite in the matrix. Chlorite (X_{Fe} = 0.56–0.77) partially replaces biotite and/or garnet in all metapelites and is interpreted as a retrograde phase.

Tab. 3.5 Representative chloritoid analyses and structural formulae.

Sample	Z 270-6	Z 270-6	Z 270-6
Analysis	ctd1p2	ctd1p5	ctd2p3
Location	rim-St	core	rim-Grt
SiO_2	24.18	24.38	24.44
Al_2O_3	39.99	40.27	40.10
TiO_2	0.00	0.02	0.01
Cr_2O_3	0.03	0.04	0.00
FeO	26.77	26.43	26.60
MgO	1.31	1.56	1.57
MnO	0.18	0.12	0.11
CaO	0.00	0.00	0.01
Na_2O	0.00	0.01	0.00
Total	92.46	92.82	92.84
Structural formulae on a basis of 12 oxygens			
Si	2.021	2.024	2.030
Al^{IV}	3.000	3.000	3.000
Al^{VI}	0.939	0.940	0.925
Ti	0.000	0.001	0.001
Cr	0.002	0.003	0.000
Fe^{2+}	1.871	1.835	1.848
Mg	0.163	0.193	0.194
Mn	0.013	0.008	0.008
Ca	0.000	0.000	0.001
Na	0.000	0.002	0.000
Total	2.988	2.981	2.977
XFe	0.92	0.90	0.90

Tab. 3.6 Representative garnet analyses and structural formulae.

Sample	Z 221-1	Z 221-1	Z 222-1	Z 222-1	Z 223-1	Z 270-5	Z 270-5	Z 270-5	Z 270-5	Z 270-6	Z 270-6	Z 270-6	Z 270-6
Analysis	grt1p60	grt1p25	grt4p21	grt4p40	grt1p5	grt1p4	grt1p5	grt1p23	grt1p25	grt2p3	grt2p4	grt2p20	grt2p22
Location	rim	core	core	rim	core	rim	rim	core	core	rim	rim	core	core
SiO_2	37.84	38.63	37.74	38.16	38.82	38.11	37.86	38.00	37.97	37.49	37.51	37.09	37.36
Al_2O_3	21.78	22.02	21.50	21.77	21.96	21.11	21.21	21.14	21.18	20.99	21.17	20.76	20.82
FeO	29.85	29.23	26.61	25.59	27.07	33.39	34.05	33.68	33.76	37.19	37.19	34.73	34.36
MgO	4.63	6.36	2.13	2.78	3.74	3.31	3.26	2.61	2.60	2.83	2.80	0.83	1.05
MnO	2.35	0.49	2.91	0.98	0.75	0.29	0.35	0.55	0.55	0.61	0.64	3.24	2.87
CaO	4.05	4.15	9.35	10.59	9.52	5.28	4.99	5.68	5.92	2.47	2.20	5.14	5.10
Total	100.50	100.88	100.24	99.87	101.86	101.49	101.72	101.66	101.98	101.58	101.51	101.79	101.56
Structural formulae on a basis of 24 oxygens													
Si	5.960	5.982	5.982	6.004	5.992	6.005	5.97	6.001	5.983	5.976	5.977	5.958	5.989
Al	4.044	4.018	4.018	4.036	3.994	3.921	3.942	3.934	3.934	3.943	3.976	3.930	3.933
Fe^{2+}	3.932	3.786	3.528	3.368	3.494	4.400	4.490	4.448	4.449	4.957	4.956	4.665	4.606
Mg	1.086	1.468	0.504	0.650	0.860	0.778	0.766	0.614	0.611	0.672	0.665	0.199	0.251
Mn	0.314	0.064	0.390	0.131	0.098	0.039	0.047	0.074	0.073	0.082	0.086	0.441	0.390
Ca	0.684	0.690	1.588	1.786	1.574	0.891	0.843	0.961	1.000	0.422	0.376	0.885	0.876
Total	6.016	6.008	6.010	5.935	6.026	6.108	6.146	6.097	6.133	6.133	6.083	6.190	6.123
XFe	0.78	0.72	0.88	0.84	0.80	0.85	0.85	0.88	0.88	0.88	0.88	0.96	0.95
Alm	65	63	59	57	58	72	73	73	73	81	82	75	75
Grs	11	11	26	30	26	15	14	16	16	7	6	14	14
Prp	18	24	8	11	14	13	13	10	10	11	11	3	4
Sps	5	1	6	2	2	1	1	1	1	1	1	7	6

$Fe^{2+} = Fe^{tot}$

Tab. 3.7 Representative plagioclase analyses and structural formulae.

Sample	Z 221-1	Z 221-1	Z 222-1	Z 223-1	Z 270-5	Z 270-5	Z 270-6II	Z 270-6II	8HC 234	8HC 234
Analysis	pl2p22	pl4p8	pl4p2	pl1p1	pl1p1	pl3p3	pl4p1	pl6p2	pl2p2	pl5p1
Location	near grt	matrix	corona	corona	rim	core	core	rim	core	core
SiO_2	61.15	62.30	52.45	67.44	57.5	58.17	63.01	62.44	68.18	67.49
Al_2O_3	24.91	23.81	30.69	21.69	27.78	27.07	22.93	24.26	19.33	19.12
Fe_2O_3	0.04	0.06	0.20	0.19	0.05	0.03	0.05	0.07	0.26	0.05
CaO	6.11	4.93	12.78	2.01	9.88	9.16	4.66	5.99	0.09	0.14
Na_2O	7.96	8.69	4.29	9.86	6.13	6.56	9.09	8.25	11.22	11.37
K_2O	0.04	0.05	0.03	0.10	0.03	0.06	0.06	0.03	0.03	0.07
Total	100.21	99.84	100.44	101.28	101.37	101.05	99.8	101.04	99.11	98.24
Structural formulae on a basis of 8 oxygens										
Si	2.708	2.761	2.368	2.914	2.545	2.579	2.793	2.740	3.000	2.999
Al^{IV}	1.300	1.244	1.633	1.105	1.449	1.414	1.198	1.255	1.002	1.001
Total	4.008	4.005	4.001	4.018	3.994	3.993	3.991	3.995	4.002	4.000
Fe^{3+}	0.002	0.002	0.008	0.007	0.002	0.001	0.002	0.002	0.009	0.002
Ca	0.290	0.234	0.618	0.093	0.469	0.435	0.221	0.282	0.004	0.007
Na	0.684	0.747	0.376	0.826	0.526	0.564	0.781	0.702	0.957	0.979
K	0.002	0.003	0.002	0.005	0.002	0.003	0.003	0.002	0.002	0.004
Total	0.977	0.986	1.003	0.931	0.999	1.003	1.007	0.988	0.972	0.992
An	29.7	23.8	62.1	10.1	47.0	43.4	22.0	28.6	0.4	0.7
Ab	70.1	75.9	37.7	89.4	52.8	56.3	77.7	71.2	99.4	98.9
Kfs	0.2	0.3	0.2	0.6	0.2	0.3	0.3	0.2	0.2	0.4

Tab. 3.8 Representative cordierite analyses and structural formulae.

Sample	Z 103-2	Z 103-2
Analysis	crd5p1	crd5p2
Location	rim-ky	rim-ky
SiO_2	50.81	50.53
Al_2O_3	34.09	33.63
TiO_2	0.04	0.00
FeO	2.89	2.66
MgO	12.25	12.30
MnO	0.00	0.01
CaO	0.00	0.04
Na_2O	0.09	0.14
Total	100.17	99.31
Structural formulae on a basis of 18 oxygens		
Si	5.005	5.018
Al^{IV}	0.995	0.982
Al^{VI}	2.963	2.954
Ti	0.003	0.000
Total	2.966	2.954
Fe^{2+}	0.238	0.221
Mg	1.799	1.821
Mn	0.000	0.001
Total	2.037	2.043
Ca	0.000	0.004
Na	0.017	0.027
Total	0.017	0.031
XFe	0.12	0.11

Tab. 3.9 Representative talc analyses and structural formulae.

Sample	Z 103-2	Z10312	Z 103-12	8HC 234	Z 230-1	Z 230-1	Z 244-1	Z 244-1	Z 245-1	Z 245-1
Analysis	tlc1p1	tlc4p1	tlc4p2	tlc5p1	tlc2p3	tlc2bp3	tlc2p2	tlc3p4	tlc1p6	tlc6p1
Location	rim-oamp	matrix	matrix	matrix	matrix	matrix	matrix	matrix	matrix	matrix
SiO_2	59.90	59.83	61.60	61.28	62.30	62.21	61.43	62.12	62.18	62.34
Al_2O_3	3.39	4.41	2.29	2.00	1.42	1.64	2.24	1.70	1.22	1.41
TiO_2	0.13	0.00	0.00	0.06	0.00	0.03	0.20	0.04	0.06	0.09
FeO	4.71	1.80	1.25	0.61	0.28	0.25	0.42	0.34	0.17	0.20
MgO	27.60	29.07	29.80	30.32	29.54	29.28	29.15	29.08	29.51	29.46
MnO	0.04	0.01	0.04	0.00	0.02	0.01	0.00	0.03	0.00	0.01
CaO	0.11	0.01	0.01	0.00	0.00	0.00	0.00	0.00	0.00	0.00
Na_2O	0.29	0.49	0.27	0.16	0.14	0.19	0.20	0.14	0.16	0.15
K_2O	0.03	0.35	0.03	0.02	0.00	0.00	0.00	0.00	0.01	0.00
Total	96.20	95.97	95.36	94.45	93.70	93.62	93.64	93.44	93.30	93.66
Structural formulae on a basis of 22 oxygens										
Si	7.683	7.607	7.832	7.834	7.989	7.981	7.898	7.988	8.003	7.995
Al^{IV}	0.317	0.393	0.168	0.166	0.011	0.019	0.102	0.012	-0.003	0.005
Al^{VI}	0.195	0.268	0.175	0.134	0.204	0.230	0.237	0.245	0.188	0.208
Ti	0.013	0.000	0.000	0.006	0.000	0.003	0.020	0.004	0.005	0.008
Fe^{2+}	0.505	0.191	0.133	0.066	0.030	0.027	0.045	0.036	0.018	0.022
Mg	5.277	5.511	5.649	5.778	5.647	5.600	5.586	5.574	5.662	5.632
Mn	0.004	0.001	0.004	0.000	0.002	0.001	0.000	0.003	0.000	0.001
Ca	0.015	0.002	0.001	0.000	0.000	0.000	0.000	0.000	0.000	0.000
Na	0.072	0.120	0.067	0.040	0.035	0.047	0.050	0.036	0.039	0.038
K	0.005	0.056	0.005	0.004	0.000	0.000	0.000	0.000	0.001	0.000
Total	6.087	6.150	6.032	6.028	5.917	5.908	5.938	5.898	5.913	5.909
Al Total	0.512	0.843	0.661	0.300	0.215	0.248	0.339	0.257	0.186	0.212
XFe	0.087	0.034	0.023	0.100	0.005	0.005	0.008	0.006	0.003	0.004

3.5.2. Lufilian Arc: Whiteschists and associated rocks

The *whiteschists* of the Lufilian Arc have the mineral assemblages: talc-kyanite-quartz-tourmaline-haematite-rutile. The greenish whiteschist variety of the Chowe river was not found, but a brownish variety with the assemblage phlogopite-phengite-quartz-kyanite-chlorite occurs. Kyanite is cm-sized and all other minerals are in the mm-range. Kyanite usually has inclusion free cores and poikiloblastic rims clouded with inclusions. Talc has lower Al contents compared to the Chowe river samples. The mean Al ranges between 0.12 and 0.15 p.f.u, but can reach ~0.20 p.f.u. in some flakes. The X_{Fe} is also lower and ranges between 0.005 and 0.007, assuming Fe^{2+} as Fe^{tot}. Chlorine and F were not detected. Tourmaline is Fe-rich dravite and has greenish cores and yellow rims. There is a sharp boundary between these colour zones which differ in Fe_2O_3 (core ≈ 6.0 wt.%; rim ≈ 3.5 wt.%), MgO (core ≈ 8 wt.%; rim ≈ 10 wt.%), CaO (core ≈ 1.1 wt.%; rim ≈ 0.8 wt.%) and Na_2O (core ≈ 2.0 wt.%; rim ≈ 2.3 wt.%). Hematite is very common and can constitute up to 20 % of the rock. Magnesian-chlorite was not found in any of the investigated whiteschists sensu stricto. The phengite of the brownish variety has Si-contents of about 3.25 p.f.u. and contains 0.5 to 1.0 wt.% Na_2O. The phlogopite has a X_{Fe} value of 0.05-0.06 and contains ~0.8 wt.% TiO_2 and ~0.5 wt.% Na_2O. Within the brownish variety no talc was found and hematite is less common, but Mg-chlorite occurs as a minor phase.

Biotite-kyanite-garnet gneiss: The mineral assemblage is biotite-quartz-plagioclase-kyanite-garnet. Kyanite can occurs in sizes up

Tab. 3.10 Representative staurolite analyses and structural formulae

Sample	Z 103-2	Z 103-2	Z 270-5	Z 270-5	Z 270-6II	Z 270-6II	Z 270-6II
Analysis	st1p1	st1p3	st4p1	st5p2	st3p7	st4p1	st5p3
Location	rim	core	rim	core	core	core	rim
SiO_2	28.58	28.77	28.07	27.8	28.59	27.82	28.62
Al_2O_3	53.42	53.63	53.04	52.94	53.97	54.19	53.99
TiO_2	0.56	0.52	0.68	0.66	0.70	0.62	0.65
Cr_2O_3	0.12	0.02	0.03	0.00	0.02	0.06	0.06
FeO	11.75	11.92	13.33	14.02	12.22	12.19	11.16
MgO	4.22	4.18	1.28	1.18	0.60	0.55	0.46
MnO	0.02	0.06	0.06	0.03	0.09	0.09	0.11
ZnO	0.11	0.00	1.23	1.14	1.47	1.75	2.14
Total	98.78	99.1	97.72	97.77	97.66	97.27	97.19
	Structural formulae on a basis of 46 oxygens						
Si	7.788	7.812	7.826	7.772	7.925	7.764	7.958
Al	17.157	17.163	17.430	17.444	17.632	17.824	17.694
Ti	0.115	0.106	0.143	0.139	0.146	0.130	0.136
Cr	0.026	0.004	0.007	0.000	0.004	0.013	0.013
Fe^{2+}	2.678	2.707	3.108	3.278	2.833	2.845	2.595
Mg	1.714	1.692	0.532	0.492	0.248	0.229	0.191
Mn	0.005	0.014	0.014	0.007	0.021	0.021	0.026
Zn	0.022	0.000	0.253	0.235	0.301	0.361	0.439
Total	29.505	29.498	29.313	29.367	29.111	29.187	29.052
XFe	0.61	0.62	0.85	0.87	0.92	0.93	0.93

Tab. 3.11 Representative muscovite analyses and structural formulae.

Sample	Z 270-5	Z 270-5	Z 270-6II	Z 270-6II
Analysis	ms1p1	ms2p2	ms1p2	ms2p1
Location	matrix	matrix	matrix	matrix
SiO_2	46.17	46.84	46.17	46.39
Al_2O_3	34.66	33.81	34.46	34.31
TiO_2	0.63	0.77	0.61	0.61
Cr_2O_3	0.05	0.02	0.03	0.01
FeO	2.23	2.33	2.71	2.58
MgO	0.55	0.81	0.68	0.67
MnO	0.02	0	0.04	0.00
Na_2O	0.85	0.87	1.09	1.07
K_2O	10.2	10.22	9.76	9.91
Total	95.36	95.67	95.55	95.55
	Structural formulae on a basis of 11 oxygens			
Si	3.084	3.120	3.082	3.095
Al^{IV}	0.916	0.880	0.918	0.905
Al^{VI}	1.813	1.774	1.792	1.793
Ti	0.032	0.039	0.031	0.031
Cr	0.003	0.001	0.002	0.001
Fe^{2+}	0.125	0.130	0.151	0.144
Mg	0.055	0.080	0.068	0.067
Mn	0.001	0.000	0.002	0.000
Total	2.029	2.024	2.046	2.036
Na	0.11	0.112	0.141	0.138
K	0.869	0.868	0.831	0.843
Total	0.979	0.98	0.972	0.981
XFe	0.69	0.62	0.69	0.68

to 1 cm, while all other minerals have grain sizes in the mm-range. Greenish biotite grew within and crosscutting the foliation. Biotite has a greenish colour and matrix biotite differs chemically from biotite associated with garnet. Matrix biotite has X_{Fe} of around 0.36, TiO_2 > 1 wt.% and Cl ≈ 0.20-0.25 wt.%, while biotite associated with garnet has X_{Fe} of around 0.38, TiO_2 < 1 wt.% and Cl ≈ 0.25-0.30 wt.%. Garnet is almandine-rich, with Alm_{62-66}, Grs_{11-12}, Prp_{18-24} and Sps_{1-5}. The garnet zonation is restricted to a small retrograde rim with slightly higher pyrope contents in the cores than at rims, while almandine and spessartine contents increase towards the rim. Also the X_{Fe} value increases from 0.72 to 0.78 towards the rim (Fig. 3.6c). Plagioclase that occurs close to garnet, is slightly zoned with An_{27} in the core and An_{30} at the rim. Matrix plagioclase shows no zoning and has An_{24}. Tiny muscovite flakes occur as inclusion in some quartz and plagioclase grains. Further accessories are apatite and magnetite.

The mineral assemblages of the garnet-amphibolites are amphibole-quartz-garnet-plagioclase±biotite±scapolite±epidote. The amphibole is a ferroan pargasite with TiO_2 contents between 0.5 and 0.9 wt.%. The Cl content ranges between 0.5 and 1.0 wt.%. X_{Fe} values of amphiboles in the matrix are c. 0.55-0.60, and close to garnet they can be as high as 0.62. Most amphiboles contain relics of former pyroxenes in the cores, in some amphiboles tiny inclusions of titanite occur. Garnet is slightly zoned and shows preserved growth zoning and retrograde zoning near the rims. Core compositions are Alm_{56-57}, Grs_{26-28}, Prp_{09-11} and Sps_{09-05} and compositions of the retrograde rims are Alm_{57-60}, Grs_{22-30}, Prp_{11-12} and Sps_{03-06}. The X_{Fe} value range from 0.80 to 0.88, with higher X_{Fe} in the core (~0.88) than at the retrograde rims (~0.84). Plagioclase is zoned with An_{44} in the core and An_{50-56} at the rim. Where plagioclase is associated with garnet and biotite, the An content can increase up to An_{65}. In sample Z 223-1 only albitic

plagioclase (An_{10}) is preserved as inclusion in amphibole. In this rock usually scapolite and associated with epidote occur. Chlorine contents were below the detection limit in epidote. Biotite has TiO_2 contents of 2.2-2.3 wt.%. The Cl content ranges between 0.50 and 0.54 wt.%, and the X_{Fe} value is 0.44-0.45. Biotite is usually associated with garnet and plagioclase (Fig. 3.5f). Ilmenite, magnetite, titanite and apatite are common accessories.

3.6 Reaction history and P-T evolution

3.6.1 Zambesi Belt: Chowe River rocks

Mineral assemblages of the different rock types of the Chowe River section, including whiteschist, gedrite-kyanite-cordierite gneiss and metapelite, indicate amphibolite facies temperatures and pressures. All the rock types also have in common reaction textures pointing to decompression after peak metamorphism (e.g., cordierite-rims surround kyanite). These shared characteristics as well as the close association of the rocks in the field indicate that they experienced the same metamorphic evolution. Most information on the different stages of the metamorphic evolution can be obtained from the metapelites, whilst some crucial reactions also occur in the whiteschists and gedrite-kyanite-cordierite gneisses.
Peak metamorphic conditions were estimated with the garnet-biotite Fe-Mg exchange thermometer and the equilibrium garnet-alumosilicate-quartz-plagioclase (GASP). The Grt-Bt thermometer calibration of Kleemann & Reinhardt (1994) was applied since it considers the influence of Al^{VI} and Ti in biotite and the spessartine content in garnet. Its calibration is based on the two experimental data sets of Ferry & Spear (1978) and Perchuk & Lavrent'eva (1983). For GASP-barometry the calibration of Koziol (1989) was applied.

3.6.1.1 Prograde evolution

A prograde reaction texture is preserved in the gedrite-cordierite-kyanite gneiss, in which staurolite forms inclusions in amphiboles (Fig. 3.5b). These relics are attributed to the reaction

St + Chl ↔ Ged + Ky (1).

Based on observations of natural assemblages in amphibolites in New Hampshire, Spear & Rumble (1986) proposed a petrogenetic grid (FMASH-system) placing this reaction at about 550–600°C (Fig. 3.7). However, these temperatures are not well constrained (Spear, 1993).

The next preserved step on the P-T path is a staurolite-breakdown reaction in Fe-rich metapelites. Inclusions of staurolite in kyanite and garnet indicate that the prograde sliding reaction

St + Ms + Qtz ↔ Grt + Ky (2)

has taken place (Fig. 3.5d). However, the terminal reaction for staurolite-breakdown (Spear & Cheney, 1989)

St + Ms + Qtz ↔ Grt + Ky + Bt (3)

has not been reached. This limits the metamorphic temperatures to below c. 710 °C (Fig. 3.7).

3.6.1.2 Peak-metamorphic conditions

Two different samples of metapelites were investigated and they have slightly different mineral assemblages. One sample contains kyanite in the matrix, in the other kyanite occurs only as inclusion in garnet. The outer parts of garnet in the latter type (sample Z 270-6) contain inclusions of quartz, kyanite and plagioclase, the mineral assemblage which can be used for GASP barometry. Pressure estimates for a relative late stage of garnet growth are based on these inclusions. However, the estimates are hampered by the lack of well constrained temperature information for this

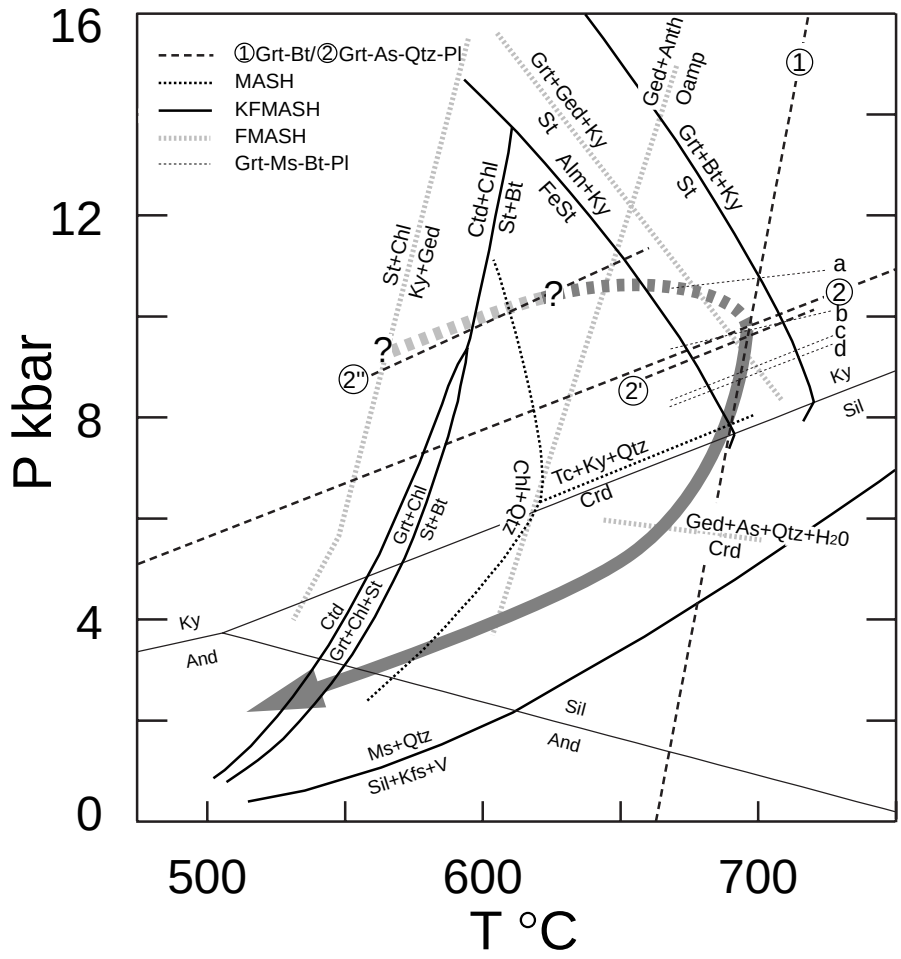

Fig. 3.7 P-T diagram with relevant reaction curves for the P-T evolution of the Chowe River section rocks. Al_2SiO_5 triple point after Holdaway (1971), MASH system for whiteschists after Massonne (1989), KFMASH system for metapelites after Spear & Cheney (1989) and FMASH system for cordierite-gedrite gneisses modified after Spear & Rumble (1986). Curve (1): garnet-biotite thermometry (Kleemann & Reinhardt, 1994). Barometry with garnet-alumosilicate-quartz-plagioclase equilibrium (Koziol, 1989): curve (2) using matrix plagioclase and matrix garnet rim (Z 270-5), curve (2') using rim of plagioclase inclusion and surrounding garnet rim (Z 270-6), and curve (2'') using core of plagioclase inclusion in garnet (Z 270-6) as explained in text. Tiny dashed curves a-d: garnet-muscovite-biotite-plagioclase barometry (a: Powell & Holland, 1988; b: Hoisch -Mg, 1990; c: Hodges & Crowley, 1985; d: Hoisch –Fe, 1990).

stage of the P-T evolution. Because the inclusions occur only in the outer parts of garnet, we assume that they were probably trapped at/or above 600°C and not close to the Grt-in temperature near 500 °C. According to the preserved prograde garnet growth zoning, which shows a slightly higher Grs content and X_{Fe} value in the core than in the rim (Fig. 3.6b), the prograde heating path seems to have had a flatter dP/dT slope than the GASP-equilibrium curve (Fig. 3.7). Plagioclase inclusions (c. 0.10-0.01 mm) are zoned from core (An_{21}) towards the rim (An_{32}), while the surrounding garnet is zoned towards the inclusion (Grs_{14} and Grs_{11}). Assuming that the rims of the plagioclase inclusions (An_{32}) were in equilibrium with the surrounding Grt rims (Grs_{11}) and that the Pl cores (An_{21}) were in equilibrium with those parts of the garnet not affected by the late stage equilibration with the

inclusions (Grs_{14}), both composition pairs were used for reconstructing the pressure evolution. The pressure estimates of 10-11 kbar using core compositions of Pl inclusion and corresponding garnet compositions at an assumed temperature of about 600–650 °C are attributed to a stage of the prograde P-T evolution (curve 2'' in Fig. 3.7). The combination of the inclusion rim with the surrounding garnet rim results in a GASP equilibrium curve c. 2 kbar lower than the one of the core estimates (curve 2' in Fig. 3.7). The latter pressure estimate is similar to that for peak metamorphism which was calculated from rim compositions of minerals (Grt, Pl, Bt) of the rock sample that contains kyanite in the matrix (sample Z 270-5). These peak estimates reveal conditions of about 700 ±25 °C at 10 ±1 kbar (curves 1 and 2 in Fig. 3.7). Garnet-muscovite-biotite-plagioclase (GMBP) barometry (Hodges & Crowley, 1985; Powell & Holland, 1988; Hoisch, 1990) yields similar estimates of c. 9 to 11 ±1 kbar at 700 ±25 °C (curves a-d in Fig. 3.7). The high Al_2O_3 content of talc in the whiteschists is in agreement with the high temperatures obtained (Massonne, 1995).

3.6.1.3 Retrograde evolution

Three different stages of the retrograde P-T path can be deduced from mineral reaction textures. The first stage is based on cordierite reaction rims surrounding kyanite in a talc-quartz matrix (Fig. 3.5a), which can be attributed to the decompression reaction

$$Tlc + Ky + Qtz \leftrightarrow Crd \quad (4)$$

(Schreyer & Seifert, 1969; Massonne, 1989).

In the gedrite-cordierite-kyanite gneiss cordierite again forms rims surrounding kyanite (Fig. 3.5c). Applying the FMASH grids of Spear & Rumble (1986) and Schumacher & Robinson (1987), this cordierite rim is interpreted as a decompression texture as well (Fig. 3.7). The corresponding reaction is

$$Ged + Ky + Qtz \leftrightarrow Crd \quad (5).$$

A third retrograde stage was found in metapelites, where chloritoid replaces staurolite and garnet (Fig. 3.5e). First chlorite was produced by the resorption of biotite according to the reaction

$$St + Bt + Qtz + H_2O \leftrightarrow Chl + Grt + Ms \quad (6).$$

Subsequently, chloritoid formed by the reaction

$$Grt + St + Chl \leftrightarrow Ctd + Ms + Qtz \quad (7).$$

The grid of Spear & Cheney (1989) places these reactions between 550 and 600 °C (Fig. 3.7).

3.6.2 Lufilian Arc: Solwezi Dome rocks

Fresh rock outcrops are rare because of the strong weathering and the widespread lateritic cover and thus, the amount of samples and lithologies which can be used for petrological investigations are restricted. However, peak metamorphic conditions are estimated using the same geothermobarometers as described above as well as the garnet-hornblende Fe-Mg exchange thermometry (Graham & Powell, 1984) and the garnet-quartz-plagioclase-biotite equilibrium (Hoisch, 1990).

3.6.2.1 Metamorphic evolution and P-T path

The chemical profiles of garnets of the investigated amphibolites and gneisses show flat patterns as well as slightly preserved growth zoning, but usually only the outer part of the garnet rims are affected by retrogression. Combining the most magnesium rich part of the prograde garnet zoning with matrix amphiboles (amphibolite) and cores of homogenised garnets with matrix plagioclase cores (biotite-kyanite-garnet gneiss), estimates

of peak-temperatures give c. 740-755 ±25 °C at about 13 ±1 kbar (Fig. 3.8).

Information about the metamorphic evolution is only sparse. In amphibolites retrograde garnet resorption is probably related to the reaction

Grt + Amp ↔ Bt + Pl + Qtz (8),

which resulted in plagioclase-biotite±quartz coronas between garnet and amphibole (Fig. 3.5f). Since only little biotite was formed, the necessary K for the biotite formation could have come from the related amphibole consumption (> 1wt.% K_2O). In the biotite-kyanite-garnet gneiss garnet resorption can be attributed to the reaction

Grs + Qtz + Ky ↔ An (9)

and indicates decompression (like reaction 8). The newly formed plagioclase displays higher An contents (An_{30}) than the peak stage plagioclase (An_{24}). Using the products of reaction 8 and 9 as well as matrix biotite (biotite-kyanite-garnet gneiss) and the rim compositions of garnet, temperature estimates give c. 610-650 ±25 °C at pressures of about 9-10 ±1 kbar (Fig. 3.8).

Combining the P-T estimates and decompression features obtained from the amphibolites and gneisses, a clockwise P-T evolution is indicated with peak metamorphic conditions of about 13 ±1 kbar and temperatures of c. 750 ±25 °C (Fig. 3.8). P-T conditions of cooling and decompression are estimated with garnet-biotite thermometry as well as GASP- and garnet-plagioclase-quartz-biotite barometry. The proposed isothermal decompression after peak metamorphism is based on plagioclase ± biotite reaction-rims surrounding garnet in amphibolites and garnet resorption in the biotite-kyanite-garnet gneisses, assuming that the barometers closed for element exchange at higher temperatures than the thermometers. Hence the P-T path

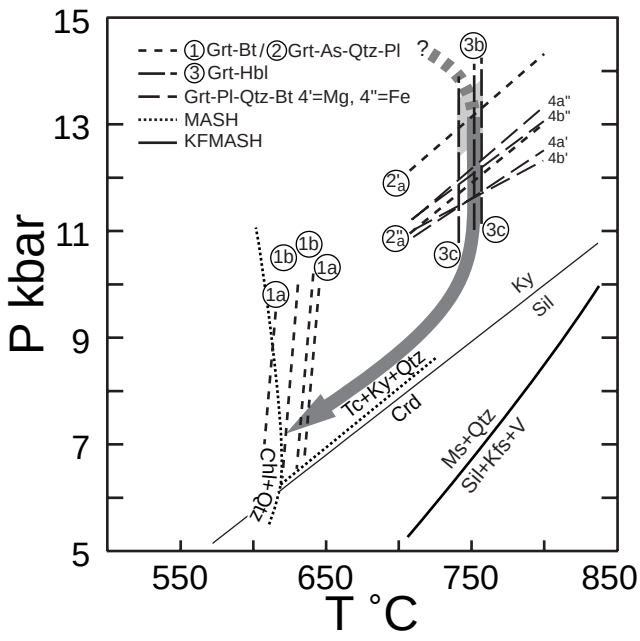

Fig. 3.8 P-T diagram with relevant reaction curves for the Solwezi Dome rocks and Lufilian Arc whiteschists. KFMASH system after Spear & Cheney (1989), MASH system for whiteschists after Massonne (1989). Thermobarometric results: Letters indicate the sample: a = Z 221-1, b = Z 222-1 and c = 223-1; curve (1) garnet-biotite thermometry (Kleemann & Reinhardt, 1994), curve (2) garnet-alumosilicate-quartz-plagioclase equilibrium (Koziol, 1989) with (2') indicate peak and (2'') retrograde conditions, (3) garnet-hornblende thermometry (Graham & Powell, 1984), 4 garnet-plagioclase-quartz-biotite equilibrium (Hoisch, 1990). Thick arrows show possible P-T path. Shaded area indicate uncertainties of P-T estimates.

crosses the barometer equilibrium curves before that of the thermometers (Fig. 3.8).

3.6.3 Discussion and comparison with previous studies

Petrographic and mineral chemical data of Zambesi Belt samples indicate peak-metamorphic conditions of about 700 ±25 °C at 10 ±1 kbar, with peak pressures presumably attained prior to peak temperatures. Mineral reaction textures suggest a clockwise P-T path with constant or slightly decreasing pressure

from maximum pressure values towards the maximum temperature. Subsequent to the thermal peak, the rocks experienced nearly isothermal decompression. The following cooling history is documented by chloritoid formation at the expense of garnet and staurolite. Also the investigations of the Lufilian Arc samples give high-pressure amphibolite facies peak-metamorphic conditions with 750 ±25 °C at 13 ±1 kbar. The mineral reactions, which are related to the garnet resorption, indicate a similar clockwise P-T evolution to that of the Zambesi Belt rocks. The only difference between the P-T evolutions of the Lufilian Arc and Zambesi Belt is the stronger exhumation of the Zambesi Belt rocks into the cordierite stability field (Figs. 3.7, 3.8), indicated by cordierite rims surround kyanite in gedrite-kyanite gneisses and very rare (one sample) in whiteschists. In the Lufilian Arc samples late stage cordierite was not found, probably simply because the retrograde reactions are poorly developed in the Lufilian Arc whiteschists (Mg-chlorite is also missing). Nevertheless, both decompression paths are interpreted to be the consequence of a significant, early tectonic crustal thickening event, which was followed by rapid erosion and/or tectonic uplift. No evidences for an eclogite facies evolution of the whiteschists were found. On the contrary, the occurrence of albite in the whiteschist assemblage (Zambesi Belt, Vrana & Barr, 1972) precludes very high pressures. The petrological results are in agreement with previous studies of different parts of the Zambesi Belt and Lufilian Arc.

Zambesi Belt: Johnson & Oliver (1998) estimated minimum P-T conditions of about 590 °C and 13 kbar for a yoderite-bearing whiteschist terrane in the Chewore Inliers (Fig. 3.2). The estimate is mainly based on the experimental study of Fockenberg & Schreyer (1994) on yoderite stability. In addition, the authors calculated metamorphic peak-conditions of 700 °C and 10.5 kbar for Grt-bearing amphibolites and metapelites in a neighbouring ophiolite terrane. Similar estimates (600–750 °C / 8–9 kbar) are given by Goscombe et al. (1998) for their M2 event in several terranes of the Chewore Inliers. The M2 event was followed by an almost isothermal decompression which is similar to the metamorphic evolution of the Chowe River section reported here. Since Vrana & Barr (1972) did not found the cordierite reaction rims in whiteschists, they proposed a more contemporaneous exhumation and cooling history of the Chowe River whiteschists than the data of this study imply.

Lufilian Arc: Cosi et al. (1992) deduced a P-T evolution characterized by two stages using phase-petrological observations obtained from amphibolite, whiteschist, and metapelite samples taken from the entire Domes Region. Their high-pressure amphibolite facies stage with temperatures between 600 and 700 °C at pressures below 13 kbar is similar to the results of this study. In addition, the results for their low-pressure amphibolites facies stage with temperatures between 600-700 °C and pressures between 5 and 6 kbar are also similar (Fig. 3.8). Cosi et al. (1992) described whiteschsists containing garnet and eclogites containing omphacite with jadeite-contents between 35 and 40 mol.% occurring in the Domes Region. They attributed the eclogite facies stage to an earlier event preceding the high-pressure amphibolite facies metamorphism since most basic rocks are amphibolites and most eclogites are pervasively amphibolitisied as well. During the field-work of this study, we were not able to find these key-rocks for the high-pressure evolution of the area, i.e., eclogites or garnet-bearing whiteschists. However, the high-

pressure amphibolite facies overprint of the eclogites at 600–700 °C and 13 kbar (Cosi et al., 1992) is similar to the peak-conditions estimated in this study.

3.7 Geochronology

The metamorphic mineral monazite is used to date the peak-stage of metamorphism, while zircons are used to date the formation of the basement of the Lufilian Arc domes. Rb-Sr cooling ages are determined to evaluate whether the basement was affected by the same metamorphism as the overlying Katangan rocks, and to clarify the cooling history of the area. Monazite-forming reactions in metapelitic rocks are starting at lower amphibolite facies conditions (e.g., Parrish, 1990; Smith & Barreiro, 1990; Bingen et al., 1996) and in comparison with zircon, monazite is less prone to Pb-loss at high-grade metamorphic conditions. The closure temperature of the U-Th-Pb system in monazite was estimated at about 700 to 750 °C (Mezger, 1990; Parrish, 1990) but it was also argued that it is higher than 800 °C (e.g., Schenk, 1980; 1990; Spear & Parrish, 1996). Thus, monazite that grew during metamorphism is ideal to date the peak stage of amphibolite facies metamorphism.

3.7.1 Sample description

One whiteschist sample of the greenish variety (Z 271-2) of the chlorite schists unit of the Rufunsa Metavolcanic Formation was selected to constrain the time of peak metamorphism within the central Zambesi Belt. To determine the age of metamorphism in the Lufilian Arc, two whiteschists of the greyish variety, from the Kabompo (Z 244-1) and the Mwombezhi Dome (Z 230-1) and one whiteschist of the brownish variety (Z 220-9) as well as one biotite-kyanite-garnet gneiss (Z221-7) from the Solwezi Dome were collected. All samples belong to the lower units of the Roan Group. The basement rocks were sampled at the Kabompo Dome (tonalitic gneiss, consisting of plagioclase-quartz-biotite-hornblende-epidote; Z 241-1) and at the Solwezi Dome (banded two-mica gneiss, consisting of plagioclase-quartz-biotite-muscovite-epidote-tourmaline; Z 220-1).

3.7.2 Analytical procedures

Monazites and zircons (60–500 µm) were separated from 3-10 kg of fresh rock material using standard techniques (steel jaw-crusher, roller mill, Wilfley table, Frantz magnetic separator, heavy liquids). Prior to dissolution, hand picked grain size fractions were washed alternating in 3 N HCl and Aqua-dest. in an ultrasonic bath to remove any surface contamination. For monazite about 5-50 (500–50 µm) individual grains were separated. The analysed zircon fractions consisted of 5–35 individual grains (200–50 µm). Dissolution and chemical extraction (anion exchange columns) of U and Pb were performed following Krogh (1973). Monazite fractions were dissolved in a mixture of 0.5 ml 6 N HNO_3:HCl (1:1) in Savillex® vials on a hotplate within 2 to 3 days. Zircon fractions were dissolved in a mixture of 1 ml concentrated HF:HNO_3 (3:1) in Savillex® vials using Teflon® bombs within screw-top steel containers at 180 °C for 5 days. The mineral separates were spiked for isotope dilution measurements with a mixed ^{205}Pb-^{235}U tracer solution prior to digestion.

Muscovite, biotite and plagioclase were separated from the same samples collected for the U-Pb studies. Fractions were enriched in micas using the same techniques as for monazite and zircon. Only the size fraction 150–200 µm has been considered for Rb-Sr dating. After hand picking, possible

contaminants between mica sheets were removed by grinding under ethanol in an agate mortar. Mica (c. 4-20 mg) and plagioclase (c. 10-40 mg) fractions were mixed with an ^{87}Rb-^{84}Sr tracer solution for isotope dilution measurements prior to dissolution in a mixture of concentrated HF:HNO_3 (5:1) in Savillex® vials on a hotplate for 5 days. Chemical extraction of Rb and Sr were performed on cation exchange columns using 2.5 N HCl.

Isotope analyses were performed at the "Zentrallaboratorium für Geochronologie" in Münster using a VG Sector 54 multi-collector mass spectrometer with Daly detector in ion-counting mode (for ^{204}Pb) or using simultaneously Faraday detectors (all other isotopes) and a NBS-type Teledyne mass spectrometer (Rb). U and Pb were loaded on Re filaments with silica gel, H_3PO_4 and 6 N HCl. Measured Pb and U isotopic ratios were corrected for 0.08% and 0.095% fractionation per atomic mass unit, based on repeated analyses of standards NBS SRM 982 and NBS SRM U 500. Total procedural blanks during the study ranged between 0.05 and 0.1 ng Pb. U blanks were not measured since the very low blanks normally obtained are negligible for the high U amounts analysed. The ages and the error ellipses of Tab. 3.12 and Figs. 3.9 & 3.10 were calculated using the recommended IUGS decay constants (Steiger & Jäger, 1977), considering the internal 2 σ error of the measurements, the uncertainty in the U-Pb ratio of the spike, the error magnification from the spike/sample ratio and the estimated uncertainty in the isotopic composition of the Pb blank. The minimum uncertainty (2 σ) of isotopic ratios were ±0.3%, based on external reproducibility of a U-Pb measurement, if the analytical error of an analysis was greater than ±0.3% (2 σ), the higher value was used. Measured ratios were corrected for initial isotope Pb composition applying the data of Kamona et al. (1999) for the monazites of the Lufilian Arc and the two-stage model of Stacey & Kramers (1975) for all other mineral fractions, using the age of the sample. Rb was loaded on Ta filaments with H_2O, Sr was loaded on W with TaF_5 liquid and 6 N HCl. Measured Rb isotopic ratios were corrected for mass fractionation using a factor of 0.9935, determined by repeated measurements of standard NBS SRM 607. Measured Sr ratios were corrected for fractionation based on an $^{86}Sr/^{88}Sr$ ratio of 0.1194. Repeated runs of standard NBS SRM 987 gave an average $^{87}Sr/^{86}Sr$ ratio of 0.710293 ± 23 (n=9). Total blanks for Rb and Sr during the measurements were less than 0.1 ng for both. For all isochron calculations in this paper a minimum uncertainty of ±0.003% (2 σ) was assumed for the measured $^{87}Sr/^{86}Sr$ ratios, based on the reproducibility of the standard. If the standard error of an analysis was higher than ±0.003% (2 σ), the higher value was used. The uncertainty in $^{87}Rb/^{86}Sr$ ratios is taken to be 1%. For age calculations the recommended IUGS decay constants (Steiger & Jäger, 1977) were used. The errors on the isochrons were calculated according to York (1969).

3.7.3 Results of U-Pb and Rb-Sr geochronology

Monazite ages

Monazite typically has high Th/U ratios with more than 5 wt.% ThO_2 and much less than 1 wt.% UO_2 (e.g., Köppel, 1974). Monazites that grew under highly oxidising conditions should incorporate even more Th than U and thus also ^{230}Th (a short-lived intermediate daughter of ^{238}U), since U occurs under such conditions mainly as U^{6+}, and is therefore not suitable for incorporation into the monazite structure. The decay from ^{230}Th to ^{206}Pb, with a half-life of about 75000 years, produce too old $^{206}Pb/^{238}U$

Tab. 3.12 U-Pb analytical results for monazite and zircon from Zambesi Belt and Lufilian Arc.

					Composition		Isotopic ratios[a, b]						Apparent ages (Ma)		
Sample	mineral	Size (µm)	Rock type	Weight (mg)	U (ppm)	Pb (ppm)	$^{206}Pb/^{204}Pb$	$^{206}Pb/^{208}Pb$	$^{207}Pb/^{206}Pb$	$^{206}Pb/^{238}U$	$^{207}Pb/^{235}U$	Correlation coefficient	$^{206}Pb/^{238}U$	$^{207}Pb/^{235}U$	$^{207}Pb/^{206}Pb$
Zambesi Belt															
Z271-2	Mnz	250-350	whiteschist	0.50	221	298	3502	0.06219	0.05484(0.28)	0.09078(0.47)	0.6864(0.55)	0.85	560.2	530.6	405.6
Z271-2	Mnz	mixed	whiteschist	1.63	292	302	1907	0.08163	0.05599(0.29)	0.08893(0.21)	0.6866(0.37)	0.64	549.2	530.8	425.1
Z271-2	Mnz	60-75	whiteschist	0.16	575	304	3623	0.1750	0.05403(0.06)	0.09011(0.18)	0.6713(0.19)	0.88	556.2	521.5	372.3
Lufilian Arc															
Z220-1	Zrn_Z1	75-100	basementgneis	0.10	571	185	4769	13.70	0.1130(0.05)	0.3154(0.19)	4.914(0.19)	0.93	1767	1805	1848
Z220-1	Zrn_Z2	75-100	basementgneis	0.15	467	148	3642	14.59	0.1125(0.05)	0.3090(0.18)	4.795(0.19)	0.92	1736	1784	1841
Z220-1	Zrn_Z3	75-100	basementgneis	0.14	429	136	3361	12.16	0.1129(0.05)	0.3057(0.18)	4.761(0.19)	0.91	1720	1778	1847
Z220-1	Zrn_Z4	<60	basementgneis	0.08	441	141	1256	13.61	0.1118(0.07)	0.3012(0.18)	4.643(0.20)	0.86	1697	1757	1829
Z220-1	Zrn_Z5	150-250	basementgneis	0.80	638	195	1887	11.46	0.1116(0.06)	0.2883(0.40)	4.436(0.40)	0.99	1633	1719	1826
Z220-9	Mnz	150-200	whiteschist	0.79	222	590	4129	0.02925	0.05314(0.11)	0.08707(0.18)	0.6379(0.22)	0.71	538.2	501.0	334.6
Z221-7	Mnz	100-150	bt-ky-grt gneis	0.18	2810	363	8055	1.466	0.05797(0.06)	0.08566(0.20)	0.6847(0.20)	0.93	529.8	529.6	528.7
Z230-1	Mnz	400-500	whiteschist	0.49	34.2	51.0	384.7	0.05376	0.05734(0.33)	0.08706(0.19)	0.6883(0.42)	0.61	538.1	531.8	504.8
Z230-1	Mnz	75-100	whiteschist	0.15	38.0	77.6	309.7	0.03879	0.05587(0.48)	0.08777(0.26)	0.6761(0.64)	0.77	542.3	524.4	447.2
Z241-1	Zrn_Za	60-75	basementgneis	0.07	74.3	27.7	429.3	4.700	0.1139(0.14)	0.3179(0.27)	4.992(0.33)	0.90	1779	1818	1862
Z241-1	Zrn_Zb	<60	basementgneis	0.07	332	120	2670	4.537	0.1141(0.05)	0.3141(0.15)	4.941(0.16)	0.76	1759	1808	1866
Z241-1	Zrn_Zc	150-250	basementgneis	0.30	142	53.9	1410	4.615	0.1141(0.07)	0.3218(0.19)	5.064(0.21)	0.90	1798	1830	1866
Z244-1	Mnz	75-100	whiteschist	0.04	255	596	752.5	0.03366	0.05608(0.27)	0.08754(0.20)	0.6768(0.37)	0.62	540.9	524.9	455.4

[a] $^{206}Pb/^{204}Pb$ is the measured ratio, all others are calculated, correction for blank, common Pb and fractionation.

[b] Number in parentheses is the relative 2σ uncertainty in %.

ages because of adding excess thorogenic ^{206}Pb to the uranogenic ^{206}Pb (Schärer, 1984). Therefore, the $^{207}Pb/^{235}U$ age represents the best age for monazites, specially if they contain high Th/U ratios (Parrish, 1990; Tomascak et al., 1996). Whiteschists have highly oxidised mineral assemblages with almost all Fe bounded in hematite resulting in the typical high-Mg silicate assemblages. Multivalent ions mainly occur in their highest oxidation state (e.g., Johnson & Oliver, 2001). Thus, the high Th/U ratios of monazites from the whiteschists (c. 100; Tab. 3.13) suggest that excess thorogenic ^{206}Pb may cause reverse discordance. A correction for excess thorogenic ^{206}Pb is not possible for metamorphic monazites, because it is not possible to evaluate precisely which minerals were in equilibrium with monazite during its formation (Parrish, 1990). In order to evaluate the significance of the $^{207}Pb/^{235}U$ ages of whiteschist monazites, different grain size fractions as well as monazites from the biotite-kyanite-garnet gneiss (Z 221-7) were analysed (Tab. 3.12).

From all samples only clear, subhedral to round monazite crystals and some fragments were selected for U-Pb geochronology. All monazite fractions of the investigated whiteschists yield strongly reverse discordant ages (Fig. 3.9). The two fractions of the Chowe River sample (Z271-2) with the larger grain sizes (mixed and 250-350 µm) yield identical $^{207}Pb/^{235}U$ ages with 531 ±2 Ma and 531 ±3Ma, but vary strongly in the $^{206}Pb/^{238}U$ ratios (Tab. 3.12). The smaller size fraction (60-75µm) has a younger $^{207}Pb/^{235}U$ age with 522 ±2 Ma and a similar $^{206}Pb/^{238}U$ age. The different size fractions of sample Z 230-1 (Lufilian Arc) yield the same $^{207}Pb/^{235}U$ age range with 532 ±2 Ma (400-500 µm) and 524 ±3Ma (75-100 µm) as well as variations in the $^{206}Pb/^{238}U$ ratios (Tab. 3.12) compared to the monazites of Z 271-2 (Zambesi Belt). The monazite fraction (75-100 µm) of sample Z 244-1 has a $^{207}Pb/^{235}U$ age of 525 ±2 Ma, which is a similar result to that of the other smaller size fractions. The monazites of whiteschist Z 220-9 (150-200 µm) yield a $^{207}Pb/^{235}U$ age of 501 ±2 Ma which is much younger than all other results (Tab. 3.12). In contrast, the monazite fraction (100-150µm) from the biotite-kyanite-garnet gneiss (Z 221-7) from the Solwezi Dome yields a concordant age of 529 ±2 Ma (Fig. 3.9).

All $^{207}Pb/^{235}U$ ages of larger size fractions of whiteschsist monazites range between 531 and 532 Ma. The analyses only differ in the $^{206}Pb/^{238}U$ ages (Fig. 3.9), indicating that thorogenic ^{206}Pb caused the strong and variable reverse discordanc (e.g., Tomascak et al., 1996). The concordant age of sample Z 221-7 with 529 ±2 Ma confirms the interpretation that the $^{207}Pb/^{235}U$ ages reflect the true ages and since all other ages, except of Z 220-9, are identical within error, 529 ±2 Ma is interpreted as being the best age estimate for the peak of metamorphism. The smaller size fractions have younger $^{207}Pb/^{235}U$ ages, ranging between 522 and 525 Ma (mean = 523 ±2 Ma), with similar variations in the $^{206}Pb/^{238}U$ ages to those of the

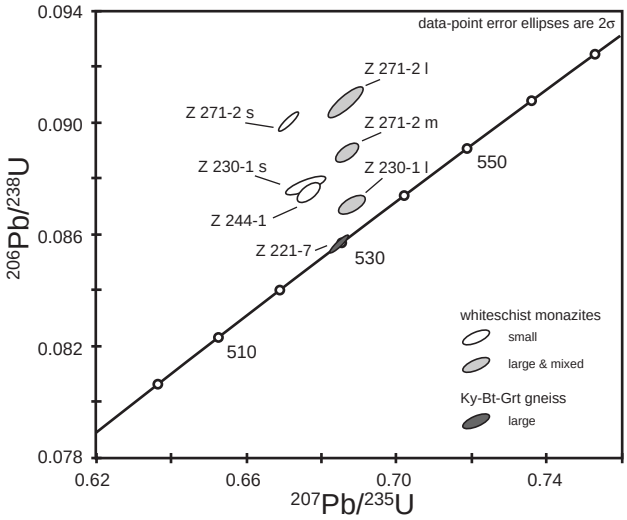

Fig. 3.9 Concordia diagram for monazite analyses of whiteschists (small size fractions = white; large size fractions = grey) and garnet-biotite-kyanite gneiss (dark grey). Sample numbers are indicated.

Tab. 3.13 Representative microprobe analyses of whiteschist-monazite and structural formulae.

Sample	Z 221-7	Z 221-7	Z 230-1	Z 230-1	Z 244-1	Z 244-1	Z 271-2	Z 271-2
Analysis	mnz3ap3	mnz3cp2	mnz1bp1	mnz1cp4	mnz4bp3	mnz4cp4	mnz2ap2	mnz2dp2
Location	core	rim	rim	core	rim	rim	core	rim
rock type	g	g	w	w	w	w	w	w
P_2O_5	31.08	31.06	30.59	31.00	31.08	30.06	30.71	30.71
SiO_2	0.08	0.06	0.00	0.01	0.08	0.00	0.11	0.19
CaO	1.04	0.72	0.51	0.20	0.75	0.71	0.93	1.17
Y_2O_3	1.86	2.57	0.02	0.57	1.62	0.54	2.26	2.21
La_2O_3	13.99	12.34	19.16	20.30	18.18	13.37	12.87	13.60
Ce_2O_3	30.37	29.48	31.84	31.82	24.74	28.34	28.36	27.43
Pr_2O_3	3.21	3.34	2.80	2.59	3.43	4.40	3.17	2.90
Nd_2O_3	12.28	13.53	11.38	10.30	12.87	16.83	12.93	11.84
Sm_2O_3	1.83	2.15	1.56	1.28	1.56	1.97	2.19	1.90
Eu_2O_3	0.44	0.54	0.38	0.34	0.50	0.31	0.64	0.57
Gd_2O_3	1.27	1.61	0.43	0.60	1.04	0.96	1.78	1.70
Dy_2O_3	0.48	0.64	0.00	0.21	0.45	0.14	0.65	0.66
Er_2O_3	0.09	0.16	0.00	0.02	0.09	0.01	0.15	0.13
ThO_2	1.41	0.95	0.67	0.22	2.69	2.70	2.72	4.44
UO_2	0.35	0.43	b.d.l.	b.d.l.	0.02	0.02	0.03	0.05
Total	99.77	99.56	99.34	99.45	99.09	100.36	99.49	99.49
			Structural formulae on a basis of 2 oxygens					
P	1.010	1.012	1.010	1.016	1.017	0.996	1.006	1.005
Si	0.003	0.002	0.000	0.000	0.003	0.000	0.004	0.008
Ca	0.043	0.030	0.021	0.009	0.031	0.030	0.038	0.049
Y	0.038	0.053	0.000	0.012	0.033	0.011	0.047	0.046
La	0.198	0.175	0.276	0.290	0.259	0.193	0.184	0.194
Ce	0.427	0.415	0.455	0.451	0.350	0.406	0.402	0.388
Pr	0.045	0.047	0.040	0.037	0.048	0.063	0.045	0.041
Nd	0.168	0.186	0.159	0.143	0.178	0.235	0.179	0.163
Sm	0.024	0.029	0.021	0.017	0.021	0.027	0.029	0.025
Eu	0.006	0.007	0.005	0.005	0.007	0.004	0.009	0.008
Gd	0.016	0.021	0.006	0.008	0.013	0.012	0.023	0.022
Dy	0.006	0.008	0.000	0.003	0.006	0.002	0.008	0.008
Er	0.001	0.002	0.000	0.000	0.001	0.000	0.002	0.002
Th	0.012	0.008	0.006	0.002	0.024	0.024	0.024	0.039
U	0.003	0.004	0.000	0.000	0.000	0.000	0.000	0.000
Total	2.001	1.997	1.998	1.991	1.990	2.004	1.999	1.997
Th/U	4	2	*	*	112	123	97	99

g = biotite-kyanite-garnet gneiss; w = whiteschist; b.d.l. = below detection limit (c. 120 ppm).
ZAF-matrix correction; measurement conditions: 60 nA, 20 kV; standards: synthetic REE phosphates, U and Th glaces.

larger size fractions. The time between 530 and 523 of c. 7 Ma is interpreted to display the duration of peak-metamorphism, rather than cooling, because metamorphic temperatures never reached values above the suggested closure temperatures of monazite. The age of sample Z 220-9 with 501 ±2 Ma is much younger than all other ages and because this rock displays the most intensive retrogression, it is interpreted to be a result of late stage fluid activity causing monazite recrystallisation.

Cooling ages

The results of the Rb-Sr dating on muscovite and biotite (Tab. 3.14) are used to constrain the cooling history of the Domes Region and to evaluate whether the basement rocks were affected by the same metamorphism as the Katangan cover rocks. The closure temperature for Rb-Sr has been estimated for muscovite at

Tab. 3.14 Rb-Sr isotope analyses for Lufilian Arc samples.

Sample	Type	Rb (ppm)	Sr (ppm)	$^{87}Rb/^{86}Sr^{ab}$	$^{87}Sr/^{86}Sr^{ab}$	Initial $^{87}Sr/^{86}Sr$	Age (Ma)[c]
Z 220-1	Muscovite	301	20.4	44.0	1.0287	0.722	489.6 ±4.8 Ma
	Biotite	556	2.44	1134	8.4182	0.722	476.3 ±4.7 Ma
	Plagioclase	104	622	0.486	0.72513		
Z 221-7	Biotite	323	3.59	309	2.7921	0.726	468.8 ±4.6 Ma
	Plagioclase	0.871	120	0.0211	0.72635		
Z 241-1	Biotite	1011	4.34	1190	8.7029	0.739	469.7 ±4.6 Ma
	Plagioclase	175	565	0.900	0.74498		

[a]Ratios corrected for fractionation, spike and blank as described in text.
[b]Uncertainties of isotopic ratios as described in text (not shown).
[c]Uncertainty in ages in million years at the 2σ confidence interval.

c. 500 ±50 °C, and in biotite at c. 350 °C (Hanson & Gast, 1967; Dodson, 1979). Thus the corresponding ages indicate the time of cooling for the temperature range of c. 500 to 300 °C.

For the biotite-kyanite-garnet gneiss (Z 221-7) sampled at the Solwezi Dome, the biotite-plagioclase isochron give an age of 469 ±5 Ma. Using the basement rock of the Solwezi Dome (Z 220-1), dating define Rb-Sr ages of 490 ±5 Ma for muscovite-plagioclase and 476 ±5 Ma for biotite-plagioclase, indicating that both samples of the Solwezi Dome experienced the same cooling history since 500 °C and thus both rocks were affected by the same tectonothermal event at about 530 Ma, dated with the U-Pb monazite ages. Rb-Sr dating of biotite-plagioclase from the basement rock of the Kabompo Dome (Z 241-1) gives an age of 470 ±5 Ma, similar to the other biotite-plagioclase ages of this study, again indicating that the rocks experienced the same metamorphic event. Using c. 530 Ma as the age of peak-metamorphism with a peak-temperature of c. 750 °C (Lufilian Arc) as well as the cooling ages for 500 °C of c. 490 Ma and for 300 °C of c. 470 Ma, the Lufilian Arc orogen cooled at a rate of c. 6-8 °C/Ma.

Zircon ages

U-Pb ages of zircons were used to date the crystallisation of the basement of the Lufilian Arc domes. From the basement sample Z 220-1 of the Solwezi Dome five fractions of different shapes and sizes were analysed (Tab. 3.12). Only pristine zircons were used, divided in groups with long prismatic shapes (Z_1), long prismatic rounded shapes (Z_2), round multiple-facet shapes (Z_3), very small crystals of round multiple-facet shape (Z_4), and large long prismatic crystals which were air-abraded (Z_5). Air abrasion was used to obtain more concordant analyses by removing metamict parts, or younger overgrowths (Krogh, 1982; Mezger & Krogstad, 1997). A discordia line through all five fractions has upper and lower intercept ages of 1863 ±25 Ma and 414 ±270 Ma, with the close spacing of the analyses generating high uncertainties on both ages. The age of peak-metamorphism with c. 530 Ma, obtained from the overlain Katangan rocks with U-Pb monazite dating, is within the error of the lower intercept age. Since the cover and the basement rocks experienced the same tectonothermal event, as indicated by the Rb-Sr mica ages, pinning of the discordia line through a 530 ±10 Ma lower intercept seems to be reasonable and results in an upper intercept age of 1874 ±9 Ma (Fig. 3.10a). The air-abraded zircon fraction gives the most discordant analysis (Fig. 3.10a) which can be explained with recrystallisation of metamict zircons during amphibolite facies metamorphism (Mezger & Krogstad, 1997). Three zircon fractions of sample Z 241-1 were used to define the time of formation of the

Kabompo Dome basement. Again only pristine zircons were used. The analysed fractions (Tab. 3.12) consist of long prismatic rounded crystals (Za), round multiple-facet crystals (Zb), and large long prismatic air-abraded crystals (Zc). Since the Rb-Sr biotite age of this rock is identical with that of the Solwezi Dome rocks, the same assumption about the metamorphic evolution as for Z 220-1 were made. The three analyses define an upper intercept age of 1884 ±10 Ma if the lower intercept is anchored at 530 ±10 Ma (Fig. 3.10b), while using the three analyses only, the upper intercept age is 1869 ±120 Ma. The upper intercept ages of 1874 ±9 Ma (Z 220-1, Solwezi Dome) and 1884 ±10 Ma (Z 241-1, Kabompo Dome) are interpreted to be best determination of the basement-formation of the of the Lufilian Arc domes. No evidences for another tectonothermal event between emplacement and peak-metamorphism at c. 530 Ma were found.

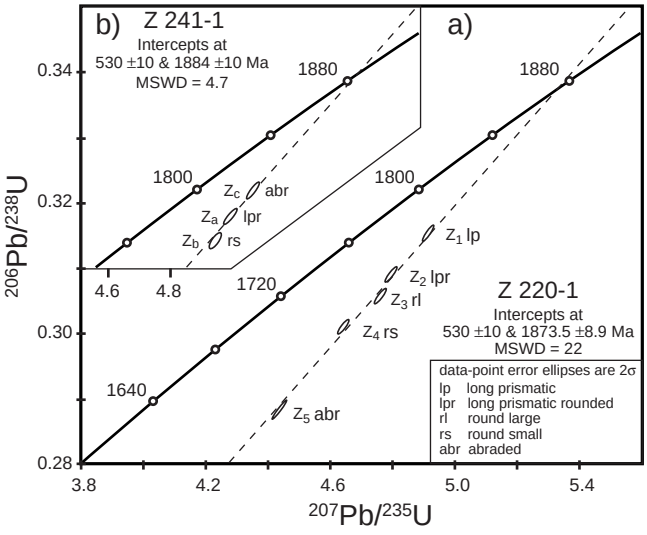

Fig. 3.10 Concordia diagrams for (a) = zircon analyses of the Solwezi Dome basement gneiss (Z 220-1) and (b) zircon analyses of the Kabompo Dome basement gneiss (Z 241-1). Sample numbers are indicated.

3.7.4 Comparison with previous studies and discussion

The emplacement of the Lufilian Arc basement within the Domes Region has been dated at 1874 ±9 and 1884 ±10 Ma and is with c. 1.9 Ga in agreement with the Palaeoproterozoic ages of basement rocks of the eastern Lufilian Arc, ranging between 2.0 and 1.8 Ga as indicated by Rb-Sr whole-rock and U-Pb SHRIMP dating (Cahen et al., 1984; Rainaud et al., 1999). The occurrence of Mesoproterozoic basement in the Domes Region was suggested by Cosi et al. (1992) mainly on the basis of a poorly constrained, regional Rb-Sr isochron. The results of the present study make this interpretation very unlikely. In addition, no evidence for a Mesoproterozoic metamorphic event was found that might have affected the rocks of the Domes Region.

A tectonothermal event between c. 550 and 525 Ma has been recently dated at several localities of the entire Lufilian Arc-Zambesi Belt (Fig. 3.11). Amphibolite to high-pressure granulite facies metamorphic events in the Zambesi Belt have been dated from east to west, in the Rushinga Area at c. 535 Ma (U-Pb zircon and titanite single grain ages, Vinyu et al., 1999), in the Mavuradonha Mountains at c. 550 Ma with 551 ±7 to 545 ±9 Ma (Pb-Pb zircon evaporation and Grt-wr Sm-Nd ages, Müller, 2001), in the Chewore Inliers at 526 ±17 Ma (SHRIMP analyses of zircon, Goscombe et al., 1998, 2000) and in the Makuti Metamorphic Complex around 542 ±10 Ma (U-Pb zircon and titanite U-Pb ages, Hanson et al., 1998). In addition, recrystallisation of uraninite due to a tectonic event at around 530 ±1 Ma has been dated with the U-Pb system at Lwiswishi, Lufilian Arc (Loris et al., 1997). All these results are in good agreement with the results of this study and thus point to

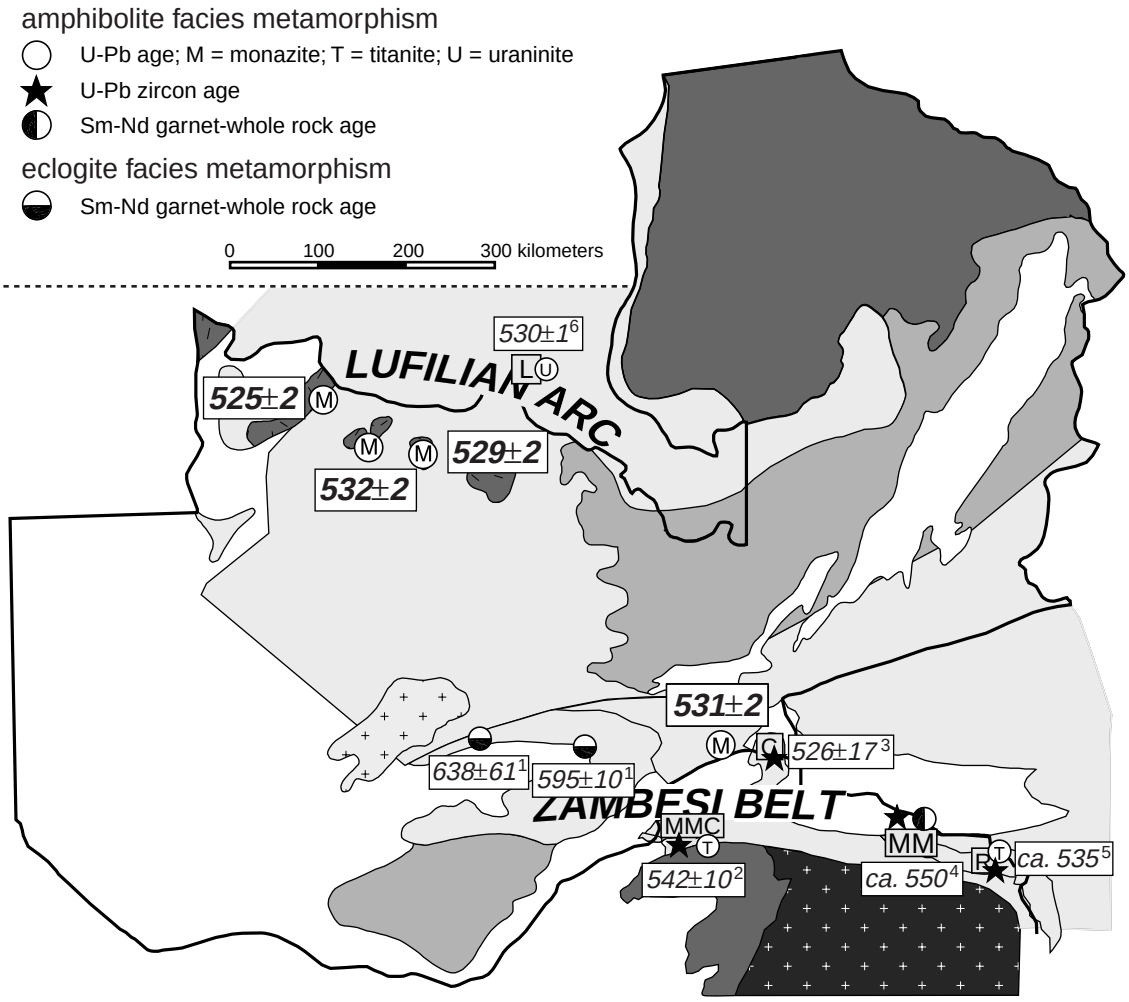

Fig. 3.11 Geological map of Zambia, Northern Zimbabwe and Western Moçambique (Legend is similar to Fig. 3.1) showing the spatial distribution of determined ages of crustal thickening (amphibolite to eclogite facies) in the Lufilian Arc-Zambesi Belt orogen. Enlarged-bold sample labels indicate the results of this study, thin numbers are literature data; 1 chapter one; 2 Hanson et al. (1998); 3 Goscombe et al. (2000); 4 Müller (2001); 5 Vinyu et al. (1999); 6 Loris et al. (1997).

one major crustal thickening event at c. 530 Ma which affected the entire Lufilian Arc-Zambesi Belt orogen almost simultaneously (Fig. 3.11). This interpretation confirms recent models of the Pan-African belts of central southern Africa, which postulate an orogenic belt, formed by collision between 560 and 500 Ma, that stretches from the Moçambique Belt either to the Damara Belt (Goscombe et al., 2000), or to the West Congo Belt (Porada & Berhorst, 2000). Goscombe et al. (2000) pointed out that the tectonic setting of this Pan-African orogenic belt is still unresolved. However, Porada & Berhorst (2000) interpreted the Lufilian Arc and northern Zambesi Belt as forming together a segment of a passive continental margin, which belongs to the southern edge of the Congo Craton. The related rifting started at c. 880 Ma (Porada & Berhorst, 2000 and references therein) and first basic intrusions within the thinned lower crust are documented to have occurred around 870 Ma (Müller, 2001). Porada & Berhorst (2000) postulated the opening and closure of a large ocean basin to

explain the deposits of passive margin sediment sequences and following thrust transport (> 150 km distance). This interpretation is in accordance with geochemical and geochronological data from MORB-type eclogites and associated gabbros of central Zambia, which are evidence for a Neoproterozoic ocean basin. The low geothermal gradient during eclogite facies metamorphism, which was caused by cold and thus old subducted oceanic lithosphere, indicates that this basin was relatively large (chapter one). However, all these models are in contrast to the model of Dirks & Sithole (1999), who proposed that the major collisional event in the Zambesi Belt occurred between 1100-945 Ma (during Rodinia consolidation), and was followed by an extensional event at around 800 Ma (reworking of the Zambesi Belt during Rodinia break up). In this model a non-oceanic basin closed without significant crustal thickening between 550–500 Ma.

The cooling ages of c. 490 ±5 Ma for muscovite and c. 470 ±5 Ma for biotite, determined for the Lufilian Arc, are similar to the results of Cosi et al. (1992) who reported Rb-Sr muscovite ages between 510 and 450 Ma (see discussion in Porada & Berhorst, 2000). Cooling at a rate of 8-6 °C/Ma for the Lufilian Arc is almost identical with the cooling history of parts of the Zambesi Belt that record rates between 4 and 16 °C/Ma (Goscombe et al., 2000 and references therein), pointing to a similar post tectonic evolution. Willigers at al. (submitted) found that relatively slow cooling, as observed here, is typical for deeply eroded orogens of Proterozoic age in contrast to the fast cooling of high-pressure terranes occurring in Phanerozoic orogens.

3.8 Conclusions

The results of this study show that the whiteschist within the Lufilian Arc-Zambesi Belt formed under high-pressure amphibolite facies conditions. Since no evidence for eclogite facies metamorphism was found in whiteschists, and the eclogites of the central Zambesi Belt were already formed at c. 600 Ma (chapter one), the high-P amphibolite metamorphism at c. 530 Ma was most likely linked to a continental collision rather than to subduction zone processes. This proposed crustal thickening event affected the entire Lufilian Arc-Zambesi Belt almost simultaneously, c. 70 Ma subsequent to the closure of an ocean basin. Consequently, it is suggested that the Lufilian Arc-Zambesi Belt represent part of the collisional plate boundary between the Congo and the Kalahari craton during Gondwana growth.

Combining the results of this study with data from the literature leads to the following evolutionary model for the Pan-African mobile belts of central southern Africa which is shown in the cartoon of figure 3.12:

1. extension (Fig. 3.12a)
Initial rifting started at c. 880-870 Ma (e.g., Müller, 2001) and is related to the dispersal of Rodinia. During the proceeding rifting a passive continental margin developed at the southern edge of the Congo craton (Porada & Berhorst, 2000) and an ocean basin formed (chapter one).

2. compression (Fig. 3.12b)
The geodynamic scenario changed from extension to compression and due to the convergence of the Congo and Kalahari cratons oceanic lithosphere was subducted and eclogites were formed at c. 600 Ma.

a) extension since ca. 880 Ma
- ocean floor formation

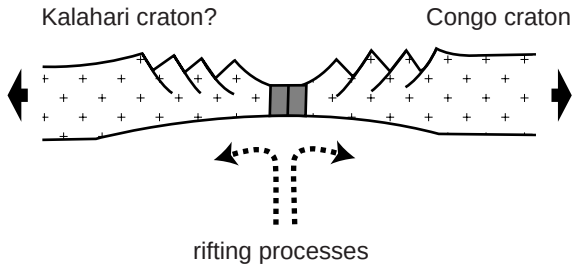

b) compression
- eclogite formation at ca. 600 Ma

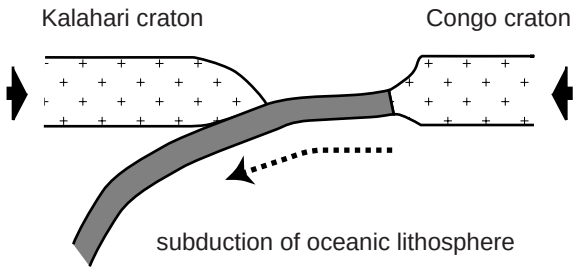

c) continental collision at ca. 530 Ma
- HP / LT metamorphism

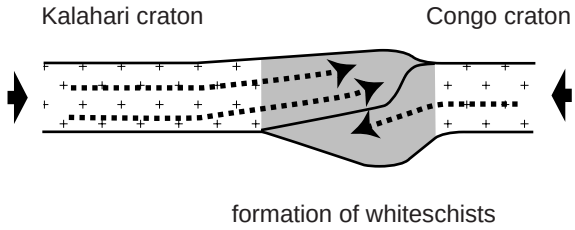

d) cooling since 530 Ma
- uplift and erosion

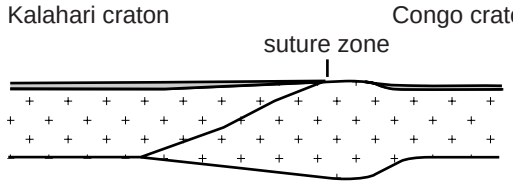

3. collision (Fig. 3.12c)
After the oceanic crust was consumed, the Kalahari craton started to override the passive continental margin of the Congo craton (Porada & Berhorst, 2000). Peak metamorphism in this thickened crust commenced at c. 530 Ma. Hence, the whiteschist formation could be related to fluids from shallow water sediments (e.g., evaporates) of the overridden plate. This could explain the existence of an “exotic fluid” during whiteschist formation, postulated by Johnson & Oliver (2001).

4. cooling (Fig. 3.12d)
When the final collision with thrusting over 150 km distance (Porada & Berhorst, 2000) came to end, it was followed by rapid erosion and/or tectonic uplift and finally cooling.

Fig. 3.12 Cartoon illustrating the proposed evolution of the Pan-African Lufilian Arc-Zambesi Belt orogen (see text), (a) the extensional stadium is related to the dispersal of Rodinia and led to the formation of an ocean basin, (b) during convergence between the Kalahari and Congo craton the ocean basin closed, (c) in the final stage of convergence the Kalahari and Congo cratons collide resulting in a continent-continent collision, and (d) the stage of cooling is characterized by denudation and uplift.

Andersen, L.S., Unrug, R., 1984. Geodynamic evolution of the Bangweulu Block, northern Zambia. Precambrian Research, v. 25, p. 187-212.

Åustrheim, H., 1986/87. Eclogitisation of lower crustal granulites by fluid migration through shear zones. Earth and Planetary Science Letters, v. 81, p. 221-232.

Åustrheim, H., 1990. The granulite-eclogite facies transition: a comparison of experimental work and a natural occurrence in the Bergen Arcs, western Norway. Lithos, v. 25, p. 163-169.

Barnes, S.-J., Sawyer, E.W., 1980. An alternative model for the Damara mobile belt: ocean crust subduction and continental convergence. Precambrian Research, v. 13, p.297-336.

Barnicoat, A.C., Cartwright, I., 1997. The gabbro-eclogite transformation: an oxygen isotope and petrographic study of west Alpine ophiolites. Journal of Metamorphic Geology, v. 15, p. 93-104.

Barr, M.W.C., 1997. Geology of the Chongwe River area: explanation of degree sheet 1529, SW quarter. Report of the Geological Survey of Zambia, No 45.

Berman, R.G., 1988. Internally-consistent thermodynamic data for minerals in the system Na_2O-K_2O-CaO-MgO-FeO-Fe_2O_3-Al_2O_3-SiO_2-TiO_2-H_2O-CO_2. Journal of Petrology, v. 29, p. 445-522.

Bingen, B., Demaiffe, D., Hertogen, J., 1996. Redistribution of rare earth elements, thorium, and uranium over accessory minerals in the course of amphibolite to granulite facies metamorphism: The role of apatite and monazite in orthogneisses from southwestern Norway. Geochimica et Cosmochimica Acta, v. 60, p. 1341-1354.

Boynton, W.V., 1984. Cosmochemistry of the rare earth elements: Meteorite studies. *In* Henderson, P., ed., Rare earth element geochemistry: Amsterdam, Elsevier, p. 63-107.

Brunsmann, A., Franz, G., Erzinger, J., Landwehr, D., 2000. Zoisite- and clinozoisite segregations in metabasites (Tauern window, Austria) as evidence for high-pressure fluid-rock interaction. Journal of Metamorphic Geology, v. 18, p. 1-21.

Caby, R., Bertrand, J.M.L., Black, R., 1981. Pan-African ocean closure and continental collision in the Hoggar-Iforas segment, Central Sahara. *In* Kröner, A., ed., Precambrian Plate Tectonics. Developments in Precambrian Geology, 4, p. 407-434.

Cahen, L., Snelling, N.J., Delhal, J., Vail, J.R., 1984. The geochronology and evolution of Africa. Clarendon, Oxford. 512 pp.

Carlson, R.W., 1991. Physical and chemical evidence on the cause and source characteristics of flood basalt volcanism. Australian Journal of Earth Science, v. 38, p. 525-544.

Carmichael, D.M., 1969. On the Mechanism of Prograde Metamorphic Reactions in Quartz-Bearing Pelitic Rocks. Contributions to Mineralogy and Petrology, v. 20, p. 244-267.

Carmichael, D.M., 1987. Induced stress and secondary mass transfer: Thermodynamic basis for tendency toward constant-volume constraint in diffusion metasomatism. *In* Helgeson, H.C., ed., Chemical Transport in Metasomatic Processes. D. Reidel Publishing Company, p. 239-264.

Carswell, D.A., O'Brien, P.J., Wilson, R.N., Zhai, M., 1997. Thermobarometry of phengite-bearing eclogites in the Dabie Mountains of central China. Journal of Metamorphic Geology, v. 15, p. 239-252.

Carswell, D.A., Wilson, R.N., Zhai, M., 2000. Metamorphic evolution, mineral chemistry and thermobarometry of schists and orthogneisses hosting ultra-high pressure eclogites in the Dabieshan of central China. Lithos, v. 52, p. 121-155.

Chopin, C., 1984. Coesite and pure pyrope in high-grade blueschists of the Western Alps: a first record and some consequences. Contributions to Mineralogy and Petrology, v. 86, p. 107-118.

Cloos, M., 1993. Lithospheric buoyancy and collisional orogenesis: Subduction of oceanic plateaus, continental margins, island arcs, spreading ridges and seamounts. Geological Society of America Bulletin, v. 105, p. 715-737.

Condie, K.C., 1989. Plate tectonics and crustal evolution. Pergamon Press, Oxford, 3rd ed., 476 pp.

Cosi, M., De Bonis, A., Gosso, G., Hunziker, J., Martinotti, M., Moratto, S., Robert, J.P., Ruhlman, F., 1992. Late Proterozoic thrust tectonics, high-pressure metamorphism and uranium mineralization in the Domes Area, Lufilian Arc, northwestern Zambia. Precambrian Research, v. 58, p. 215-240.

Coward, M.P., Daly, M.C., 1984. Crustal lineaments and shear zones in Africa: their relationships to plate movements. Precambrian Research, v. 24, p. 27-45.

Daly, M. C., 1986. The intracratonic Irumide Belt of Zambia and its bearing on collision orogeny during the Proterozoic of Africa. *In* Coward, M.P. and Ries, A.C., eds., Collision tectonics. Geological Society. Special Publication, v. 19, p. 321-328.

Dalziel, I.W.D., 1992. On the organisation of American plates in the Neoproterozoic and the breakout of Laurentia. GSA Today, v. 2, p.240-241.

Dalziel, I.W.D., 1997. Neoproterozoic-Paleozoic geography and tectonics: review, hypothesis and environmental speculation. Geological Society of America Bulletin, v. 109, p. 16-42.

Dalziel, I.W.D., Mosher, S., Gahagan, L.M., 2000. Laurentia-Kalahari collision and the assembly of Rodinia. The Journal of Geology, v. 108, p. 499-513.

Dirks, P.H.G.M., Jelsma, H.A., Vinyu, M., Munyanyiwa, H., 1998. The structural history of the Zambesi Belt in northeast Zimbabwe; evidence for crustal extension during early Pan-African. South African Journal of Geology, v. 101, p. 1-16.

Dirks, P.H.G.M., Sithole, T.A., 1999. Eclogites in the Makuti gneisses of Zimbabwe: implications for the tectonic evolution of the Zambesi Belt in southern Africa. Journal of Metamorphic Geology, v. 17, p. 593-612.

Dodson, M.H., 1979. Theory of cooling ages. *In* Jäger, E., Hunziker, J.C., eds., Lectures in Isotope Geology. Springer, p. 194-202.

Ferry, J.M., 2000. Patterns of mineral occurrence in metamorphic rocks. American Mineralogist, v. 85, p. 1573-1588.

Ferry, J.M., Spear, F.S., 1978. Experimental calibration of the partitioning of Fe and Mg between biotite and garnet. Contributions to Mineralogy and Petrology, v. 66, p. 113-117.

Fockenberg, T., Schreyer, W. 1994. Stability of Yoderite in the absence and presence of quartz: Experimental study in the system MgO-Al_2O_3-Fe_2O_3-SiO_2-H_2O. Journal of Petrology, v. 35, p. 1341-1375.

Frey, F.A., Garcia, M.O., Wise, W.S., Kennedy, A., Gurriet, P., Albarède, F., 1991. The evolution of Mauna Kea volcano, Hawaii: Petrogenesis of tholeiitic and alkalic basalts. Journal of Geophysical Research, v. 96, p. 14247-14375.

Gao, J., Klemd, R., 2001. Primary fluids entrapped at blueschist to eclogite transition: evidence from the Tianshan meta-subduction complex in northwestern China. Contributions to Mineralogy and Petrology, v. 142, p. 1-14.

Goscombe, B., Armstrong, R., Barton, J.M., 1998. Tectonometamorphic Evolution of the Chewore Inliers: Partial Re-equilibration of High-grade Basement during the Pan-African Orogeny. Journal of Petrology, v. 39, p. 1347-1384.

Goscombe, B., Armstrong, R., Barton. J.M., 2000. Geology of the Chewore Inliers, Zimbabwe: constraining the Mesoproterozoic to Palæozoic evolution of the Zambesi Belt. Journal of African Earth Sciences, v. 30, p. 589-627.

Graham, C.M., Powell, R.P., 1984. A garnet-hornblende geothermometer: calibration, testing, and application to the Pelona schist, southern California. Journal of Metamorphic Geology, v. 2, p. 13-31.

Green, D.H., Hellman, P.L., 1982. Fe-Mg partitioning between coexisting garnet and phengite at high pressures, and comments on a garnet-phengite geothermometer. Lithos, v. 15, p. 253-266.

Hacker, B.R., 1996. Eclogite Formation and the Rheology, Buoyancy, Seismicity, and H_2O Content of Oceanic Crust. *In* Bebout, G.E., Scholl, D.W., Kirby, S.H., Platt, J.P., eds., Subduction Top to Bottom. Geophysical Monograph v. 96, p. 337-346.

Hanan, B.B., Blichert-Toft, J., Kingsley, R., Schilling, J.G., 2000. Depleted Iceland mantle plume geochemical signature: Artifact of multicomponent mixing?. Geochemistry, Geophysics, Geosystems, v. 1. Nr. 1999GC000009.

Hanson, G.N., Gast, P.W., 1967. Kinetic studies in contact metamorphic zones. Geochemica et Cosmochemica Acta, v. 31, p. 1119-1153.

Hanson, R.E, Hargrove, U.S., Martin, M.W., Bowring, S.A., Krol, M.A., Hodges, K.V., Munyanyiwa, H., Blenkiskop, T.G., 1998. New geochronological constraints on the tectonic evolution of the Pan-African Zambesi Belt, south central Africa. Journal of African Earth Science, v. 18, p. 104-105.

Hanson, R.E., Wilson, T.J., Brueckner, H.K., Onstott, T.C., Wardlaw, M.S., Johns, C.C., Hardcastle, K.C., 1988. Reconnaissance geochronology, tectonothermal evolution, and regional significance of the middle Proterozoic Choma-Kalomo Block, southern Zambia: Precambrian Research, v. 42, p. 39-61.

Hanson, R.E., Wilson, T.J., Munyanyiwa, H., 1994. Geologic evolution of the Neoproterozoic Zambesi Orogenic Belt in Zambia. Journal of African Earth Science, v. 18, p. 135-150.

Hanson, R.E., Wilson, T.J., Munyanyiwa, H., 1994. Geologic evolution of the late Proterozoic Zambezi Belt in Zambia. Journal of African Earth Science, v. 18, p. 135-150.

Hanson, R.E., Wilson, T.J., Wardlaw, M.S., 1988a. Deformed batholiths in the Pan-African Zambezi, Zambia. Age and implications for regional Proterozoic tectonics. Geology, v. 16, p. 1134-1137.

Hawkesworth, C.J., Gallagher, K., Hergt, J.M., McDermott, F., 1993. Mantle and slab contributions in arc magmas. Annual Reviews of Earth and Planetary Sciences, v.21, p. 175-204.

Hickey, R.L., Frey, F.A., Gerlach, D.C., Lopez-Escobar, L., 1986. Multiple sources for arc rocks from the southern volcanic zone of the Andes (34°-41°S): Trace element and isotopic evidence for contributions from subducted oceanic crust, mantle, and continental crust. Journal of Geophysical Research, v. 91, p.5963-5983.

Hodges, K.V., Crowley, P.D., 1985. Error estimation and empirical geothermobarometry for pelitic systems. American Mineralogist, v. 70, p. 702-709.

Hoffman, P.F., 1991. Did the breakout of Laurentia turn Gondwanaland inside-out? Science, v. 252, p. 1409-1412.

Hofmann, A.W., 1988. Chemical differentiation of the Earth: the relationship between mantle, continental crust and oceanic crust. Earth and Planetary Science Letters, v. 90, p. 297-314.

Hoisch, T.D., 1990. Empirical calibration of six geobarometers for the mineral assemblage quartz + muscovite + biotite + plagioclase + garnet. Contributions to Mineralogy and Petrology, v. 104, p. 225-234.

Holdaway, M.J., 1971. Stability of andalusite and the aluminium silicate phase diagram. American Journal of Science, v. 271, p. 97-131.

Holland, T.J.B., 1979. Experimental determination of the reaction Paragonite = Jadeite + Kyanite + H_2O, and the consistent thermodynamic data for part of the system Na_2O-Al_2O_3-SiO_2-H_2O, with applications to eclogites and blueschists. Contributions to Mineralogy and Petrology, v. 68, p. 292-301.

Jahn, B-m., Caby, R., Monie, P, 2001. The oldest UHP eclogites of the World: age of UHP metamorphism, nature of protoliths and tectonic implication. Chemical Geology, v. 178, p. 143-158.

Joesten, R.L., 1991. Kinetics of coursing and diffusion-controlled mineral growth. *In* Kerrick, D.M., ed., Contact Metamorphism. Mineralogical Society of America Reviews in Mineralogy, v. 26, p. 507-582.

Johnson, R.L., Vail, J.R., 1965. The junction between the Mozambique and Zambesi orogenic belts, north-east Southern Rhodesia. Geological Magazine, v. 101, p. 489-495.

Johnson, S.P. and Oliver, G.J.H., 2001. High fO_2 metasomatism during whiteschist metamorphism, Zambesi Belt, northern Zimbabwe. Journal of Petrology, in press.

Johnson, S.P., Oliver, G.J.H., 1998. A second natural occurrence of yoderite. Journal of Metamorphic Geology, v. 16, p. 809-818.

Johnson, S.P., Oliver, G.J.H., 2000. Mesoproterozoic oceanic subduction, island-arc formation and the initiation of back-arc spreading in the Kibaran Belt of central, southern Africa: evidence from the Ophiolite Terrane, Chewore Inliers, northern Zimbabwe. Precambrian Research, v. 103, p. 125-146.

Kamona, A.F., Lévêque, J., Friedrich, G., Haack, U., 1999. Lead isotopes of the carbonate-hosted Kabwe, Tsumeb, and

Kipushi Pb-Zn-Cu sulphide deposits in relation to Pan African orogenesis in the Damaran-Lufilian Fold Belt Central Africa. Mineralium Deposita, v. 34, p. 273-283.

Katongo, C., Tembo, F., 1999. Structural and petrographic fabrics in the Chisamba area: implications for the kinematic development of the Neoproterozoic Mwembeshi Dislocation Zone. 11th International Conference of the Geological Society of Africa, Journal of African Earth Science, v. 28, p. 35.

Kleber, W., 1962. Über orientierte heterogene Keimbildung in kristallisierten Phasen. Forschung und Fortschritte, v. 36, p. 257-262.

Kleemann, U., Reinhardt, J., 1994. Garnet-biotite thermometry revisited: The effect of Al^{VI} and Ti in biotite. European Journal of Mineralogy, v. 6, p. 925-941.

Koons, P.O., Rubie, D.C., Frueh-Green, G., 1987. The effects of disequilibrium and deformation on the mineralogical evolution of quartz diorite during metamorphism in the eclogite facies. Journal of Petrology, v. 28, p. 679-700.

Köppel, V., 1974. Isotopic U-Pb ages of monazite and zircon from the crust-mantle transition and adjacent units of the Ivrea and Ceneri zones (Southern Alps, Italy). Contributions to Mineralogy and Petrology, v. 43, p. 55-70.

Koziol, A.M., 1989. Recalibration of the garnet -plagioclase-Al_2SiO_5-quartz geobarometer. EOS, Transactions American Geophysical Union, v. 70, p. 493.

Kretz, R., 1983. Symbols for rock-forming minerals. American Mineralogist, v. 68, p. 277-279.

Krogh, T.E., 1973. A low-contamination method for hydrothermal decomposition of zircon and extraction of U and Pb for isotopic age determinations. Geochimica et Cosmochimica Acta, v. 37, p. 485-494.

Krogh, T.E., 1982. Improved accuracy of U-Pb zircon dating by the creation of more concordant systems using an air abrasion technique. Geochimica et Cosmochimica Acta, v. 46, p. 637-649.

Kullerud, K., 1996. Chlorine-rich amphiboles: Interplay between amphibole composition and an evolving fluid. European Journal of Mineralogy, v. 8, p. 355-370.

Li, Z.X., Powell, McA., 1993. Late Proterozoic to early Paleozoic paleomagnetism and the formation of Gondwanaland. *In* Findlay, R.H., Unrug, R., Banks, M.R., Veevers, J.J., eds., Assembly, evolution and dispersal; proceedings of the Gondwana eight symposium. International Gondwana Symposium, v. 8, p. 9-21.

Loris, N.B.T., Chralet, J.-M., Pechmann, E., Clare, C., Chabu, M., Quinif, Y., 1997. Caractéristiques minéralogiques, critallographiques, physico-chimiques et ages desminéralisations uranifères de Lwiswishi (Shaba, Zaire). Proceedings International Cornet Symposium, Mons. Royal Academy Oversea Science, p. 285-306.

Markl, G., Bucher, K., 1998. Compositions of fluids in the lower crust inferred from metamorphic salt in lower crustal rocks. Nature, v. 391, p. 781-783.

Massonne, H.-J., 1989. The upper thermal stability of chlorite + quartz: an experimental study in the system MgO-Al_2O_3-SiO_2-H_2O. Journal of Metamorphic Geology, v. 7, p. 567-581.

Massonne, H.-J., 1995. Experimental and Petrogenetic Study of UHPM. *In* Coleman, R.G., Wang, X. eds., Ultrahigh pressure metamorphism. Cambridge University Press, p. 33-95.

Meert, J.G., Powell, C.M.A., 2001. Assembly and break-up of Rodinia: introduction to the special volume. Precambrian Research, v. 110, p. 1-8.

Meert, J.G., Van der Voo, R., Ayub, S., 1995. Paleomagnetic investigation of the Neoproterozoic Gagwe lavas and Mbozi complex, Tanzania and the assemblage of Gondwana. Precambrian Research, v. 74, p. 225-244.

Merino, E., Dewers, T., 1998. Implications of replacement for reaction-transport modeling. Journal of Hydrology, v. 209, p. 137-146.

Mezger, K., 1990. Geochronology in granulites. *In* Vielzeuf, D., Vidal, P.H., eds., Granulites and crustal evolution. NATO Advanced Study Institute, Kluwer Academic Publishers, p. 451-470.

Mezger, K., Krogstad, E.J. 1997. Interpretation of discordant U-Pb zircon ages: An evaluation. Journal of Metamorphic Geology, v. 15, p. 127-140.

Möller, A., Appel, P., Mezger, K., Schenk, V., 1995. Evidence for a 2 Ga subduction zone: Eclogites in the Usagaran belt of Tanzania. Geology, v. 23, p. 1067-1070.

Morimoto, N., Fabries, J., Ferguson, A.K., Ginzburg, I.V., Ross, M., Seifert, F.A., Zussman, J., Aoki, K., Gottardi, G., 1988. Nomenclature of pyroxenes. American Mineralogist, v. 73, p. 1123-1133.

Mørk, M.B.E., 1985a. A gabbro to eclogite transition on Flemsøy, Sunnmøre, western Norway. Chemical Geology, v. 50, p. 283-310.

Mørk, M.B.E., 1985b. Incomplete high P-T metamorphic transitions within the Kvamsøy pyroxenite complex west Norway: a case study of disequilibrium. Journal of Metamorphic Geology, v. 3, p. 245-264.

Müller, M.A., 2001. The Mavuradonha Layerd Complex: Pan-African emplacement and grenulite-facies metamorphism in the Zambezi Allochtonous Terrain of the Mt. Darwin Area, Zambezi Belt, NE Zimbabwe. unpublished dissertation, Mainz.

Oliver, G.J.H., Johnson, S.P., Williams, I.S., Herd, D.A., 1998. Relict 1.4 Ga oceanic crust in the Zambesi Valley, northern Zimbabwe: Evidence for Mesoproterozoic supercontinental fragmentation. Geology, v. 26, p. 571-573.

Parrish, R.R., 1990. U-Pb dating of monazite and its application to geological problems. Canadian Journal of Earth Sciences, v. 27, p. 1431-1450.

Pearce, J.A., Ernewein, M., Bloomer, S.H., Parson, L.M., Murton, B.J., Johnson, L.E., 1995. Geochemistry of Lau Basin volcanic rocks: influence of ridge segmentation and arc proximity, *In* Smellie, J.L. ed., Volcanism associated with extension at consuming plate margins: Geological Society Special Publications, v. 81, p. 53-75.

Perchuk, L.L., Lavrent´eva, I.V., 1983. Experimental investigation of exchange equilibria in the system cordierite-garnet-biotite. *In* Saxena, S.K. ed., Kinetics and equilibrium in mineral reactions. New York, Springer, p. 199-239.

Piper, J.D.A., 2000. The Neoproterozoic Supercontinent: Rodinia or Palaeopangaea?. Earth and Planetary Science Letters, v. 176, p. 131-146.

Pognante, U., 1985. Coronitic reactions and ductile shear zones in eclogitised ophiolite metagabbros, Western Alps, North Italy. Chemical Geology, v. 50, p. 99-110.

Porada, H., 1989. Pan-African rifting and orogenesis in southern to Equatorial Africa and Eastern Brazil. Precambrian Research, v. 44, p. 103-136.

Porada, H., Berhorst, V., 2000. Towards a new understanding of the Neoproterozoic-Early Palaeozoic Lufilian and northern Zambesi Belts in Zambia and the Democratic Republic of Congo. Journal of African Earth Sciences, v. 30, p. 727-771.

Powell, C.McA., Jones, D.L., Pisarevsky, S., Wingate, M.T.D., 2001. Paleomagmatic constraints on the position of the Kalahari craton in Rodinia. Precambrian Research, v. 110, p. 33-46.

Powell, R., 1985. Regression diagnostics and robust regression in geothermometer / geobarometer calibration: the garnet-clinopyroxene geothermometer revisited. Journal of Metamorphic Geology, v. 3, p. 231-243.

Powell, R., Holland, T.J.B., 1988. An internally consistent thermodynamic dataset with uncertainties and correlations. 3. Applications to geobarometry, worked examples and a computer program. Journal of Metamorphic Geology, v. 6, p. 173-204.

Rainaud, C., Armstrong, R.A., Master, S., Robb,L.J., 1999. A fertile Palaeoproterozoic magmatic arc beneath the Central African Copperbelt. *In* C.J. Stanley ed., Mineral Deposits: Processes to processing. Proceedings of the 5th SGA meeting and the 10th IAGOD Symposium, London. Balkema, p. 1427-1430.

Ray, G.E., 1974. The structural and metamorphic geology of northern Malawi. Journal of the Geological Society of London, v. 130, p. 427-440.

Ridley, J., Thompson, A.B., 1985. The Role of Mineral Kinetics in the Development of Metamorphic Microtextures. *In* Walther, J.V., Wood, B.J., eds., Fluid-Rock interaction during Metamorphism, p. 154-193.

Rolfo, F., Compagnoni, R., Xu, S., Jiang, L., 2000. First record of felsic whiteschists in the ultrahigh-pressure metamorphic belt of Dabie Shan, China. European Journal of Mineralogy, v. 12, p. 883-898.

Rubie, D.C., 1983. Reaction-enhanced ductility: the role of solid-solid univariant reactions in deformation of the crust and mantle. Tectonophysics, v. 96, p. 331-352.

Rubie, D.C., 1990. Role of kinetics in the formation and preservation of eclogites. *In* Carswell, D.A., ed., Eclogite Facies Rocks. Blackie, p. 111-140.

Rubie, D.C., 1998. Disequilibrium during metamorphism: the role of nucleation kinetics. *In* Treloar, P.J., O'Brien, P., eds., What Drives Metamorphism and Metamorphic Reactions?. Geological Society, London, Special Publications, v. 138, p. 199-214.

Sanders, I. S., Van Calsteren, P. W. C., Hawkesworth, C. J., 1984. A Grenville Sm-Nd age for the Glenelg eclogite in north-west Scotland. Nature, v. 312, p. 439-440.

Scambelluri, M., Piccardo, G.B., Philippot, P., Robbiano, A., Negretti, L., 1997. High salinity fluid inclusions formed from recycled seawater in deeply subducted alpine serpentinite. Earth and Planetary Science Letters, v. 148, p. 485-499.

Schärer, U., 1984. The effect of initial 230Th disequilibrium on young U-Pb ages: the Makalu case, Himalaya. Earth and Planetary Science Letters, v. 67, p. 191-204.

Schenk, V., 1980. U-Pb and Rb-Sr radiometric dates and their correlation with metamorphic events in the granulite-facies basement of the Serre, southern Calabria (Italy). Contributions to Mineralogy and Petrology, v. 73, p. 23-38.

Schenk, V., 1990. The exposed crustal cross section of southern Calabria, Italy: structure and evolution of a segment of Herzynian crust. *In* Salisbury, M.H., Fountain, D.M. eds., Exposed cross-sections of the continental crust. Kluwer Academic Publishers, p. 21-42.

Schenk, V., Appel, P., 2001. Anti-clockwise P-T path during ultrahigh-temperature (UHT) metamorphism at c. 1050 Ma in the Irumide Belt of Eastern Zambia. Berichte der Deutschen Mineralogischen Gesellschaft, Beihefte zum European Journal of Mineralogy, v. 13, p. 161.

Schmid, M.W., Poli, S, 1998. Experimentally based water budgets for dehydrating slabs and consequences for arc magma generation. Earth and Planetary Science Letters, v. 163, p. 361-379.

Schreyer, W., 1973. Whiteschist: a high-pressure rock and its geological significance. The Journal of Geology, v. 81, p. 735-739.

Schreyer, W., 1977. Whiteschists: their compositions and pressure-temperature regimes based on experimental, field, and petrographic evidence. Tectonophysics, v. 43, p. 127-144.

Schreyer, W., 1988. Experimental studies on metamorphism of crustal rocks under mantle pressures. Mineralogical Magazine, v. 52, p. 1-26.

Schreyer, W., Abraham, K., 1976. Three-Stage Metamorphic History of a Whiteschist from Sar e Sang, Afghanistan, as Part of a Former Evaporite Deposit. Contributions to Mineralogy and Petrology, v. 59, p. 111-130.

Schumacher, J.C., Robinson, P., 1987. Mineral chemistry and metasomatic growth of aluminous enclaves in gedrite-cordierite-gneiss from southwestern New Hampshire, USA. Journal of Petrology, 28, 1033-1073.

Sikatali, C., Legg, C.A., Bwalya, J.J., Ng'ambi, O., 1994. Geological and Mineral occurrence map (1: 2,000000): Geological Survey of Zambia.

Smith, H.A., Barreiro, B., 1990. Monazite U-Pb dating of staurolite grade metamorphism in pelitic schists. Contributions to Mineralogy and Petrology, v. 105, p. 602-615.

Spear, F.S., 1993. Metamorphic phase equilibria and pressure-temperature-time paths. Monograph series, Mineralogical Society of America. 799 pp.

Spear, F.S., Cheney, J.T., 1989. A petrogenetic grid for pelitic schists in the system SiO_2-Al_2O_3-FeO-MgO-K_2O-H_2O. Contributions to Mineralogy and Petrology, v. 101, p. 149-164.

Spear, F.S., Kohn, M.J., Cheney, J.T., 1999. P-T paths from anatectic pelites. Contributions to Mineralogy and Petrology, v. 134, p. 17-32.

Spear, F.S., Parrish, R.R., 1996. Petrology and cooling rates of the Valhalla complex, British Columbia, Canada. Journal of Petrology, v. 37, p. 733-765.

Spear, F.S., Rumble III, D., 1986. Pressure, temperature, and structural evolution of the Orfordville Belt, west-central New Hampshire. Journal of Petrology, v. 27, p. 1071-1093.

Stacey, J.S., Kramers, J.D., 1975. Approximation of terrestrial lead isotope evolution by a two-stage model. Earth and Planetary Science Letters, v. 26, p. 207-221.

Steiger, R.H., Jäger, E., 1977. Subcommision on Geochronology: convention on the use of decay constants in geo- and cosmochronology. Earth and Planetary Science Letters, v. 36, p. 359-362.

Tembo, F., Kampunzu, A.B., Porada, H., 1999. Tholeiitic magmatism associated with continental rifting in the Lufilian Fold Belt of Zambia. Journal of African Earth Sciences, v. 28, p. 403-425.

Thieme, J.G., 1984. Geological Map of the Lusaka Area 1:250,000 sheet. Geological Survey of Zambia, Map No. SD-35-15.

Thieme, J.G., Johnson, R.L., 1977. Republic of Zambia, Geological Map 1:1,000.000. Sheet NW. Geological Survey of Zambia.

Thompson, J.B.Jr., 1981. An Introduction to the mineralogy and petrology of the biopyriboles. *In* Veblen, D.R., ed., Amphiboles and other Hydrous Pyriboles-Mineralogy. Mineralogical Society of America Reviews in Mineralogy, v. 9a, p. 141-188.

Tomascak, P.B., Krogstad, E.J., Walker, R.J., 1996. U-Pb Monazite Geochronology of Granitic Rocks from Maine: Implications for Late Paleozoic Tectonics in the Northern Appalachians. The Journal of Geology, v. 104, p. 185-195.

Turner, F.J., Weiss, L.E., 1965. Deformational kinks in Brucite and gypsum. Proceedings of the National Academy of Sciences, v. 54, p. 359-364.

Turner, S., Hawkesworth, C., Rogers, N., Bartlett, J., Worthington, T., Hergt, J., Pearce, J. and Smith, I., 1997. ^{238}U-^{230}Th disequilibria, magma petrogenesis, and flux rates beneath the depleted Tonga-Kermadec island arc. Geochimica et Cosmochimica Acta, v. 61, p. 4855-4884.

Unrug, R., 1996. The assembly of Gondwanaland. Scientific results of IGCP Project 288: Gondwanaland sutures and mobile belts. Episodes, v. 19, p. 11-20.

Vernikovsky, V.A., Vernikovskaya, A.E, 2001. Central Taimyr accretionary belt (Artic Asia): Meso-Neoproterozoic tectonic evolution and Rodinia break-up. Precambrian Research, v. 110, p. 127-142.

Vidale, R.J., 1974. Vein Assemblages and Metamorphism in Dutchess County, New York. Geological Society of America Bulletin, v. 85 2, p. 303-306.

Vinyu, M.L., Hanson, R.E., Martin, M.W. Bowring, S.A., Jelsma, H.A., Krol, M.A., Dirks, P.H.G.M., 1999. U-Pb and $^{40}Ar/^{39}Ar$ geochronological constraints on the tectonic evolution of the easternmost part of the Zambezi orogenic belt, northeast Zimbabwe. Precambrian Research, v. 98, p. 67-82.

Vinyu, M.L., Martin, M.W., Bowring, S., Hanson, R., Jelsma, H.A., Dirks, P.H.G.M., 1997. Tectonothermal evolution of the polymetamorphic Zambesi Belt in NE Zimbabwe: constraints from U-Pb single grain zircon data. Intraplate Magmatism and Tectonics of Southern Africa, Abstract Volume, p. 52.

Vrána, S., Barr, W.C., 1972. Talc-kyanite-quartz schists and other high-pressure assemblages from Zambia. Mineralogical Magazine, p. 837-846.

Vrana, S., Prasad, R., Fediuková, E. 1975. Metamorphic Kyanite Eclogites in the Lufilian Arc of Zambia. Contributions to Mineralogy and Petrology, v. 51, p. 139-160.

Walther, J.V., Wood, B.J., 1984. Rate and mechanism in prograde metamorphism. Contributions to Mineralogy and Petrology, v. 88, p. 246-259.

Waters, D.J., Martin, H.N., 1993. Geobarometry of phengite-bearing eclogites. Terra Abstracts. v. 5, p. 410-411.

Wayte, G.J., Worden, R.H., Rubie, D.C, Droop, G.T.R., 1989. A TEM study of disequilibrium plagioclase breakdown at high pressure: the role of infiltrating fluid. Contributions to Mineralogy and Petrology, v. 101, p. 426-437.

Weil, A.B., Van der Voo, R., Mac Niocaill, C., Meert, J.G., 1998. The Proterozoic supercontinent Rodinia: paleomagnetically derived reconstructions for 1100 to 800 Ma. Earth and Planetary Science Letters, v. 154, p. 13-24.

Wendt, J.I., Regelous, M., Niu, Y., Hékinian, R., Collerson, K.D., 1999. Geochemistry of lavas from the Garrett Transform Fault: insights into mantle heterogeneity beneath the eastern Pacific. Earth and Planetary Science Letters, v. 173, p. 271-284.

Whittington, A., Busbey, A., Hanson, R., Morgan, K., 1999. Remote-sensing study of structural relations between the Pan-African Zambesi and Mozambique orogenic belts in NE Zimbabwe and adjacent parts of Mozambique. Geological Society of America Abstracts with Programs, v. 31, A37.

Willigers, B.J.A., van Gool, J.A.M, Wijbrans, J.R., Krogstad, E.J., Mezger, K. submitted. Apparent contrasting orogenic cooling histories in the Precambrian and the Phanerozoic. The Journal of Geology.

York, D., 1969. Least squares fitting of a straight line with correlated errors. Earth and Planetary Science Letters, v. 5, p. 320-324.